

UNIVERSITY OF CYPRUS | POLYTECHNIC SCHOOL



Master Science MSc Thesis

Growth & Characterization of Cuprous Oxide

Cu_2O

ANDREAS IOANNOU

DEPARTMENT OF MECHANICAL AND
MANUFACTURING ENGINEERING

ADVANCED MATERIALS & NANOTECHNOLOGY

MAY 2024



UNIVERSITY OF CYPRUS | POLYTECHNIC SCHOOL

DEPARTMENT OF MECHANICAL AND
MANUFACTURING ENGINEERING

Growth & Characterization of Cuprous Oxide Cu_2O

Andreas Ioannou

Supervisor:

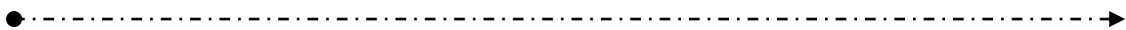
Associate Professor Dr. Matthew Zervos

The Master Science Thesis was submitted in partial fulfillment of the requirements
for the MSc in Advanced Materials and Nanotechnology of Mechanical and
Manufacturing Engineering

May 2024

ACKNOWLEDGMENTS

For the exposure of my MSc Thesis, first and foremost I am extremely grateful to my supervisor, Professor Matthew Zervos, for his invaluable advice, continuous support, and patience during the whole period of my postgraduate studies. His immense knowledge and plentiful experience have encouraged me in all time of my research at university. Furthermore, I want to thank the other postgraduate students of our lab, Argiris Tilemachou and Andreas Georgiou for the training at lab, on the use of equipment, operation of machines and learning of the experimental methods at the lab. Last, I want to thank Mr. Panagiotis Ioannou, a PhD holder at Nanomaterials at our department, which helps me at the lab and learning to me different experimental methods, where they belong to his lab.



ABSTRACT

In MSc Thesis, the characteristics, properties, and applications of Cuprous Oxide (Cu_2O) are extensively analyzed. First, is carried out an extensive literature review on this material, with the previous research with target to find out how we must proceed the investigation on Cu_2O . The purpose is to grow up a stable and high-efficient semiconductor material to become ready for use at industrial scale, since the energy amounts of our planet are increased rapidly. We described the whole procedure of the experiments that we done for the growth of our material on several substrates, to find out the optimum conditions for the deposition by Sputtering and post vacuum annealing by CVD, of a pure Cu_2O . The methods that are used for growth and characterization of the materials, are described. We did fundamental research on Cu_2O to understand the structural and optical properties of the material, and to explain the findings of characterization methods, of XRD, SEM, Raman Spectroscopy and Ultrafast Pump Probe Spectroscopy. Last, the next article is published by the collaboration with other investigators.

APL Energy

ARTICLE

pubs.aip.org/aip/ape

Critical and controversial issues pertaining to the growth and properties of Cu_2O in the context of energy conversion

Cite as: APL Energy 1, 036102 (2023); doi: [10.1063/5.0165856](https://doi.org/10.1063/5.0165856)

Submitted: 30 June 2023 • Accepted: 9 October 2023 •

Published Online: 20 October 2023



View Online



Export Citation



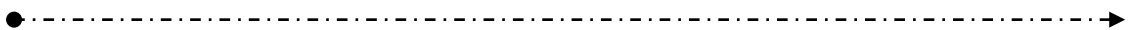
CrossMark

Eleni Prountzou,¹  Andreas Ioannou,²  Dimitrios Sapalidis,¹  Eleni Pavlidou,¹  Maria Katsikini,¹ 
Andreas Othonos,³  and Matthew Zervos^{2,a)} 

Contents

Chapter 1 – Introduction	7
Chapter 2 - Literature Review on Cu ₂ O	10
2.1. Characteristics	10
2.2. Applications	10
2.3. Fabrication Methods	12
2.3.1. Sputtering Technique	12
2.3.2. Annealing process of samples – Hydrogen Treatment	17
Chapter 3 – Fabrication Methods.....	22
3.1. Preparation Methods	22
3.1.1. Sputtering technique.....	22
3.1.2. Chemical Vapor Deposition (CVD) technique.....	24
3.2. Characterization Methods.....	27
3.2.1. X – Ray Diffraction (XRD) technique.....	27
3.2.2. Scanning Electron Microscopy (SEM) technique.....	29
Chapter 4 - Growth of Cu ₂ O	33
4.1. Introduction.....	33
4.2. Reactive Sputtering Conditions	33
4.2.1. Initial Materials for Reactive Sputtering	33
4.2.2. Initial Conditions for Reactive Sputtering	34
4.2.3. Optimum Conditions for Reactive Sputtering	34
4.3. Experiment 1 - Use of Optimum Reactive Sputtering Conditions with simple use of Chemical Vapor Deposition technique (CVD).....	35
4.3.1. Experimental process	35
4.3.2. Initial Conditions for CVD	35
4.3.3. XRD Characterization & Results.....	37
4.4. Experiment 2 - Use of Vacuum Pressure in CVD Furnace for Thermal Annealing – Change of O ₂ percent in Reactive Sputtering	39
4.4.1. Vacuum pressure instead of atmospheric pressure.....	39
4.4.2. Change of O ₂ percent in Reactive Sputtering.....	39
4.4.3. Experimental Process	39
4.4.4. XRD Characterization and Results	40
4.5. Experiment 3 – Use of Hydrogen gas (H ₂) in Vacuum Thermal Annealing.....	45

4.5.1. Benefits of introduction of Hydrogen	45
4.5.2. Experimental process – Reactive Sputtering.....	45
4.5.3. Experimental process – Thermal Vacuum Annealing.....	46
4.5.4. XRD Characterization and Results	47
4.5.5. Optimum Conditions for pure Cu ₂ O	55
4.6. Preparation of samples for SEM Characterization, Raman Spectroscopy and Ultrafast Pump Probe Spectroscopy (UPPS).....	55
4.6.1. Experimental process - Preparation of Cu ₂ O thin films.....	56
4.6.2. SEM and Raman Spectroscopy Results.....	56
4.6.3 UPPS Results and Discussion	57
Chapter 5 – Conclusion.....	62
Supplementary Material.....	63
Experiment 1	63
Experiment 2	64
Experiment 3	65
Experiment 4	67
References.....	69



Chapter 1 – Introduction

Nowadays, there are serious energy and environmental crises, and a huge increase of industry, which needs too much higher amounts of energy. To solve these problems, it is necessary to exploit new renewable and sustainable sources. This will be happened using the science of nanotechnology.

Nanotechnology is the science which involved the design, synthesis, characterization, and application of materials and devices whose have dimensions on nanometer scale, at least in one dimension [1]. On more simple definition of nanotechnology, is “technology at the nanoscale”, which explains the previous phrase, and give us the scale of this technology. The nanoscale covers the range from 1 to 100nm. The important of combination of science and engineering at nanoscale is the discovery of new fundamental and unique properties that open the range of what modern technology can succeed.

The solar energy is one of the best sources on the category of renewable and sustainable sources. Is renewable and sustainable, and we can have this kind of energy in high amounts, to produce electricity by the photovoltaic cells. So, the production of electricity by photovoltaic cells, helps in two ways, to the growing demand for energy as we said before, and to mitigation of global climate change by increasing of this energy and reducing of the production of energy by fossil fuels [2].

Furthermore, the solar cells that are produced by the industry are almost only, monocrystalline silicon cells because of their high efficiency. On laboratory scale, this efficiency was 25% before two decades, and on our days, increased slightly to 26.6% [2]. Because of the small increase on the efficiency for a long time, scientists are exploring alternative materials for the solar cells and manufacturing processes to create it, to reach higher efficiencies.

On these materials, is our material, cuprous oxide (Cu_2O), which is a promising oxide-based p-type semiconductor, appropriate to develop a p-n junction for a solar cell. This material belongs to the category of thin films materials. The efficiency that succeeded from the incorporation of Cu_2O is 2%. This is a heterojunction solar cell which was done by deposition of transparent conducting oxide (TCO) films on Cu_2O substrates [3].

Also, for the concerning of climate crisis the certain material is used to reduction the CO_2 with purpose the reduce of carbon emissions, with final positive effect on the planet. The CO_2 in atmosphere has risen up over the last century from 280 ppm above the 400ppm according to climate information from National Oceanic and Atmospheric Administration (NOAA) about the atmospheric carbon dioxide [4]. Specifically, in 2023 rise on 424 ppm, which was a new record, and the prediction until the new century is to rise to 700 ppm. So, the purpose is to discard CO_2 or convert into a valuable resource. Cu_2O is a potential material to use as a catalyst for CO_2 reduction, because

of its many advantages, including the interfacial charge separation and transportation. CO₂ transformations take place by photochemical and electrochemical phenomena. Sathya M. et al, on their review provides an idea of current photochemical and electrochemical CO₂ fixing techniques by using Cu₂O-based materials [5]. Further analysis will take place on Chapter 2 on this application of cuprous oxide.

In addition to previous examples on applications of Cu₂O in nanotechnology we have more, including the solar water splitting by the use of Cu₂O as an emerging photocathode [6], and the use of Cu₂O to understand the novel properties of excitons [7], etc. The interesting on this material is high, and therefore has been done big research. Many scientists have worked and are working on Cu₂O, at last 80 years. At next Chapter (Ch.2) we have a literature review on our material, including the characteristics, properties, and applications of Cu₂O. We emphasize on fabrication methods, how other researchers have deposited and form the Cu₂O, by Sputtering technique and after how they did the annealing process of prepared sample, what pressure and inlet gases they have used.

Next, at Chapter 3 we analyzed the methods that we have used on the lab for our experiments. We have worked with Sputtering and CVD techniques, for the deposition and growth up of the thin film at its final form, and we used XRD and SEM techniques, to characterize the prepared material. The principles, and the operation of these four techniques are described on this Chapter, with examples from the experiments on Cu₂O, that we have done.

In the next Chapter is described the whole procedure on the experimental part of work. The main purpose it is the growth of pure Cu₂O, therefore we must find the optimum conditions for the best formation of this material. For the growth we used two techniques, Sputtering and CVD techniques, and we set different parameters for each technique, to start the experiments. The basic parameters that we changed are the time, cycles, and sputter current, at Sputtering technique, and the time, temperature, pressure, and inlet gases at CVD for the annealing process of prepared samples. Several combinations have been made to execute the optimum conditions. After each set of experiments, we characterized the samples by XRD to identify the material, that we grow up. All these combinations, the series of experiments, and the results from XRD are analyzed in detail at this Chapter, with execution of the optimum conditions from the best result.

The cuprous oxide (Cu₂O) due to its characteristics and properties is a promising material for the future of nanotechnology, and the fields that we refer before. Except from the other characteristics about structure, to form this material we need Cu and O₂, which are two materials highly abundance in earth, and non-toxicity. So, for the concerning of planet these characteristics are important. Also, very important is the low cost and simplicity of synthesis. It is important for us to use simple techniques, for example the Sputtering technique to form this material in simple way, and to have a lot of experiments due to low cost. Much more are important for the field of industry

because they want to have a production, so they need low cost of fabrication, and high profits.

Generally, the purpose of this research and thesis is the investigation of cuprous oxide (Cu_2O), by a fundamental point of view, thus on the way that the cuprous oxide gets its final form, how it's the structure, and what properties exhibit at the end. This will be achieved by the investigation, first on characteristics, properties, and applications of Cu_2O that referred in literature, second on fabrication methods that referred again in literature, and finally on our experiments that are based on two previous steps. Also, the results from the characterization methods are important to execute conclusions about the findings for the structural and optical properties. The use of UPPS and Raman Spectroscopy give as more data about the properties. The target is to have a Cu_2O thin film with high purity and good crystal quality, with final target the use of this material on an application.

Also, we have published an article at APL Energy magazine [8], for the critical and controversial issues pertaining to the growth and properties of Cu_2O in the context of energy conversion, which involves the results from this thesis. Amongst others, is the literature review for Cu_2O , the optimization of conditions for Sputtering and Annealing techniques, and the introduction of hydrogen in the Annealing process. The article is found at supplementary material.

APL Energy ARTICLE pubs.aip.org/aip/ape

Critical and controversial issues pertaining to the growth and properties of Cu_2O in the context of energy conversion

Cite as: APL Energy 1, 036102 (2023); doi: 10.1063/5.0165856
Submitted: 30 June 2023 • Accepted: 9 October 2023 •
Published Online: 20 October 2023

[View Online](#) [Export Citation](#) [CrossMark](#)

Eleni Prountzou,¹ [ORCID](#) Andreas Ioannou,² [ORCID](#) Dimitrios Sapalidis,¹ [ORCID](#) Eleni Pavlidou,¹ [ORCID](#) Maria Katsikini,¹ [ORCID](#)
Andreas Othonos,³ [ORCID](#) and Matthew Zervos^{2,a)} [ORCID](#)

Figure 1.1. Critical and controversial issues pertaining to the growth and properties of Cu_2O in the context of energy conversion [8].

Chapter 2 - Literature Review on Cu₂O

2.1. Characteristics

Cu₂O (cuprous oxide) is a promising oxide-based p-type semiconductor, which has been recognized as oldest p-type binary oxide material. A lot of research in the fields of optoelectronics and solar technology has been done the last 80 years on this material. Most of the theory of semiconductors was developed based on the Cu₂O devices. Due to low band gap energy, Cu₂O was the first choice to the researcher as photovoltaic applications rather than other TCO applications.

However, there are very few papers, published in a last two decades on the use of Cu₂O as a material on a solar cell. Recently, the interest was raising on oxide-based materials in the electronic fields due to some important factors for the general today situation in our planet. These factors are important for the environment. It's nontoxic material, the raw materials to create it are abundant in the earth and the cost for its production is low [9].

It is very important to standardize a material by proper synthesise technique. Even a material gets importance in the field of industrial usage by its cost and the way of production [10].

Cuprous Oxide has very promising characteristics for several applications. Is a p-type semiconductor with photoelectronic properties like the energy band gap of 2.1eV, large optical absorption, optical gap of 2.62eV, and high carrier mobility. Also, this material has other characteristics, which are important for the environment. It's nontoxic material, the raw materials to create it are abundant in the earth and the cost for its production is low [9]. Furthermore, has a cubic crystal structure with lattice parameter of 4.27Å, and the theoretical energy conversion efficiency is about on 20% [11].

2.2. Applications

This material could be involved in some important applications. First, as an active p-type layer in a structure of solar cell. For the fabrication of a heterojunction with the deposition of transparent conducting oxide (TCO) films on Cu₂O substrates, like the Cu₂O/ZnO [9], the Cu₂O/SnO₂ [12], the Cu₂O/SnO₂ and Cu₂O/In₂O₃ [3], or a solar cell structure based on silicon [13].

The Cu₂O with the narrow direct band gap of 2.17eV, and the negative CBM (Conduction Band Minimum) of -1.4V ~ -0.3V vs NHE, has a photogenerated electrons which can easily be captured to achieve photocatalysis. However, there are limits for this application of cuprous oxide, which are the poor stability in aqueous solution under light irradiation, and further the oxidization of material to CuO. Also has low photocatalytic activity. These issues may be solved by modifying the Cu₂O into a heterostructure.

On review of Indrajit V. Bagal et al [6], researchers among others, described the different strategies to reduce the photocorrosion and improve photocurrent density, and the advantages and disadvantages of Cu_2O to use as photocathode for photoelectrochemical solar water splitting. They analyzed the existing issues and described the improvements in this Cu_2O photocathode the last years, for enhanced H_2 production.

Furthermore, the CO_2 reduction is one application of Cu_2O , which is important in view of escalating climate crisis. As we said on Chapter 1, according to NOAA [4], the CO_2 was increased on our planet from 280ppm to more than 400ppm and will increase further to 700ppm, the next century.

The Cu_2O is used as catalyst for CO_2 reduction, because of its many advantages, including the interfacial charge separation and transportation, enhanced surface area, quantum efficiency, and feasibility of modification via composite development or integration of the favorable surface functional groups. CO_2 transformations take place by photochemical and electrochemical phenomena. Sathya M. et al [5], on their review provides an idea of current photochemical and electrochemical CO_2 fixing techniques by using Cu_2O -based materials. Also, one other research team on their investigation is trying to understand the chemical transformations in metal oxides, and the Cu_2O , to achieve sustainable production of solar fuels and chemicals. This will happen by mitigation of degradation mechanisms in Cu_2O photoelectrodes for CO_2 reduction to ethylene [14].

In addition to previous applications, Cu_2O is used from researchers as an archetype for understanding the novel properties of excitons [7]. So, it is important to have thin films of Cu_2O with high purity, and good crystal quality [8].

2.3. Fabrication Methods

There are several examples of Cu_2O -based PV devices reported in the literature using simple low-cost synthesis techniques. The Cu_2O thin films can be prepared by various methods, like the reactive (DC or RF Magnetron) sputtering process [9][10][15][16][17][18][19][20][21][22][23][24][25][26][27][28][29][30], chemical and thermal oxidation [31][10], electrodeposition [10], and sol gel spin coating technique [11]. Here we will discuss analytically the sputtering technique which is used broadly the last years for the synthesis of Cu_2O .

2.3.1. Sputtering Technique

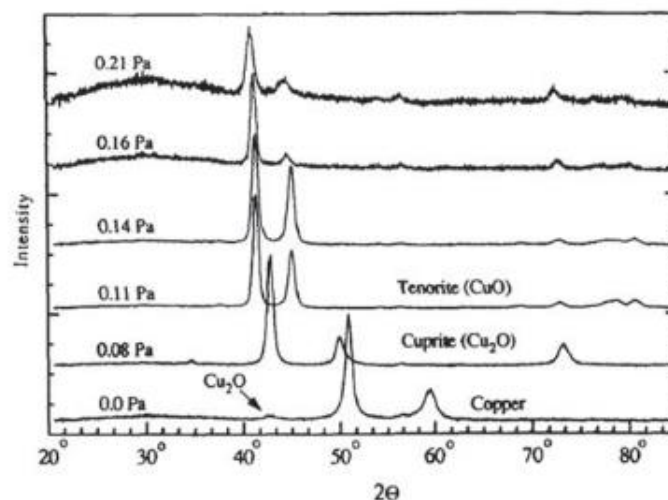
The Sputtering technique is one of the best methods for the preparation of thin films. It provides very good characteristics, like the low cost and easy synthesis. Also, there is high quality uniform film deposition in a large area and controlling of parameters with precision. So, it is useful for material synthesis and much more for the device fabrication.

Some of the sputtering parameters that can be varying are the oxygen partial pressure, gas flow rate, chamber pressure, substrate temperature, sputtering power, and the distance between the target material to the substrate. After the optimization of the conditions, we can produce by the Sputtering method very good thin films [10]. So, for the cuprous oxide (Cu_2O), the Sputtering is useful technique to grow up the material, with high precision by controlling the partial oxygen in the chamber. The most important is to find the phase of copper oxide by the control of Oxygen. There are a lot of publications on this issue.

Parrettam et al. [2] had grown up the Cu_2O on different partial oxygen pressures, on reactive rf magnetron sputtering, with a pure Cu target in an oxygen-argon atmosphere at 300 K. By the results of XRD on figure (2.1) they had showed that the phase of copper oxide films depends on the oxygen partial pressure, because we had a formation of different phases of copper oxides films. Also, they had showed that on higher pressures is more possible the formation of CuO films instead of Cu_2O .

They got single phase Cu_2O film on the optimized oxygen partial pressure (0.08 Pa). It is also reported that the different substrate temperature can influence the phase of Cu during the deposition.

Figure 2.1: XRD graphs of Parrettam et al. [2].



On [18] the researchers reported the effect of oxygen partial pressure on the optical and electrical properties of copper oxide thin film deposited by DC reactive magnetron sputtering technique.

Recently [19], by use of reactive DC Sputtering they succeed single phase of Cu_2O at a relatively low substrate temperature using constant 200 watt DC power with varying oxygen flow rate. By that they observed a variation in band gap values from 1.62 eV to 2.54 eV. The surface sheet resistivity at room temperature was found to vary with the deposition parameters and film thickness.

For Sputtering process, they have used glass substrates, pure solid copper target (99.99%) and two gases, the Oxygen (reactive gas) and the Argon (sputtering gas). In the chamber of Sputtering the vacuum pressure was 5×10^{-6} mbar. The flow rate of Ar was constant at 20 Sccm, and the flow rate of O_2 which was controlled by mass flow controllers and gas regulators interfaced to a computer, started from 2.5 Sccm, and increased to 25 Sccm. They have grown up different copper oxides thin films in each ratio depends on the flow rate of Oxygen. The temperature was kept constant at 325K and time at 15 minutes.

According to the authors, the values of band gap is dependent on the kinetics of the oxide's formation and the kinetics of the formation of oxides of copper during thin film deposition is dependent on following factors:

- The nucleation rates of Cu, Cu_2O and CuO during the growth
- the sticking coefficient/sticking probability of the particles
- re-evaporation and migration by the impinging copper and
- the different growth rates of the nucleated specie.

And all these factors depend on the sputtering power and the oxygen flow rate during the deposition. Also, the effective sticking probability is important to understand which type of oxide is formed, the Cu_2O or the CuO. It's depending on the flux ratio of both of gases. Further, the kinetics of CuO formation is much slower than that of Cu_2O .

On [20] they have grown up the Cu_2O by cryo-pumped vacuum chamber (CVC) magnetron sputtering. Again, the started materials were a solid copper target of (99.99%) and the two gases (Ar & O_2). The Ar was set at 50 Sccm, and the O_2 increase from 4 to 10 Sccm, at different ratios again. Now the power was set from 200 to 800W. Compared to the previous publication, now the time of Sputtering is 30 seconds.

They showed that the power on Sputtering process plays a significant role in the optical transmission as we can see on figure 2.2, and on optical bandgap of the films. They have varied this power from 200W to 800W, and the result was the succeed of rich Cu_2O and CuO TFs. Also, the highest optical transmission was succeeded on the lowest power of 200W. These parameters have significant influence on the properties of thin films and affect the electrical sheet resistance of the prepared films.

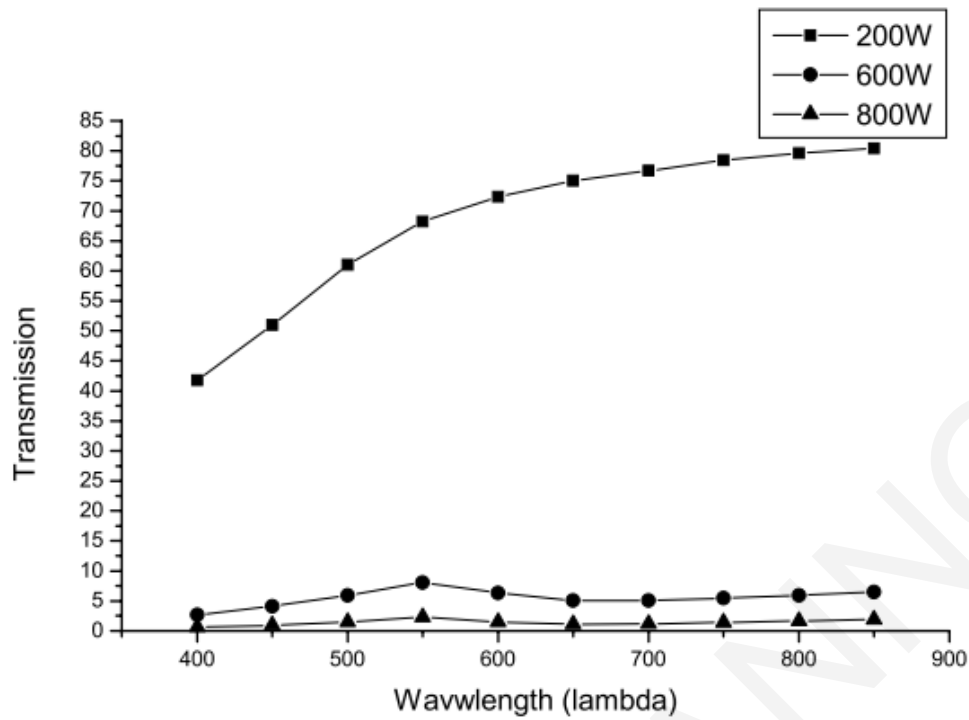


Figure 2.2: Transmission of Copper Oxide TFs on 200, 600, 800W, by 4 Sccm of O₂ [20].

Recently [17], they prepared Cu₂O TFs, by reactive sputtering in a mixture gas of Ar and O₂, on transparent conducting oxide (TCO) on a glass substrate with TCO composed of double layers of SnO₂:Sb (ATO) and ITO. The thicknesses of TFs were varied from 2 to 5 μm. The quality of these layers on TCO substrate was high, by using this technique and precise O₂ flow control. By their measurements on XRD, the highest transmittance was obtained at the lowest impurity ratio of Cu and CuO. This is presented clearly by figure 2.3.

Furthermore, the highest efficiency of 8.4%, was succeeded again on the lowest impurity ratio. This efficiency is the highest that was succeeded for this thin film material for solar cells. Also, according to device simulation analysis, a higher efficiency (over 10%) of Cu₂O TFs, can be obtained by decreasing the surface velocity v_s at p-n interfaces and increasing n-type carrier density n_{GaO} at the n-layer.

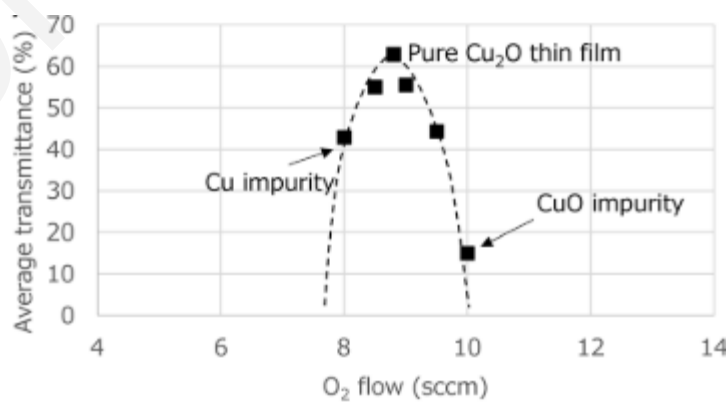


Figure 2.3: O₂ flow dependence of average transmittance of Cu₂O thin films on TCO substrates [17].

The same investigation obtained high crystallinity on almost single component Cu_2O thin films on the TCO substrate. The figure 2.4 shows the XRD patterns of the samples with this crystallinity. On these patterns there are small peaks from impurities from CuO and Cu that are marked by asterisks on the figure.

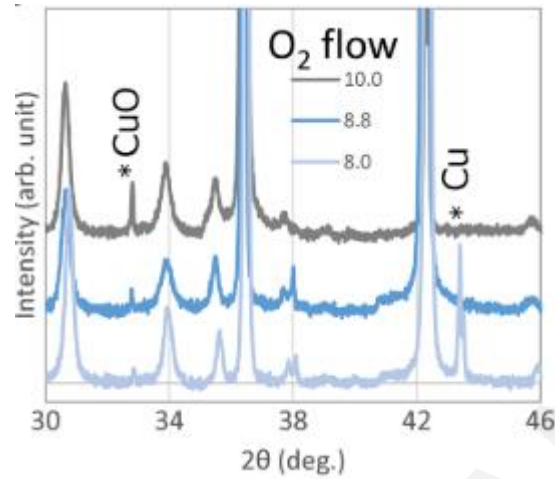


Figure 2.4: Magnified view of x-ray diffraction patterns of Cu_2O thin films on the TCO substrate. Small impurity peaks are marked by asterisks [17].

Other researchers have grown up the Cu_2O thin film by doping of nitrogen in the material [16]. They have incorporated the basic gases (Ar & O_2) with N_2 . They keep constant the total gas flow on 50 Sccm, the flow of O_2 at 7.5 Sccm, and the varied the Ar/N_2 ratio as following:

$\text{N}_2/\text{Ar}/\text{O}_2$ (sccm)
0/42.5/7.5
1/41.5/7.5
2/40.5/7.5
3/39.5/7.5
5/37.5/7.5
10/32.5/7.5
15/27.5/7.5

Table 2.1: $\text{N}:\text{Cu}_2\text{O}$ thin film sample gas flows used during the sputter deposition process [16].

Also, there are some differences on this deposition by reactive DC Magnetron Sputtering. The first one is the substrate temperature at 400°C instead of room temperature, the rotation of sample stage at a constant speed of 12 rotations per minute, and the reduced compared to previous papers, deposition power at 100W.

In general, the doping of Cu_2O by Nitrogen does not affect the structural and optical properties of the material. However, as they have shown, the electrical properties can be modified by nitrogen doping. These include the decrease of resistivity and decrease of hole mobility with increase of doping level of Nitrogen. For example, this type of thin film can be incorporated at the back side of the Cu_2O absorber layer in a $\text{ZnO}/\text{Cu}_2\text{O}$

heterojunction solar cell to reduce the charge carrier recombination at the rear surface and to form a low resistivity ohmic contact at the rear interface.

S. Ghosh et al [15], did the deposition of copper oxides films by sputtering, and the varied the substrate temperature. They did three runs on 30°C, 150°C and 300°C. They have succeeded at 30°C (figure 2.5) and 150°C (figure 2.6) the formation of Cu₂O, and at 300°C (figure 2.7) the CuO.

First, the increase of temperature from 30°C to 150°C, make the XRD peak [1 1 1] of Cu₂O, stronger with higher intensity, so the crystallinity is better.

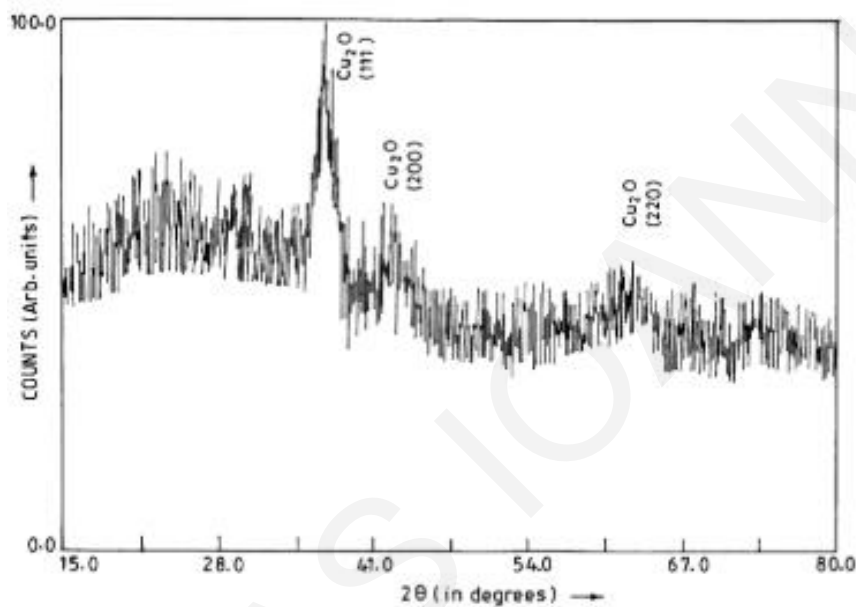


Figure 2.5: XRD pattern of Cu₂O with substrate at 30°C [15].

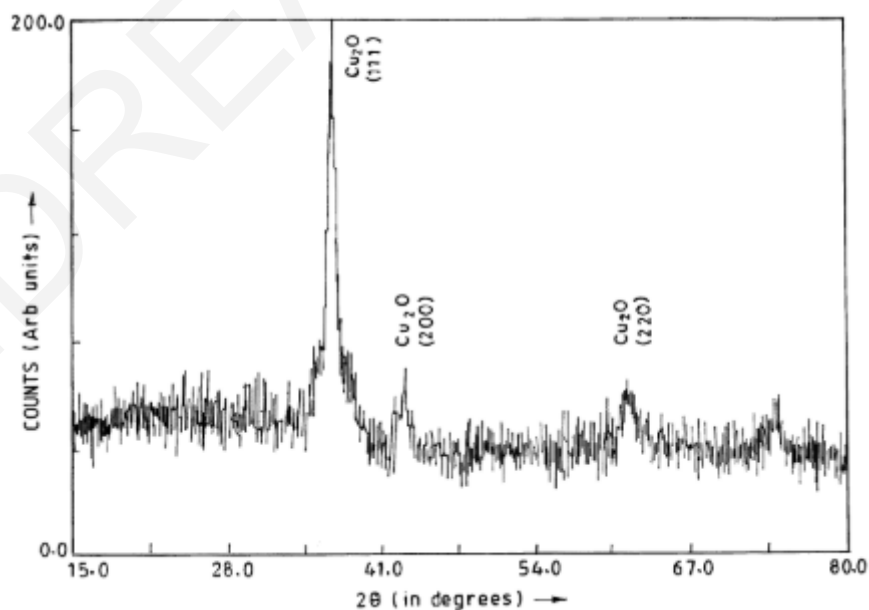
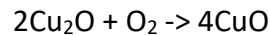


Figure 2.6: XRD pattern of Cu₂O with substrate at 150°C [15].

Secondly, the increase of temperature from 150°C to 300°C, leads to the formation of CuO. This is described by the following reaction:



Initially, at low temperatures the formation of Cu₂O take place. According to this investigation, after the 200°C the Cu₂O starts to react with O₂, with result the formation of CuO, as we can see below at figure 8, with the [-1 1 1] and [2 0 0] XRD peaks.

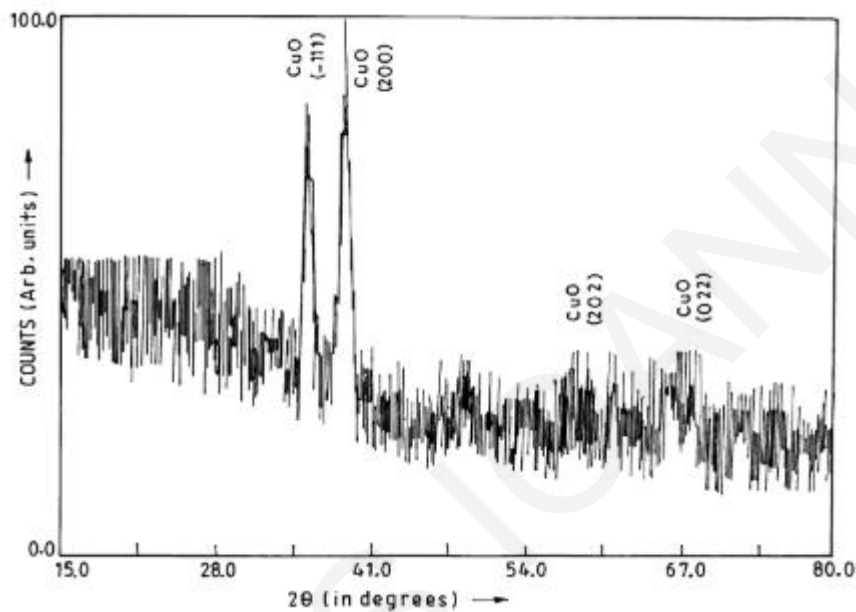


Figure 2.7: XRD pattern of Cu₂O with substrate at 300°C [15].

2.3.2. Annealing process of samples – Hydrogen Treatment

Furthermore, the Sputtering technique is combined in a lot of situations with a second technique for the growth of Cu₂O. This technique is used for an annealing step to the prepared samples, with purpose the increase of temperature. As we know from the previous paper [15], with increase of temperature, the crystallization of the material increased.

With similar parameters on Sputtering with previous references, Raj Kumar et. al [13], after the deposition on Sputtering with temperature on 400°C, they did annealing process on the samples in higher temperature. The temperature was set at 900°C for rapid thermal annealing, in an Annealsys Micro rapid thermal annealing (RTA) furnace, for 3 minutes, to improve the structural, optical, and electrical properties. After that, a hydrogen implantation step was done on the Cu₂O TFs by a NEC Tandem accelerator at room temperature, with the implantation energy on 36keV. This was done to passivate the acceptor/defects levels in Cu₂O material. Following that, a second annealing step, at different temperatures in a range from 100°C to 600°C, at Ar atmosphere.

The results after the annealing process shown higher crystallinity compared to as-deposited film with showing preferential orientation growth, but the hydrogen implantation does not affect the Cu₂O TFs. Furthermore, the [9] did an annealing step by RTA (Rapid Thermal Annealing) for 30s in an Ar atmosphere at various temperatures up to 600°C.

Also, on passivation of defects of Cu₂O TFs, has worked one more research team [21]. The worked-on passivation by the hydrogen or the cyanide treatment. Again, they grow up the material by the sputtering technique, with substrate temperature on 400°C. The difference here is that they have used Oxygen and Nitrogen with Argon. The flow rate of oxygen was fixed at 200 ml/min, and the flow rate of nitrogen was varied from 0 to 20 ml/min. The nitrogen gives a p-dopant phase on a single phase of Cu₂O. The hydrogen treatment was done by exposing the films to hydrogen plasma generated from the gas mixture of Ar and H₂. The cyanide treatment was done by the immersing of films in a solution containing cyanide.

The results from this experiment are the following. The Cu₂O TFs which prepared are polycrystalline with the typical grain size of 0.2-0.4µm. According to the authors, for that reason is expected from the material to have many dangling bonds, which may act as non-radiative recombination centers or carrier traps, on the surface of polycrystalline grains. On figure 2.8, we can see the results of a PL spectra of Cu₂O TFs before and after hydrogen or cyanide treatment. Before, there is not luminescence peak on as deposited film. After the hydrogen and cyanide treatment, is observed an emission of Cu₂O at around 680nm, which was assigned as a nitrogen acceptor-related luminescence. By this we the result, that the H (hydrogen) and CN (cyanide) passivate the non-radiative recombination centers on and in polycrystalline grains. So, the treatment is important because we have improved optical and electrical properties of the material due to better configuration of film.

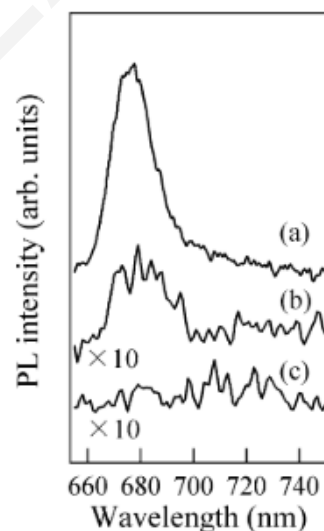


Figure 2.8: PL spectra of nitrogen doped Cu₂O thin films measured at 77K after: (a) hydrogen treatment, (b) cyanide treatment, and (c) before treatment [21].

The following research [22] is like the previous. They researchers did a similar experiment, with hydrogen treatment of samples. In figure 2.9 are the results from electrical measurements, before and after this treatment. We observed a significant improvement in electrical properties of the material for the same reason as the previous research, for the passivation of defects by hydrogen. Hydrogen can indeed be beneficial in optimizing the properties of such thin films for use as active material in solar cells and may offer new pathways for raising the cell efficiencies of solar cells based on such films. Also, K. Hering et al [23], have used the Hydrogen in the Sputtering process. By this it is not necessary a post-growth treatment on the film, so in this way they have avoid an additional process step, fact that is important because is contributed to cost effectiveness in device fabrication.

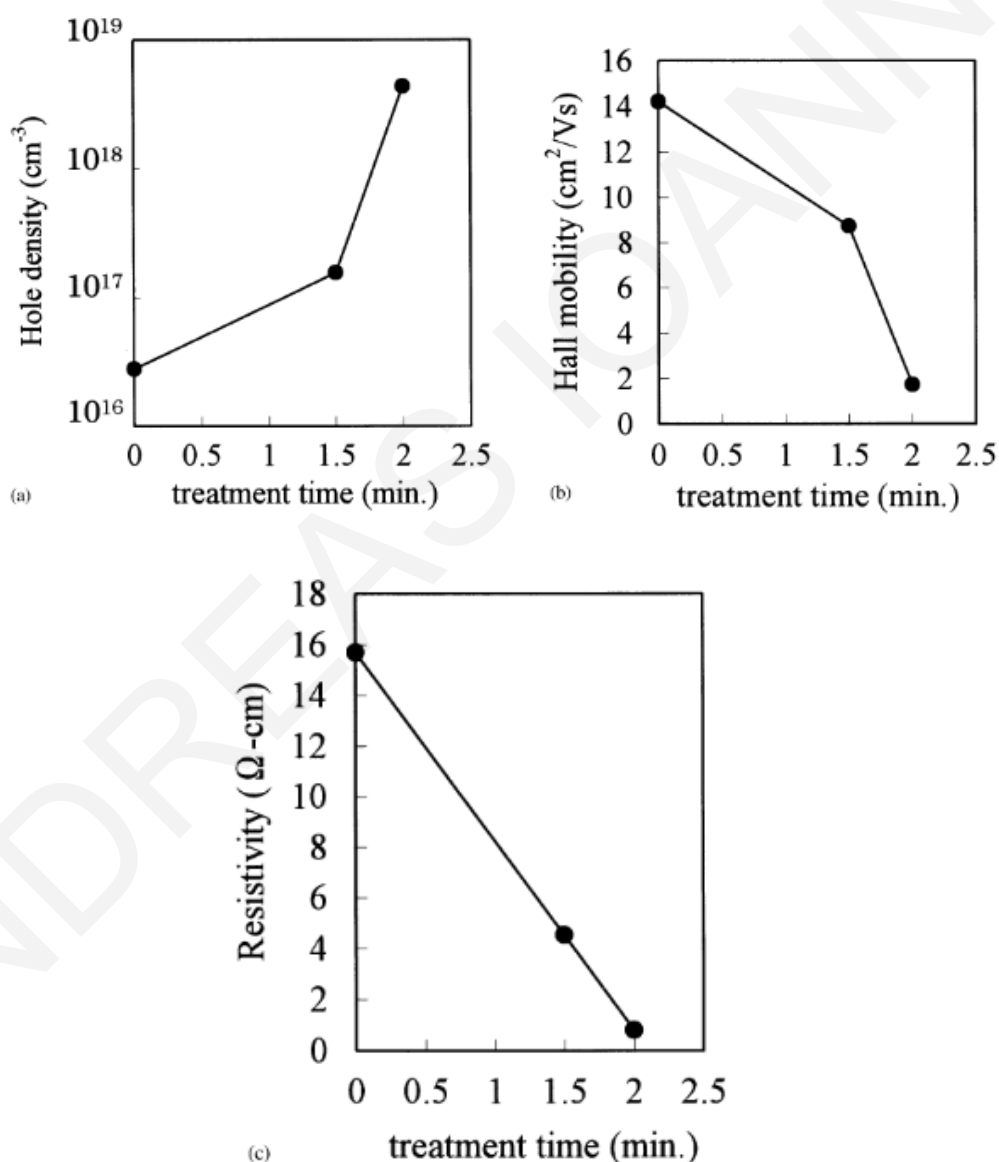


Figure 2.9: Variations of hole density (a), Hall mobility (b) and resistivity (c) with hydrogen treatment time for nitrogen doped Cu₂O [22].

Other projects [24] used copper sheet to form Cu_2O by oxidation at 700°C for 1 hour, and after that they have worked on magnetron sputtering. On the following investigation [28], they have synthesized Cu_2O TFs from CuO . First, they synthesized CuO TFs by using the magnetron sputtering technique at room temperature. After that they did a vacuum annealing on CuO samples using these parameters, 5×10^{-6} mbar at 430°C for 1 hour, with result the Cu_2O thin film.

The Cu_2O films have enhanced crystallinity and larger grains. This was observed by XRD measurements on figure 2.10. We can observe first, the change of material from CuO (red line) to Cu_2O (green line) according to the shift of peaks to theoretical peaks of material. Secondly, the intensity of peaks is higher after the vacuum annealing and formation of Cu_2O , thus, enhancement crystallinity.

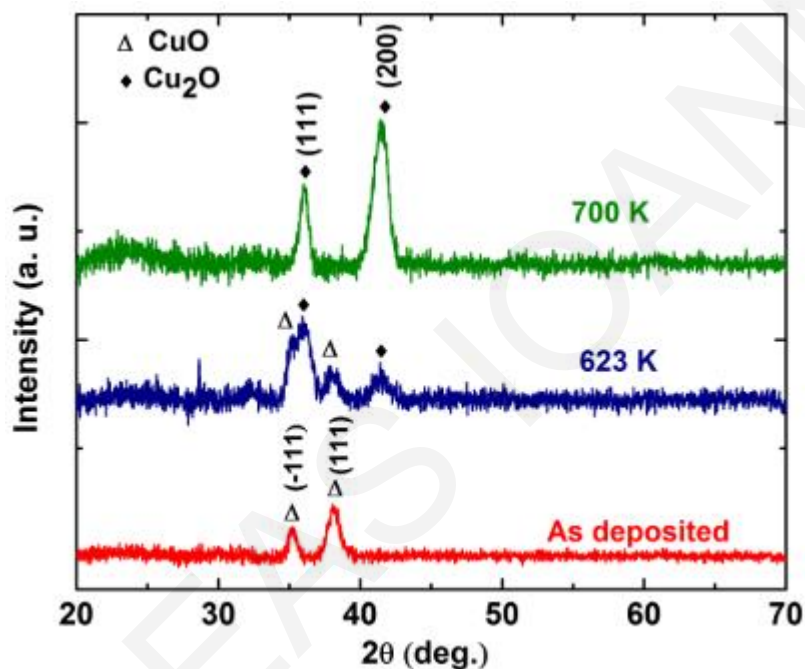


Figure 2.10: XRD of copper oxide thin films: “as deposited”, annealed in vacuum at 623K, and annealed in vacuum at 700K [28].

Using the Debye – Scherrer empirical formula, they calculated the grain sizes of CuO and Cu_2O as 12.8 nm and 58.4 nm respectively. So, we have larger grains on Cu_2O . This was verified by SEM images, figure 2.11, where the Cu_2O image shows us larger grains at size. The above observations confirms that vacuum annealing changes the structure and composition of copper oxide thin films.

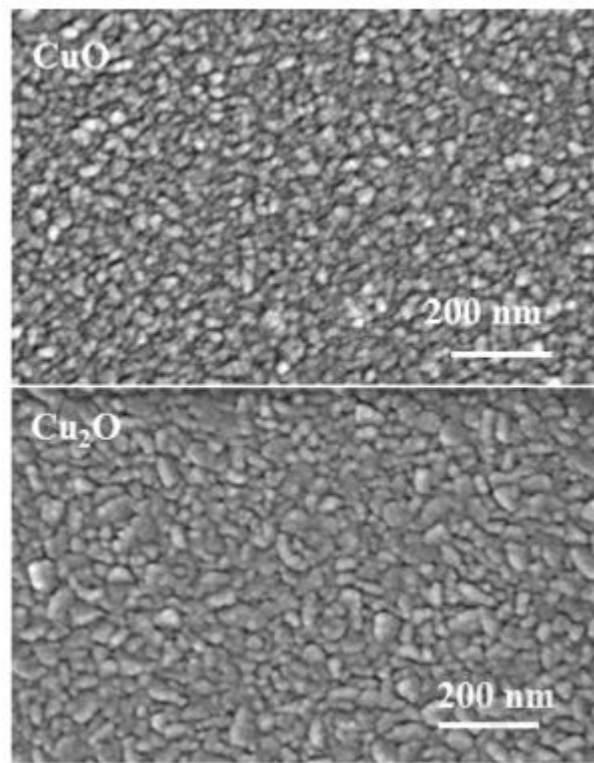


Figure 2.11: SEM images of as deposited CuO and annealed in vacuum at 700K (Cu_2O) [28].

Chapter 3 – Fabrication Methods

On this Chapter will we analyzed the four methods that are used for fabrication of Cu_2O thin film. The first two are the preparation methods, the Sputtering, and Chemical Vapor Deposition (CVD) technique. These methods are responsible for the growth of this material, at its final form. The next two, are the characterization methods, thus, the X-Ray Diffraction (XRD) technique, and the Scanning Electron Microscopy (SEM) technique. These two are responsible for the analysis and identification of the growth material.

3.1. Preparation Methods

3.1.1. Sputtering technique

The first method that is used is the Sputtering. The Sputtering technique is one of the best methods for the preparation of thin films. It provides very good characteristics, like the low cost and easy synthesis. Also, there is high quality uniform film deposition in a large area and controlling of parameters with precision. So, it is useful for material synthesis and much more for the device fabrication. In our case it is important because we have the initial materials in a form that are useful for the Sputtering [10]. For growing of Cu_2O thin film is important because it allows effective control, high deposition rate, low resistivity, and uniform substrate heating during the deposition of the films. The physical properties of the deposited films depend critically on the sputtering parameters such as the oxygen partial pressure, sputtering pressure, substrate temperature, sputtering power, and distance from the target to the substrate. So, the Cu_2O films with electrical resistivities from 10^2 to $10^4 \Omega\text{cm}$, hole mobility of $1\text{-}10\text{cm}^2/\text{V}/\text{s}$ and optical band gap of $2.0\text{-}2.6\text{eV}$, needs precise management of the oxygen partial pressure and sputtering power, so it's important to use the Sputtering technique for the deposition of these thin films [27].

The two main ways of Sputtering are the DC (Direct Current) Sputtering, and the second is the RF (Radio Frequency, 13.56MHz) Sputtering. In RF Sputtering, the physical properties of the deposition film as we said before can be tuned to find the optimum conditions. In our lab we have the DC Sputtering technique as we can see in figure 3.1.



Figure 3.1: DC Sputtering

The specific instrument is too much easy to work on it because it's simple. The process is next. The first thing that we must do is the check of chamber if it is clear. This is necessary because we want to avoid reactions from elements from previous experiments in the same chamber. After the preparation of samples (cutting, cleaning etc.) and at same way, preparation of the target, we must put in the base of the chamber, which is in the middle of the chamber, and the target exactly perpendicular above from the base in his place (figure 3.2).

Furthermore, we must open the flow of gases of our choice. There are several bottles with gases, Ar 100%, Ar:O₂ - 90:10, Ar:O₂ - 75:25, Ar:O₂ - 50:50. Then the Sputtering instrument, and set the parameters that we need for the experiment. The parameters are the following:

- Sputter Current (mA)
- Number of Cycles
- Time of each cycle (seconds)

By setting the Sputter Current, we set the power that we want for the experiment. This parameter is dependent on the material of target. Some materials have low melting point, so they don't need high values of current, for example the lead, because the target will be destroyed. The copper is not in this category because has high melting point, but the high current in cooperation with a certain number of cycles may cause a damage in the copper target. For that reason, it is good to run each cycle separately from the others, to cool down the temperature of the target.

For the deposition of copper on substrates, we use a Sputter Current of 120mA, which is a high value. Also, the number of cycles is on 3 and the time is the maximum that this instrument provides, 4 minutes. After the choose of parameters we start the experiment. One pump that is connected to Sputtering, create a high vacuum in the chamber where the substrates are placed.

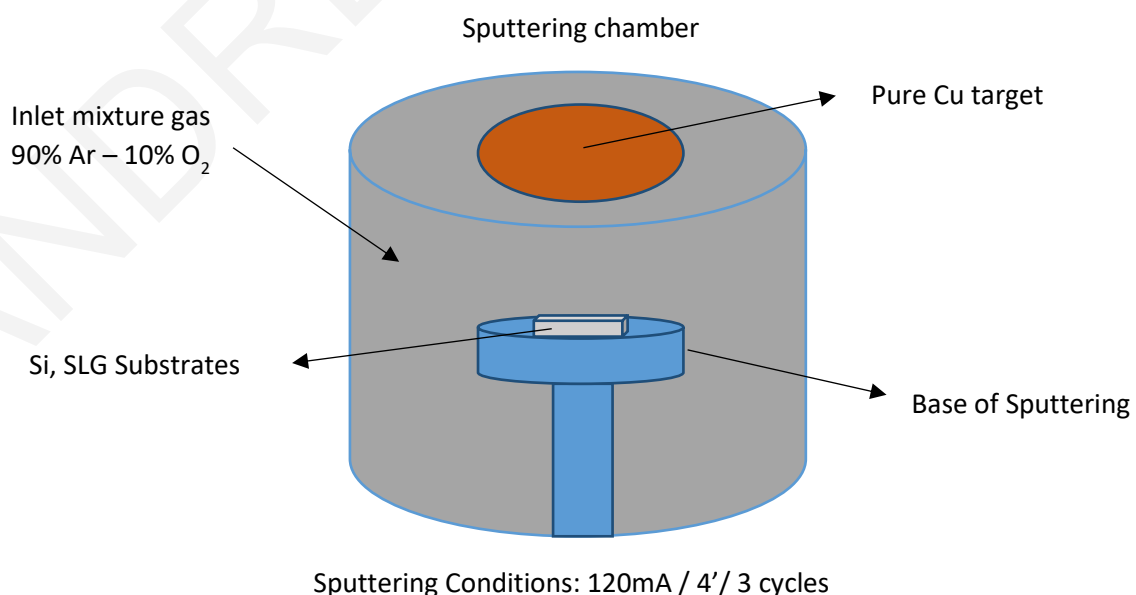


Figure 3.2: Schematic illustration of DC

After the creation of vacuum the experiment is start with the insert of gases in the chamber. For the deposition of the material, is necessary the development of voltage difference between the target and the base. With this difference is created the plasma. The plasma is a gas, which it contains atoms, ions, from the material of the target and from the inlet gases. The high voltage that is created, hit the target as a result the remove of material by this and the deposition on the substrates. The color of plasma is dependent on the inlet gases. For example, if the inlet gas is pure Argon, plasma will has a purple color. Furthermore, the creation of plasma is the evidence of the right operation of the system.

At the end of the run, the vacuum is venting automatically, and the opposite procedure take place to remove the prepared samples and closed the whole system, closing of flow gases, turn off Sputtering instrument.

3.1.2. Chemical Vapor Deposition (CVD) technique

The second technique that is used is the chemical vapor deposition, the CVD. This technique is used to take the advantage of using too much higher temperatures compared to the Sputtering technique, which is operated in room temperature. Specifically, chemical vapor deposition is one technique in which the deposited phase is produced *in situ* by chemical reaction(s). At this reaction a solid material is deposited from gaseous precursors onto a substrate. The substrate is typically heated to promote the deposition reaction and to provide sufficient mobility of the atoms to form the desired structure [32].

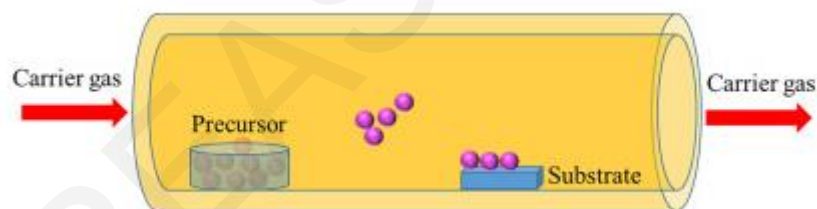


Figure 3.3: Reaction of materials in the chamber by introduced gas and precursor and deposition of the mixture on substrate [32].

On figure 3.3, we can see the reaction in the chamber of CVD. The two reactive materials are the introduced mixture of gases, and the precursor material which is usually a solid material. The increase of temperature leads to the evaporation of the solid material to a gaseous phase and the deposition on the substrate.

The advantage of this technique is several. The high deposition rate is one of the most important, which can be greater than tens of micrometers per hour. Other advantages are the too much high precision, the high purity, the control of stoichiometry, morphology, crystal structure, and orientation, which can be controlled by controlling deposition parameters. In contrast, some of disadvantages are the typical corrosiveness and the toxicity of the process gases.

The CVD technique, due to high range of temperatures (200°C-1600°C) has been used broadly for several purposes. Some of them are the annealing process on prepared samples, the oxidization, the initial deposition on substrates etc [33].

There are several types of the CVD technique. First, is the TACVD, the thermally activated CVD, where the deposition is initiated and maintained by heat. The second is the plasma activated CVD. On this method, photons, electrons, and ions may induce and maintain the reaction of CVD.

Also, we have:

- APCVD: Atmospheric pressure CVD
- LPCVD: Low pressure CVD
- UHVCVD: Ultrahigh vacuum CVD
- AACVD: Aerosol-assisted CVD
- DLICVD: Direct liquid injection CVD
- MPCVD: Microwave plasma-assisted CVD
- RPECVD: Remote plasma-enhanced CVD
- ALCVD: Atomic layer CVD
- HWCVD: Hot wire CVD
- MOCVD: Metal-organic CVD
- HPCVD: Hybrid physical CVD
- RTCVD: Rapid thermal CVD

We used CVD technique for annealing process on our experiments. Annealing is a heat treatment process of materials which is used to increase the ductility and reduce the hardness of a material. This happened because of the reduction of dislocations in the crystal structure of the material being annealed. The three stages of annealing process as the temperature of the material are increased are, recovery, recrystallization, and grain growth.

We want the annealing step on our experiment to increase the crystallization of prepared film (Cu_xO) on previous technique, Sputtering, for the formation of pure Cu_2O thin film. There is control of the experiments by connected software on the instrument. On figure 3.4 is on the left the CVD instrument, and on the right the software.



Figure 3.4: CVD instrument and software

The operation of the system is the following. First, we insert the prepared samples in the tube, we closed the system, switch on the sensor to check if the system it is ready to start. After that, we turn on the flow of necessary gases, and we set the flow of each on software, as we can see on the right picture above. The available gases are the following, Argon (Ar), Oxygen (O₂), Ammonium (NH₃), and Hydrogen (H₂). If we want to apply a vacuum pressure on the tube, we must turn on the pump for this purpose. We start the experiment when the pressure is the appropriate.

On the software we set the steps of the procedure on CVD. First, we have the purge of the chamber, that is the remove of all gaseous species. This lasts 10 minutes. After that we have the increase of temperature on the selected temperature. We set the step of this ramp. This step is 30°C/min and wants around 30 minutes to reach the setting temperature. for example, if we set the temperature on 1060°C, the second step of procedure lasts 35 minutes. At the same time, we have the insert of the gases, in low amounts because we want only the purge of chamber and the increase of temperature. On the third step, we hold the temperature for 10 minutes and we introduced much more higher amounts of gases that we already used, or we introduced the rest of gases that we need for the reaction. Usually, at the next steps we keep stable the temperature, and increase the time for each step. After that, step by step, we removed the gases, and if we want, we introduced other gases. The last step of procedure is the cool down of chamber on room temperature at the same ramp step of 30°C/min.

So, the parameters that we can change are the following:

- Temperature
- Pressure
- Time

On the figure 3.5, we can see the horizontal gas flow in the chamber of the furnace, which it's take place in our experiments.

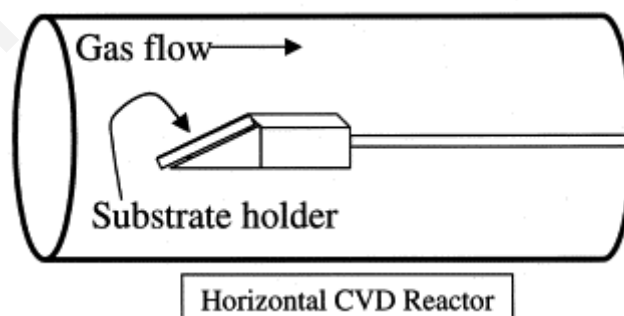


Figure 3.5: Horizontal gas flow in the chamber [33].

3.2. Characterization Methods

After the formation of Cu₂O thin film by Sputtering and CVD techniques, we need the next two characterization methods, to analyze and identify the material.

3.2.1. X – Ray Diffraction (XRD) technique

The first technique is the X-Ray Diffraction, where the basic operation is to identify the crystal structure of the material.

The techniques based on X-rays divided into three categories. The first one is the X-ray fluorescence spectroscopy, which is used for qualitative and quantitative chemical analysis, and the second one is the X-ray radiography which is an imaging technique based on the registration of the intensity passing through an object by using films or detectors. The third category includes the methods where X-rays diffracted by the crystals in that way on which we can distinguish the crystalline phases of material.

It's important to identify the crystal structure to know what material is, by the different data from an XRD graph. The peak position needs to investigate the lattice parameters, space groups, chemical composition, macrostresses, or qualitative phases analysis. The peak intensity gives information about crystal structure, thus atomic positions, temperature factor, occupancy, texture, and quantitative phase analysis. Also, the peak shape gives information about sample broadening contributions, thus microstrains and crystallite size [34].

For our experiments we used the X-ray Diffraction where the X-rays diffracted by crystalline materials. The principle of this method is based on the diffraction of X-rays by periodic planes and the angle of the diffracted signal. This phenomenon is described by the Bragg's law:

$$n\lambda = 2d_{hkl} \sin(\theta)$$

On this equation, the n is the order of diffraction, λ the wavelength of the incident beam in nm, d_{hkl} the lattice spacing in nm and θ the angle of the diffracted beam in degree [34]. On figure 3.6 is the schematic illustration of the incident and diffracted beam of X-rays on a crystalline material.

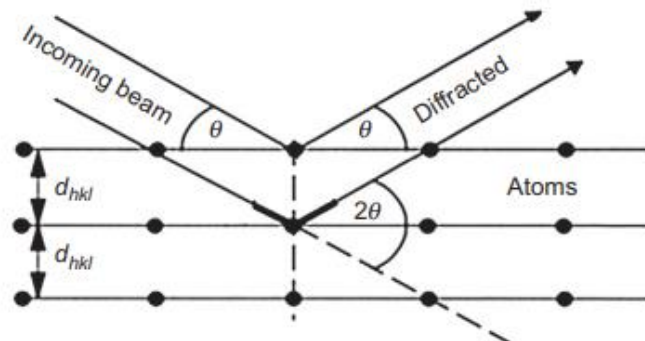


Figure 3.6: Geometrical condition for diffraction from lattice planes [35].

The procedure for the XRD characterization of the materials is the next. First, we insert the prepared sample on a base in the chamber of Miniflex Rigaku XRD instrument (figure 3.7). After that we turn on the cooler of XRD to reduce the temperature at 19-20°C. When this will succeed, we turn on the XRD, the software on P.C. and we set the parameters we want for the measurements. The parameters are the degrees of angle that will be scanned, the time, and the size of our sample. Finally, we turn on the X-rays to start the procedure.

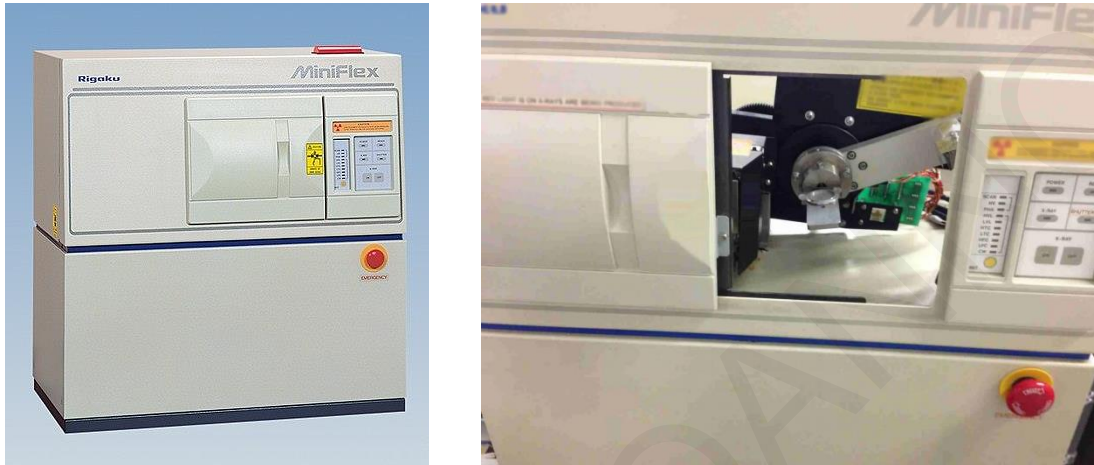


Figure 3.7: Hardware - Miniflex Rigaku

At the end of the measurement, the executed data will be analyzed in the software of Origin. The executed graph has at y-axis the intensity of the peaks of the material, and at x-axis is the angle of diffracted beam at material, which is 2θ . To analyze the results, we compared them with the corresponding theoretical diffraction patterns that we expect to be closed to our results. We compared the peaks of patterns. If the peaks are the same, we succeed the material that we want. If are not the same, probably we are closed to theoretical peaks, and we must change (increase/decrease/remove) parameters to succeed the material.

The XRD can be used to determine the crystallinity by comparing the integrated intensity of the background pattern to that of the sharp peaks. The crystalline patterns consisting well-defined, narrow, sharp, and significant peaks, the amorphous do not give clear peaks and have noise signals, and the semicrystalline patterns have a form of halo pattern. At figure 3.8 and 3.9, we can see the patterns with their differences [36].

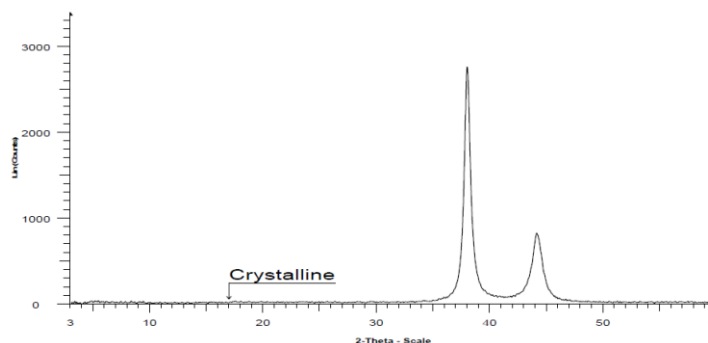


Figure 3.8: Crystalline XRD pattern [36].

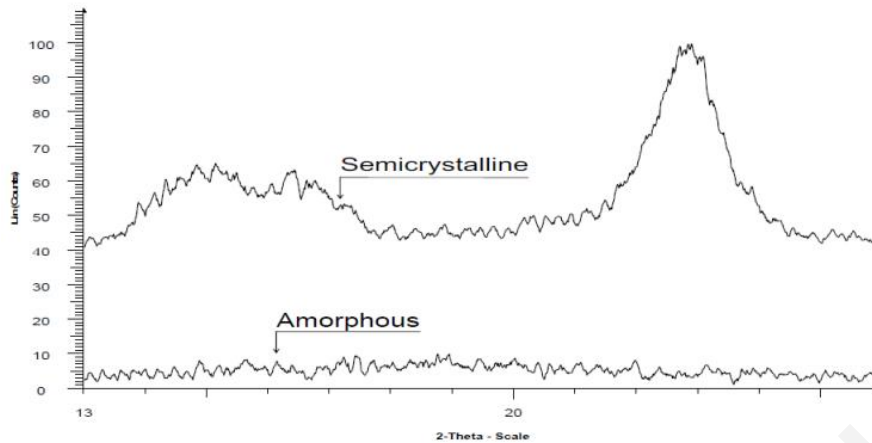


Figure 3.9: Semicrystalline and Amorphous XRD patterns [36].

For example, our material, the Cu_2O has three main theoretical high intensity peaks. These peaks are very closed to CuO peaks, and we must distinguish which material is between the two. Sometimes we have both on our sample. The best result is to have pure Cu_2O with high intensity on the peaks on a crystalline pattern.

3.2.2. Scanning Electron Microscopy (SEM) technique

The second characterization technique that we used is the Scanning Electron Microscopy, SEM. This microscope is used for imaging at micro- and nanoscale on samples at these dimensions, like our samples. Gives the opportunity of high-resolution images compared to simpler techniques like the optical microscopy. The magnifications are up to 100000x, while in optical microscopy is on 1000-2000x.

Also, the great depth of field at very low and high magnifications on producing images is an important advantage. This is happened with use of Secondary Electron Detector, which is one of the two detectors that are used on this microscope. The second one is the Backscattering Electron Detector where we can get useful information on chemical identity. At figure 3.10, is the configuration of a SEM microscope.

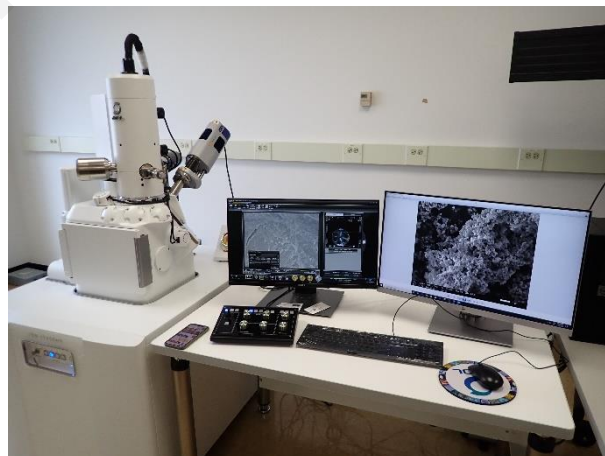


Figure 3.10: Scanning Electron Microscope configuration.

The principle of SEM microscope is the next: this microscope utilizes a focused beam of high energy electrons to generate a variety of signals (figure 3.11) at the surface of solid specimens [37]. After that the electron signal is converted to an electronic signal which is portrayed on a cathode ray tube.

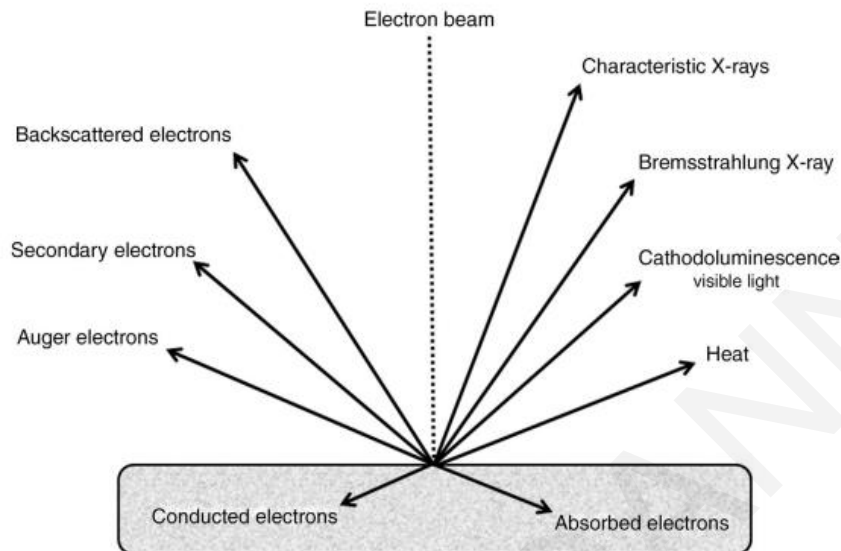


Figure 3.11: Schematic illustration of signals in SEM [37].

So, the secondary electrons are used from SE Detector for topographical information, the backscattered electrons are used from BSE Detector for atomic number and topographical information, and the Auger electrons are responsible for compositional information, thus the element analysis of a sample. The last operation is done by EDS (Electron Dispersive Microscopy), the technique that is on the same system with SEM, with only difference the operation of the procedure on different software.

The procedure on SEM needs a careful sample preparation. The samples that are getting in SEM, must be small. It depends on the microscope, how many positions offers, and how many samples we want to input for our purpose. The form of samples is mainly solid, and it is necessary for that to be conductive, for the reaction of them with the electrons. If are not conductive, needs a thin layer of a conductive material on their surface, to be conductive. This can happen by a deposition in the Sputtering.

The operation of SEM microscope starts with a venting of chamber, because is in vacuum when is off. So, after the turn on of computer software and SEM, we vent the chamber. For that is necessary to open the gas (N_2) to break the vacuum. After the venting of chamber, we must put the samples in the base of microscope (figure 3.12), and then we pump the chamber to create the vacuum again. We wait for the pressure to reduce to 9×10^{-3} mbar, to start taking images. We must set the High Voltage from 10KV to 30KV, turn on the heat and the HV (High Voltage) and the system is ready to take images.



Figure 3.12: Base of SEM – Placement of samples on the base

The process of imaging is shown at figure 3.13. At the left of figure is what we can see from the microscope, at right is the camera where we can see the base from inside of chamber, and all the parameters that we can change to take the best image. The important parameters are below:

- The speed that the sample is scanned: for the best image the speed must increase above the 7, which is a very low speed.
- The necessary magnification
- The WD (working distance), which is the depth on the surface of sample that we can get in and take better and cleaner image.
- The PC (Probe Current): how many current (electrons) we send to samples to absorb.
- The Signal (Gain/Black): the change in black and white color, that means how black or white is the image.



Figure 3.13: Imaging process

To take images from the BSE detector, it is necessary to change the choice on the parameters, from SE to BSE. The BSE detector is getting above the samples manually from the outside.

To have clear images to have detailed information about the surface regions of sample, it is necessary to reduce the speed of scanning at 7-8 and increase accordingly the magnification on 13-14kx. We used mainly the SE Detector, because we want information from sample surface. The secondary electrons are coming from the inelastic interactions between the primary electron beam and the sample and have lower energy than the backscattered electrons. So, are useful for the topographic characteristics of the sample surface.

For our experiments on Cu_2O , we want to have images from samples, to see how the configuration on the surface is. We want a smooth, stable, and periodic surface with the same patterns. These characteristics leads to a crystalline structure of the material, and to a stable material, which is important to use the specific material in a structure synthesis with other materials. On figure 3.14 we can see examples of images from samples of Cu_2O , which are promising results for next experiments.

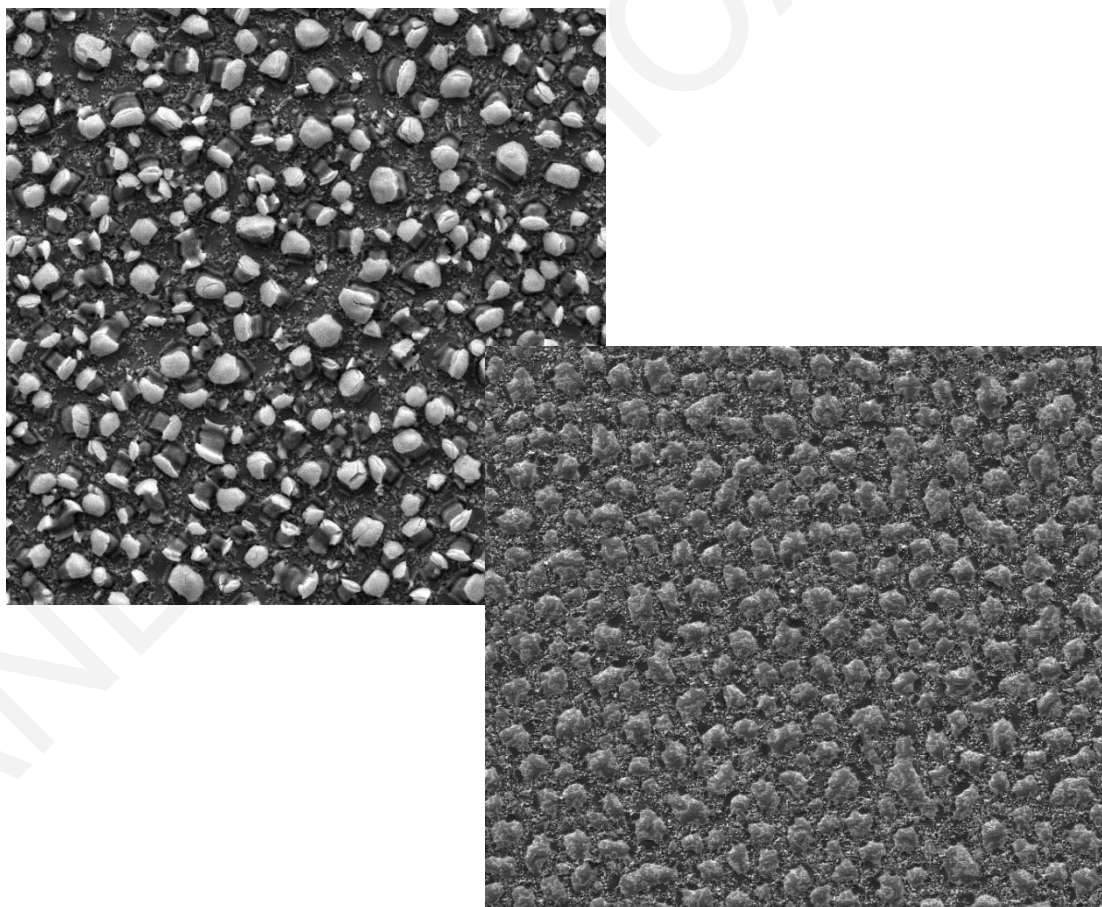


Figure 3.14: Imaging examples of Cu_2O on 1kx and 500x

Chapter 4 - Growth of Cu₂O

4.1. Introduction

At this chapter we described the whole procedure which was done for the growth of Cuprous Oxide (Cu₂O). The techniques were used for the growth of Cu₂O thin films are the Reactive Sputtering following by Chemical Vapor Deposition (CVD). The characterization was done by X-Ray Diffractometer (XRD), and finally the analysis of the XRD results was done by the Origin software. The purpose of these experiments is to export the optimum conditions for the Reactive Sputtering and CVD, thus creating a pure Cu₂O. We divide the experiments on four main parts. The first one is the optimization of Reactive Sputtering Conditions, the second is the simple use of CVD, the third is use of vacuum pressure on process of CVD, and the last one is the introduction of Hydrogen on process of CVD. After the optimization of conditions, we are talking about the preparation of samples for measurements at Raman Spectroscopy, SEM characterization and Ultrafast Pump Probe Spectroscopy, as well the results from these measurements.

4.2. Reactive Sputtering Conditions

The first part of Cu₂O thin films' growth has the deposition of one thin amorphous layer on a substrate by Reactive Sputtering (figure 4.1). This layer must be a form of Cu₂O thus become a pure Cu₂O, after crystallization by thermal annealing. For observation of layer after Sputtering we need the XRD characterization. If the results are good, we must proceed furthermore by thermal annealing. So, the first step is to optimize the conditions of Reactive Sputtering.

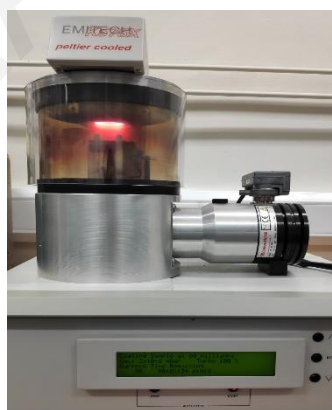


Figure 4.1: Reactive Sputtering

4.2.1. Initial Materials for Reactive Sputtering

The initial materials must be the pure Copper (Cu) which is the solid target (figure 4.2), and the Oxygen (O₂) which is the inlet gas in the chamber, to have a reaction between them and the deposition of the Cu_xO amorphous layer on a substrate. Substrates (figure 4.3) are crystalline n-type Silicon (Si) and amorphous soda-lime glass (SLG).

First, we clean the pure target of Cu by Isopropanol (IPA) and substrates by the TMA (trichloroethylene, methanol, and acetone), IPA, and DI Water (Deionized Water), and we dried all of them by nitrogen gas.



Figure 4.2: Cu target

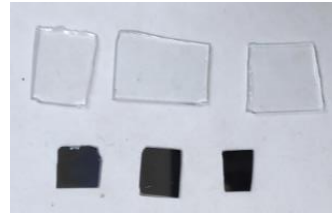


Figure 4.3: Si & SLG substrates

4.2.2. Initial Conditions for Reactive Sputtering

By these materials may grow up several combinations of thin films. The most possible combinations are the Cuprous oxide (Cu_2O) and the Copper Oxide (CuO). For that reason, it is necessary to define the optimum conditions for the growth of Cu_2O , which is the desirable material.

Compared to CuO , the Cu_2O needs less O_2 to form, so less oxygen in Sputtering, more possibilities to have Cu_2O thin films. The oxygen is getting in the chamber in a mixture with Argon (Ar). The Argon is noble gas, so it is not get involved in the procedure, only controlled the quantity of O_2 . So, the first condition is the quantity of O_2 in the inlet mixture gas. Initially, we did the experiment with a ratio of 90%Ar – 10% O_2 .

The second parameter is the Sputter Current. The variation is from 60mA to 120mA. With low current (60mA) we have low deposition of Cu_2O , and with high current (120mA) we have higher deposition. This highest value was chosen because in higher values than this, may the target become to failure. The two last parameters are the number of cycles of each run, and the time of each cycle.

So, in the first experiment we did three different runs. We keep the minimum time, that means, 4 minutes and 1 cycle, and the sputter current it was 60, 80, and 120mA, respectively. After the deposition, all films had low deposited material. We need more, because in the next step of experiment we want the crystallization of film by thermal annealing.

4.2.3. Optimum Conditions for Reactive Sputtering

After the last observation, the parameters were change to maximum. The sputter current and the time of each cycle are kept constant, at 120mA and 4 minutes, respectively. The number of cycles change to 3 cycles for each deposition. By this, we have a very good, deposited material, appropriate for thermal annealing. This was verified by XRD measurements, where the results have peaks very closed to the desired material, the Cu_2O .

So, the optimum conditions for Reactive Sputtering are the 90%Ar – 10% O_2 as inlet mixture gas, sputter current at 120mA, 4 minutes per cycle, and 3 cycles of deposition.

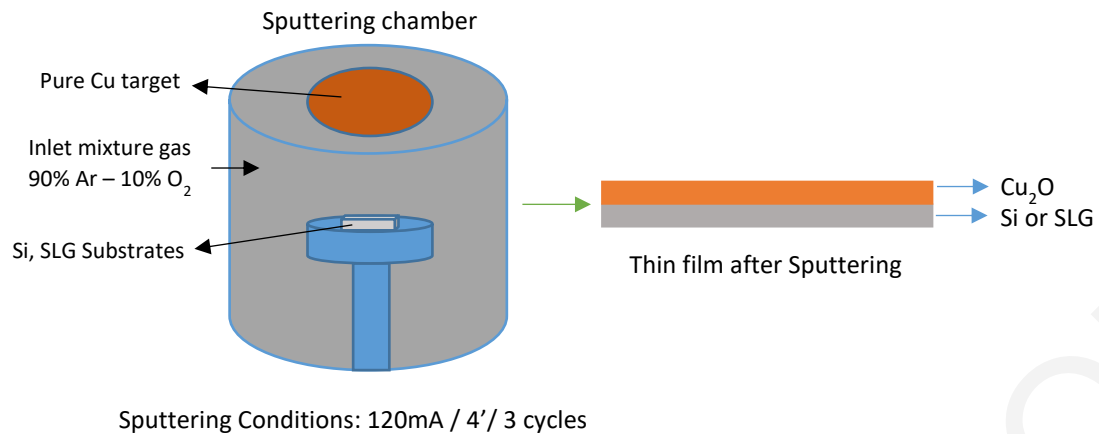


Figure 4.4: Optimum Conditions on Reactive Sputtering

4.3. Experiment 1 - Use of Optimum Reactive Sputtering Conditions with simple use of Chemical Vapor Deposition technique (CVD)

After the optimization of R.S. Conditions, we have the first complete experiment. The combination of two processes, deposition of material by Reactive Sputtering following by Chemical Vapor Deposition. By using the CVD process, we can increase the temperature, as a result the thermal annealing of film, and the enhance of crystallization on Cu_2O . After the growth of thin films, we must characterize them, by X-Ray Diffractometer (XRD), for observation of results.

4.3.1. Experimental process

Initially, we prepared samples on Si and SLG by Sputtering. The conditions are 90%Ar – 10% O_2 as inlet mixture gas, sputter current at 120mA, 4 minutes per cycle, and 3 cycles of deposition. All information about the Sputtering deposition is in Table 4.1 at Supplement.

4.3.2. Initial Conditions for CVD

The prepared samples now will get in the furnace of CVD for thermal annealing (figure 4.5). The conditions must be simple, to observed how effect the samples. At the first runs we keep constant the time and pressure and inlet gas, but we change the temperature.

The time it is on 60 minutes, the pressure on 1Bar, and the inlet gas is the noble gas Argon (Ar). This was happened because we want the succeed of thermal annealing only, without any reaction of sample and gas.



Figure 4.5: CVD Furnace

The only varied parameter is the temperature, which is varied from 300°C to 600°C. So, we did four runs in the CVD furnace, at 300°C, 400°C, 500°C, and 600°C. All information about the CVD process of experiment 1 is in Table 4.2.

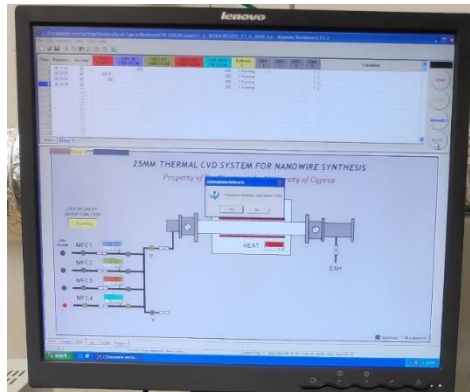


Figure 4.6: Software for CVD

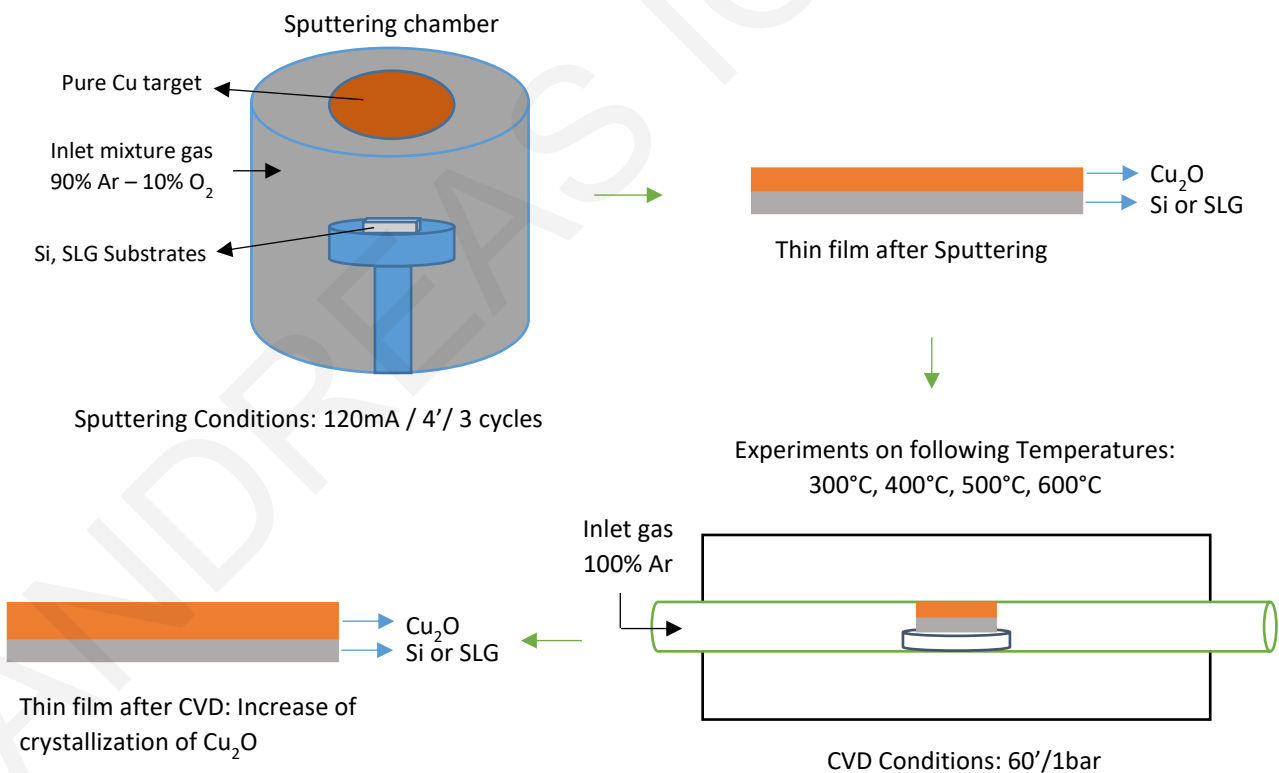


Figure 4.7: Schematic Illustration of Experiment 1

4.3.3. XRD Characterization & Results

The final material needed to characterize to understand exactly what material is. The method of XRD is used for this purpose by the export of the crystallographic structure. The two possible materials that may grow up by the previous techniques, are the copper oxide (CuO) and the cuprous oxide (Cu₂O). So, by the crystallographic structure we understand what material is, according to the peaks on XRD graphs.

At the next figures there are the crystallographic structures of materials at each temperature, from 300°C to 600°C. At the figure 4.8 the growth materials have Si substrate and at the figure 4.9 is on SLG substrates.

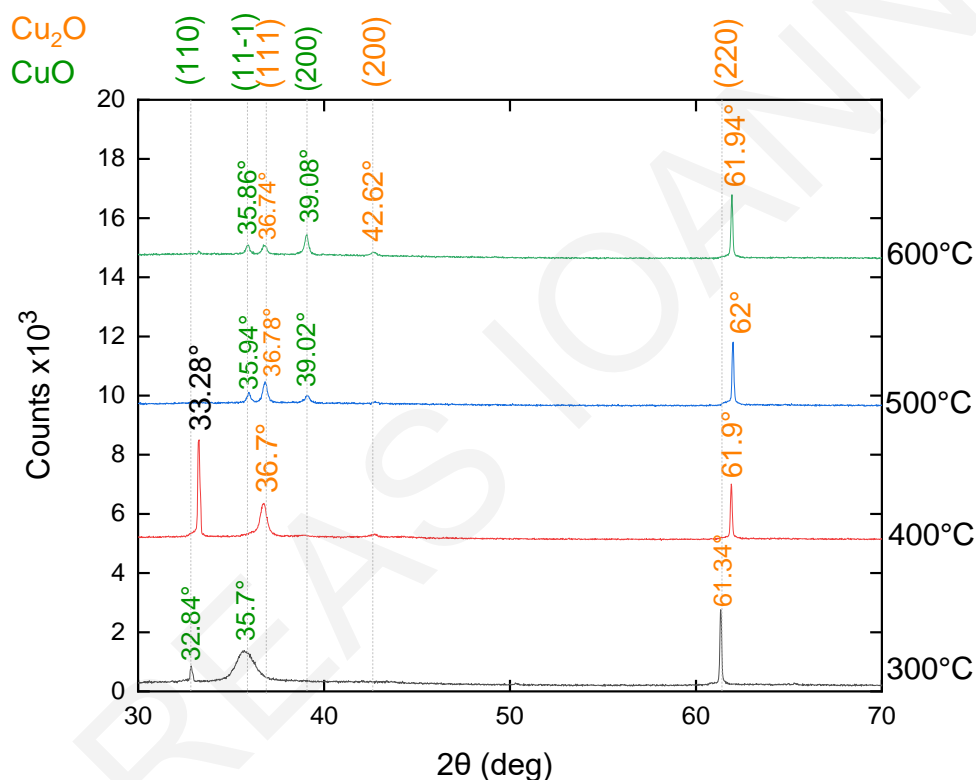


Figure 4.8: Si/Cu₂O TFs, Constant Ar:O₂ - 90:10, Thermal Annealing at 1bar, Increase of Temperature from 300°C to 600°C

Firstly, we can say that in both of substrates we can observed peaks of the desirable material Cu₂O but also, we have peaks of CuO, and some peaks from other materials, for example the peak at 33.28° on 400°C, at figure 4.8. For the comparison of two substrates, we can say that the use of Si substrate gives us better uniform deposition of material compared to SLG substrate, and higher intensity peaks of material.

The important result from graphs, especially from figure 4.8 is that the peaks are closed to the high intensity peaks of Cu₂O, at 36,41°, 42,29°, 61,34°. Furthermore, at figure 4.8 the peak of Cu₂O at 61-62° is constantly high at all temperatures.

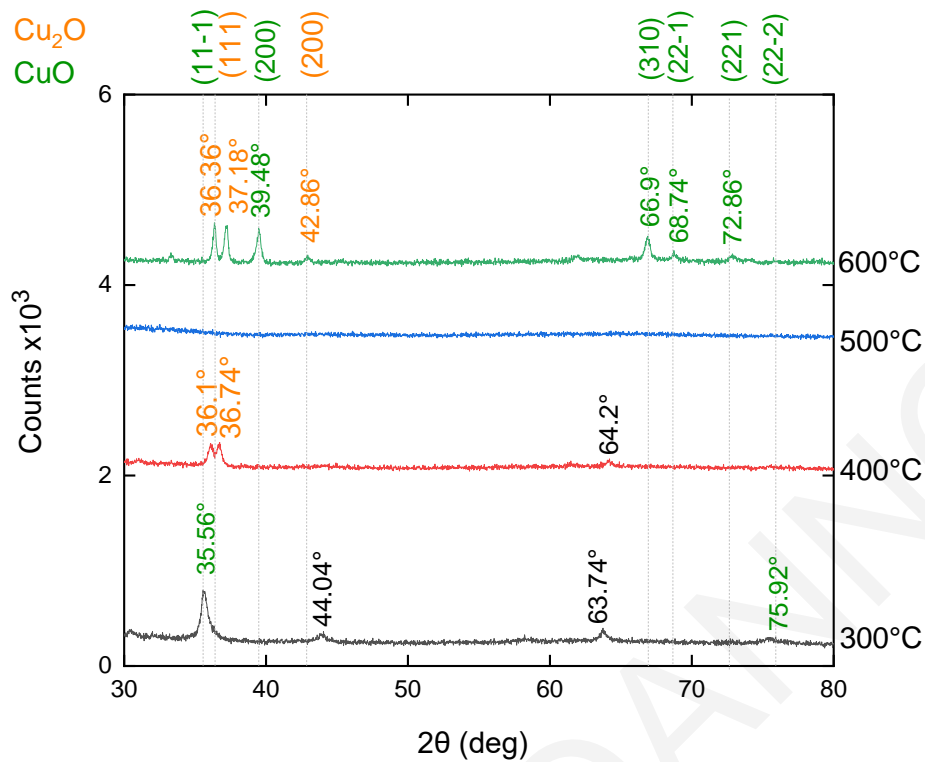


Figure 4.9: SLG/Cu₂O TFs, Constant Ar:O₂ - 90:10, Thermal Annealing at 1bar, Increase of Temperature from 300°C to 600°C

Generally, we can't decide now which temperature is the best to proceed on this experiment. The only important result from figure 4.9 is that at 600°C, we have growth of CuO much more than Cu₂O. So, we can avoid this temperature in the next experiments. Also, the growth material is not a pure Cu₂O, which is the purpose of these experiments, but the results in a first phase are promising to have pure Cu₂O, because we can distinguish the peaks of material.

We can change several parameters to have better results, such as the pressure and the inlet gases at CVD furnace, and at the chamber of Sputtering the inlet mixture gas. We need to change the parameters to have more comparisons between the results. We have already some good parameters, which may be the optimum for the experiments, such as the percentage of Oxygen (10%) in the inlet mixture gas of Sputtering.

4.4. Experiment 2 - Use of Vacuum Pressure in CVD Furnace for Thermal Annealing – Change of O₂ percent in Reactive Sputtering

At the next step of experiment, we change two parameters. The first one is the pressure in the CVD furnace, which is now vacuum pressure instead of atmospheric pressure and the second one is the inlet mixture gas ratio on Reactive Sputtering, where we used more ratios of gases with change of quantity of O₂.

4.4.1. Vacuum pressure instead of atmospheric pressure

The vacuum pressure offers to thermal annealing process one cleaner furnace without any elements and dusts from the atmospheric air. Also, prevent collisions between the vapor particles with a result the higher uniformity of material. In our experiment we need the vacuum to prevent the further oxidation of our samples due to oxygen in atmospheric pressure. This is necessary because if we have more reaction of Cu₂O thin film with O₂ the Cu₂O will convert to CuO, which is not the desirable material. So, the pressure in the furnace is 10⁻¹mbar now.

4.4.2. Change of O₂ percent in Reactive Sputtering

The 10% of O₂ in the Reactive Sputtering is very good percentage, because as we said before we need little quantity to grow up the Cu₂O, and we don't want the formation of CuO which is need more oxygen. However, at experiment 2 we change the quantity of oxygen to cover the whole range of possible quantities of oxygen in Reactive Sputtering, and to observed how all the combinations with the second step of annealing act and what is the final growth material. The minimum oxygen was 10%, goes to 25%, 50% and finally it was 100% O₂ in the chamber. The rest of gas at first three quantities was again the Argon.

4.4.3. Experimental Process

The experiment 2 has the same steps as the first one. In the same way we cleaned the substrates (Si & SLG) and the pure Cu target. We used the optimum conditions for Reactive Sputtering, thus the Sputter Current at 120mA, the time on 4 minutes per cycle and the 3 cycles for each deposition. Now, as we said we used four different inlet gases. All information about the deposition by Reactive Sputtering is on Table 4.3 at supplement.

After that we keep the same procedure as the first experiment, for thermal annealing, except that we changed the pressure to vacuum pressure. The temperature varied from 300°C to 600°C, the time was on 60 minutes and the inlet gas was Argon 100%. All the information for thermal vacuum annealing process is on Table 4.4 of supplement. On figure 4.10 is the schematic illustration of experiment 2.

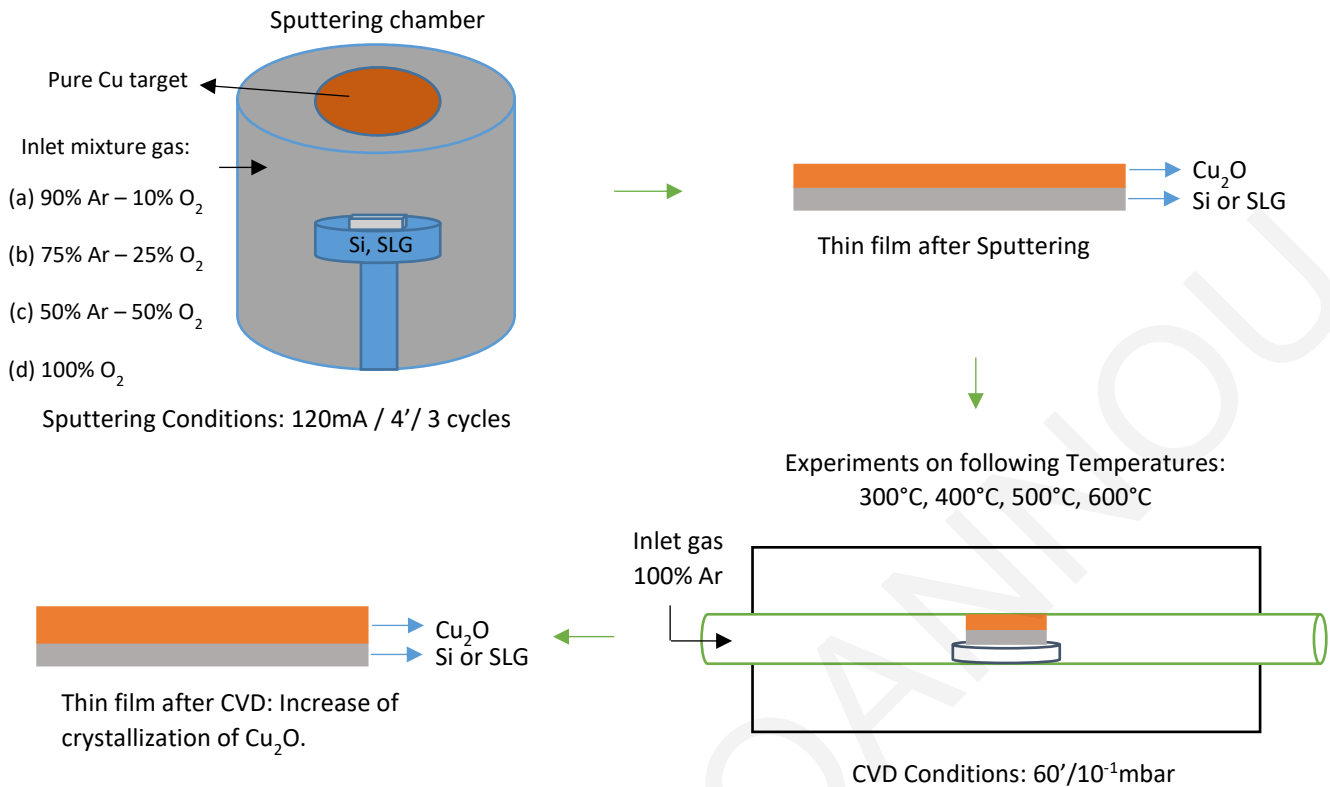


Figure 4.10: Schematic Illustration of Experiment 2

4.4.4. XRD Characterization and Results

After the growth and annealing of material we characterized all samples by XRD technique. We have been exported several XRD combination graphs to determine the results as best we can. We execute 8 combination graphs as below:

- Constant ratio of mixture gas on Sputtering (90:10, 75:25, 50:50), Si substrate, change of temperature (3 XRD graphs)
- Constant ratio of mixture gas on Sputtering (90:10, 75:25, 50:50), SLG substrate, change of temperature (3 XRD graphs)
- Constant temperature at 500°C, Si substrate, change of ratio of mixture gas (90:10, 75:25, 50:50) (1 XRD Graph)
- Constant temperature at 500°C, SLG substrate, change of ratio of mixture gas (90:10, 75:25, 50:50) (1 XRD Graph)

This was happened to understand how the increase of temperature at Thermal Vacuum Annealing at each gas ratio of Sputtering process was affect the growth of material. Also, the combination of graphs with constant temperature on 500°C was done because at 500°C, there is more purity of Cu₂O instead of CuO, with higher peaks. Below are the results and some of the graphs on figures.

Generally, we can observe an improvement on samples by the vacuum pressure compared to the previous experiment with atmospheric pressure. By vacuum annealing there is more uniformity and higher – stronger peaks on XRD graphs. The Cu_2O is purer now by vacuum annealing. Also, in comparison between substrates, at materials with Si substrate at all ratio gases, there are higher peaks at 61° , and at materials with SLG substrates the higher peaks are at the 36° and 42° .

At figure 4.11 we keep constant the inlet mixture gas on Reactive Sputtering at ratio of 90:10 ($\text{Ar}:\text{O}_2$), because the 10% of O_2 is very good low quantity. The temperature is increased from 300°C to 600°C . The results are good, but we don't have pure Cu_2O . We can observe at 61° a strong peak of Cu_2O , but the other two main theoretical peaks of Cu_2O at 36° and 42° are low. Also, we have peaks from the CuO .

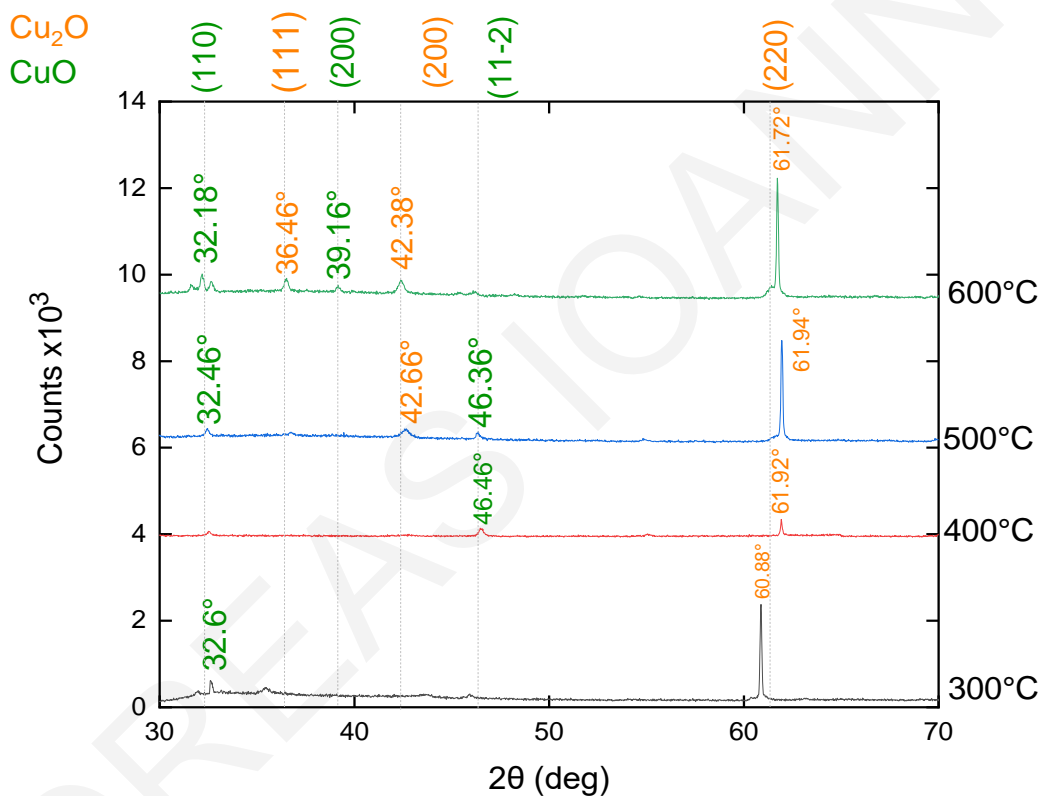
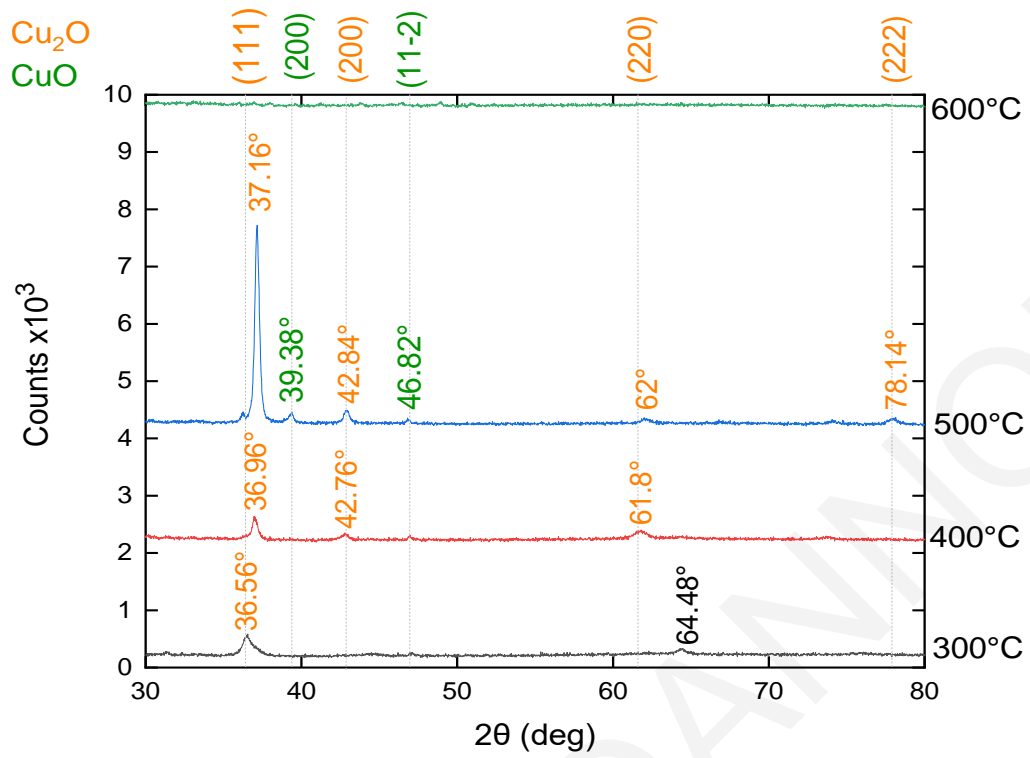


Figure 4.11: Si/Cu₂O TFs, Constant $\text{Ar}:\text{O}_2$ - 90:10, Vacuum Annealing, Increase of Temperature from 300°C to 600°C

At figure 4.12 again, we keep constant the inlet mixture gas on Reactive Sputtering at ratio of 90:10 ($\text{Ar}:\text{O}_2$) on SLG substrate this time. Same with previous graph, the temperature is increased from 300°C to 600°C . Now we can observe that we have very good growth materials at the temperature of 300°C to 500°C . The most important is the pure Cu_2O on 400°C at this graph, but also at 500°C , the growth of Cu_2O is very good with the appearance of main theoretical peak, strong and high. Also, we have and the other peaks of Cu_2O and two peaks of CuO which are very low. We can say that at 500°C with 10% O_2 we can grow a very good Cu_2O thin film.



Graph 4.12: SLG/Cu₂O TFs, Constant Ar:O₂ - 90:10, Vacuum Annealing, Increase of Temperature from 300°C to 600°C

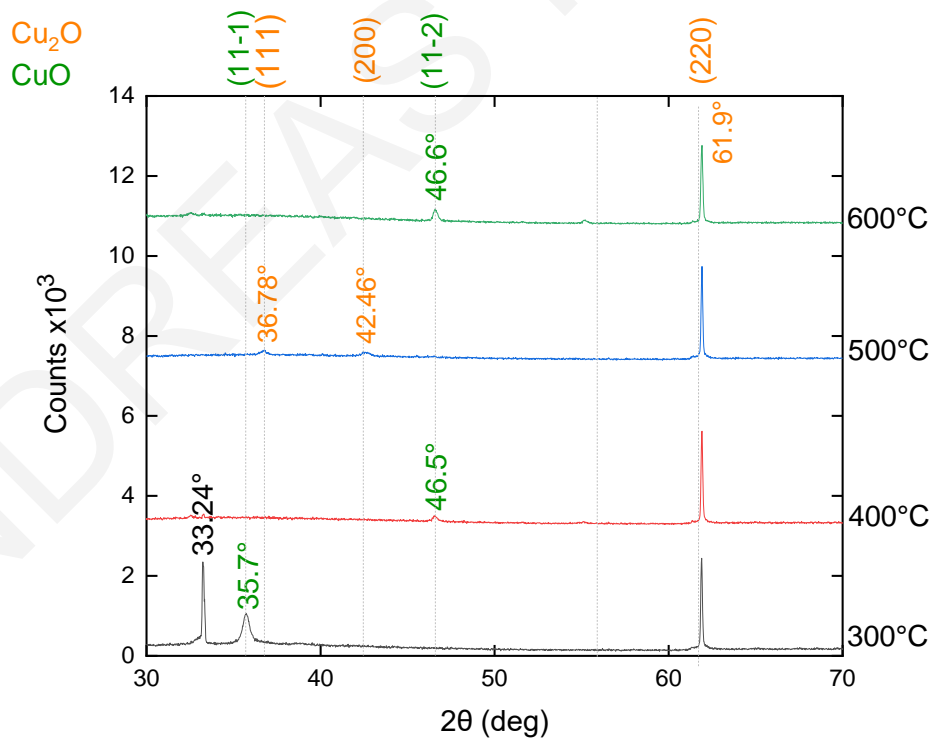


Figure 4.13: Si/Cu₂O TFs, Constant Ar:O₂ - 75:25, Vacuum Annealing, Increase of Temperature from 300°C to 600°C

Next, at figures 4.13 & 4.14 we have the same analysis of data with only change, the inlet mixture gas on Reactive Sputtering. From 90:10 (Ar:O₂), we have 75:25 (Ar:O₂) now. Also, the 25% of O₂ is low quantity of oxygen, so we can have good growth Cu₂O TFs.

At figure 4.13 (Si substrate) we observed again the strong peak of Cu₂O at 61° at all different temperatures. At 500°C we have pure Cu₂O, but the peaks on 36° and 42° are too much lower from the theoretical. At figure 4.14 (SLG Substrate) we have again pure Cu₂O with low peaks. Furthermore, at 300°C the growth material is Cu₂O with one stronger peak than the peaks of higher temperatures.

In general, the range of temperature from 300°C to 500°C, provide good and pure growth Cu₂O. At 600°C, we observe low peaks of both of materials, Cu₂O and CuO. Maybe, the further increase of temperature is not appropriate for the growth of Cu₂O by this way. At this point we can't say for sure that the higher temperatures are not appropriate. We must have extended experiments on higher temperatures to execute more and clear results about the optimum temperature.

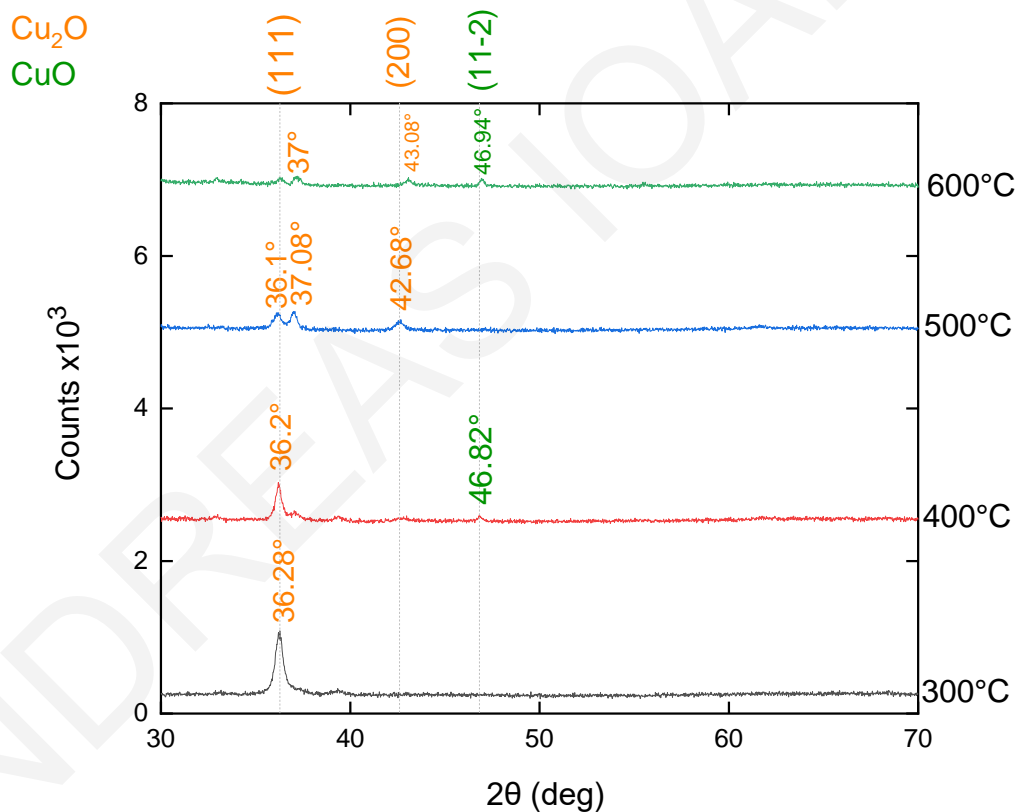


Figure 4.14: SLG/Cu₂O TFs, Constant Ar:O₂ - 75:25, Vacuum Annealing, Increase of Temperature from 300°C to 600°C

The experiments that have been done by the ratio of 50:50 (Ar:O₂) in the Reactive Sputtering shows as that this percentage of oxygen is high for the desirable material. With higher amounts of oxygen, we observed better growth of CuO than the Cu₂O.

At the next two figures, 4.15 & 4.16, we keep the temperature at 500°C, due to the previous results, which are shows us that one very good annealing temperature is this. With constant temperature at 500°C, we combine all the different ratios of inlet mixture gas at Reactive Sputtering, and we execute the following graphs. The figure 4.15 is on Si substrate and the figure 4.16 is on SLG substrate.

At figure 4.15 (Si substrate) we distinguish the strong constant peak at all different quantities of O₂, at 61°. Also, we can say that the better growth material is at 25% and 10% of O₂, compared to other two (50% and 100% of O₂). At 100% of O₂ we can observe a mix phase of Cu₂O and CuO with addition of one third material according to the peak at 33°. So, as we said before the higher quantities of O₂ are not the appropriate for the growth of Cu₂O.

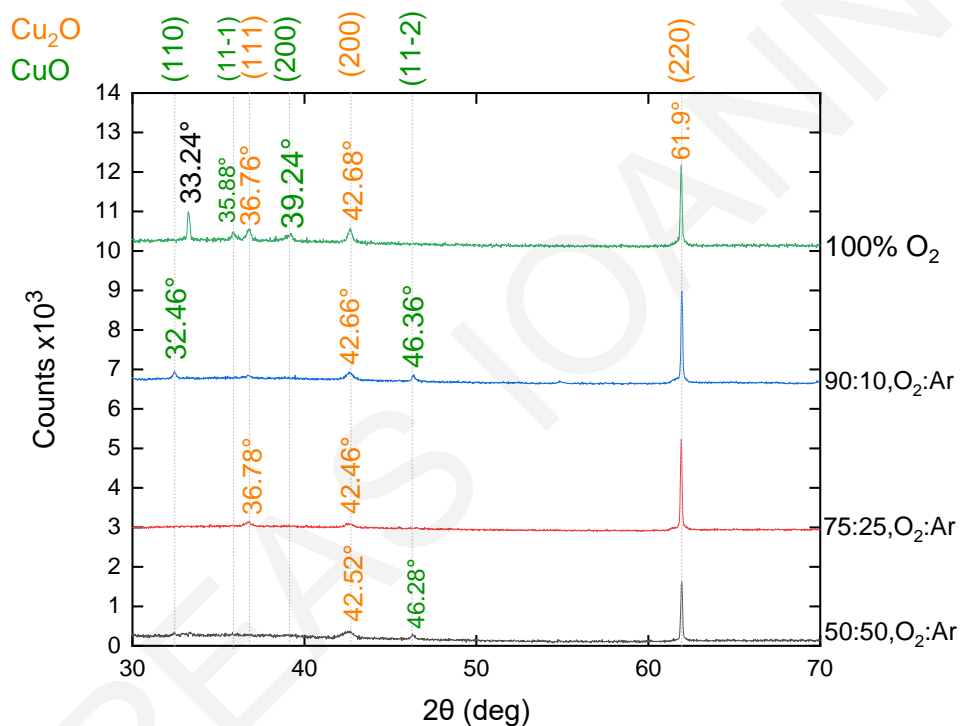


Figure 4.15: Si/Cu₂O TFs, Constant T at 500°C, Vacuum Annealing, Increase of O₂

At figure 4.16 (SLG substrate), again, we can say that the better growth material is at 10% and 25% of O₂, compared to other two (50% and 100% of O₂), as the previous graph. The other two percentages of O₂ they don't give us something good, we have an amorphous layer.

In general, we can avoid the 100% of O₂, we can have some more experiments by using 50% of O₂ and changing of other parameters after the deposition on Reactive Sputtering.

The time of 1 hour for thermal vacuum annealing seems very good. We can vary this parameter to see how affect our experiment.

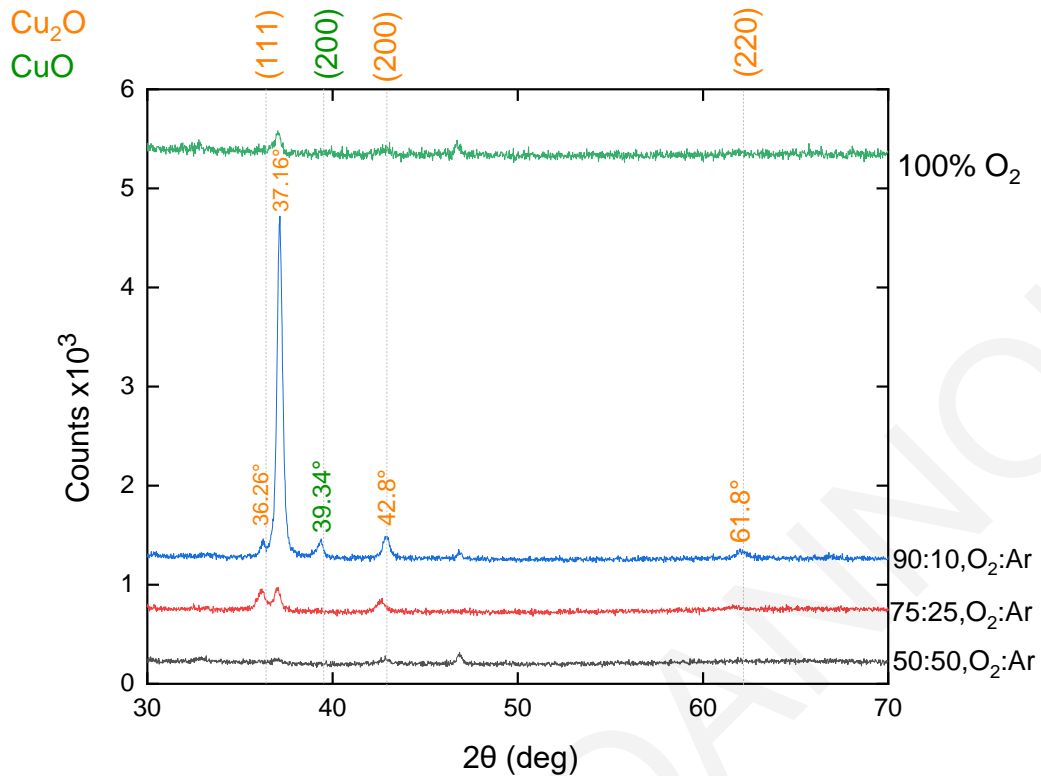


Figure 4.16: SLG/Cu₂O TFs, Constant T at 500°C, Vacuum Annealing, Increase of O₂

Finally, compared to the previous experiment on atmospheric pressure the results are much better. We succeed pure Cu₂O, however, there is not a pure and quality phase of Cu₂O on samples by vacuum annealing, yet.

4.5. Experiment 3 – Use of Hydrogen gas (H₂) in Vacuum Thermal Annealing

The new parameter that is change in procedure is the introduce of Hydrogen (H₂) in the inlet mixture gas of CVD furnace, for the vacuum thermal annealing. Also, have been done some experiments in higher temperatures and more time, compared to previous experiments. This was happened to have accuracy about the optimum parameters.

4.5.1. Benefits of introduction of Hydrogen

The introduction of H₂ passivate defects and fills the holes, as a result the better electronic configuration of growth material. By the flow of H₂, we can suppress the oxidation and reduced the Cu₂O layers.

4.5.2. Experimental process – Reactive Sputtering

The process is the same as previous experiments. In Reactive Sputtering we have Si and SLG substrates, with the same ratio gases. We avoid the 100% of O₂, because the results from this were not the expected. Also, we keep the other three ratios to see

how the results will be, after the introduction of H₂. The oxygen varied from 10% to 50% in incorporation with Argon. All information about the conditions in Reactive Sputtering is on Table 4.5 on supplement.

4.5.3. Experimental process – Thermal Vacuum Annealing

For the second step of Annealing, we keep the vacuum pressure of 10⁻¹mbar. We make the runs for one hour, and at some runs we change the time from 1 to 2 hours, to observed how affect the last result this increase. For the same reason we change the range of temperatures. We did the experiments at three different temperatures to cover the whole possible range. We started from 300°C goes to 500°C, which is the best temperature until now, and we did some experiments at 800°C, to verify the optimum temperature.

Subsequently, we have the important parameter of inlet gas. Now, the inlet gases are the Argon (Ar) and the Hydrogen (H₂). Again, we vary the H₂ from 10% to 100% to cover the whole possible range. We use at three different ratios, 10%, 50% and 100%. At the first two ratios the rest of inlet mixture gas is the noble Argon. All information about the conditions on CVD furnace was on supplement at table 4.6.

At the figure 4.17 we have the procedure of experiment 3.

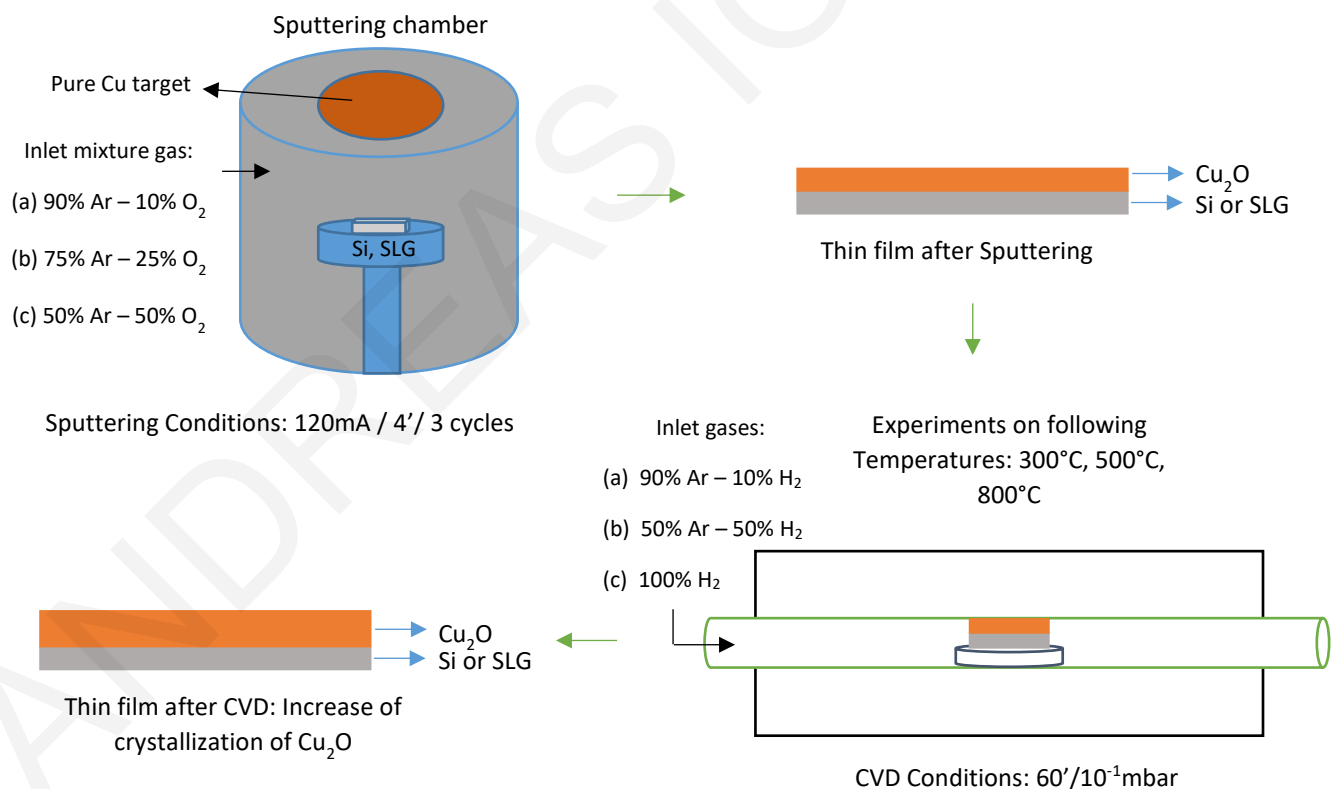


Figure 4.17: Schematic Illustration of Experiment 3

4.5.4. XRD Characterization and Results

For the analysis of data, we must make combination XRD graphs with constant parameters, e.g., the Temperature, the inlet mixture gas at Reactive Sputtering or the inlet mixture gas at CVD furnace, or a combination of them. These combinations were done to understand the behavior of Hydrogen for the formation of Cu_2O in the experiment. Below are the prepared graphs in summary.

For samples with Si substrate:

- Constant T at 500°C , Constant Ar: O_2 at 90:10, Decrease of H_2 (100% to 10%)
- Constant T at 500°C , Constant Ar: H_2 at 50:50, Increase of O_2 (10% to 50%)
- Constant T at 300°C , Constant Ar: H_2 at 50:50, Decrease of O_2 (50% to 25%)
- Constant Ar: H_2 & Ar: O_2 at 90:10, Increase of T (300°C to 500°C)

For samples with SLG substrate:

- Constant Ar: H_2 & Ar: O_2 at 90:10, Increase of T (300°C to 500°C)
- Constant T at 500°C , Constant Ar: H_2 at 50:50, Decrease of O_2 (50% to 10%)
- Constant T at 500°C , Constant Ar: O_2 at 90:10, Increase of H_2 (10% to 100%)
- Constant Ar: H_2 at 50:50, Ar: O_2 at 75:25, Increase of T (300°C to 500°C)
- Constant Ar: H_2 & Ar: O_2 at 50:50, Decrease of T (500°C to 300°C)
- Constant T at 300°C , Constant Ar: H_2 at 50:50, Increase of O_2 (50% to 25%)

At figure 4.18, we keep constant the best optimum conditions until now. The temperature at 500°C , and the inlet mixture gas in Reactive Sputtering, the 10% of O_2 . We vary the H_2 from 100% to 10% at three levels. We did this decrease on H_2 because as we can observed from each separate graph, as we decrease the H_2 , the peaks of growth Cu_2O become higher and stronger.

The results are too much better than the previous series of experiments. First, the H_2 gives to growth materials high uniformity and more clear and almost pure Cu_2O . As we can see on this figure with 10% of H_2 , we succeed the three main theoretical peaks of desirable material, but we have also one small peak of CuO . This peak is the lowest from the other three. Compared to all the other graphs of the whole work on this growth of Cu_2O , the peak at 36.24° , is the strongest and very close to theoretical value of Cu_2O , the 36.41° .

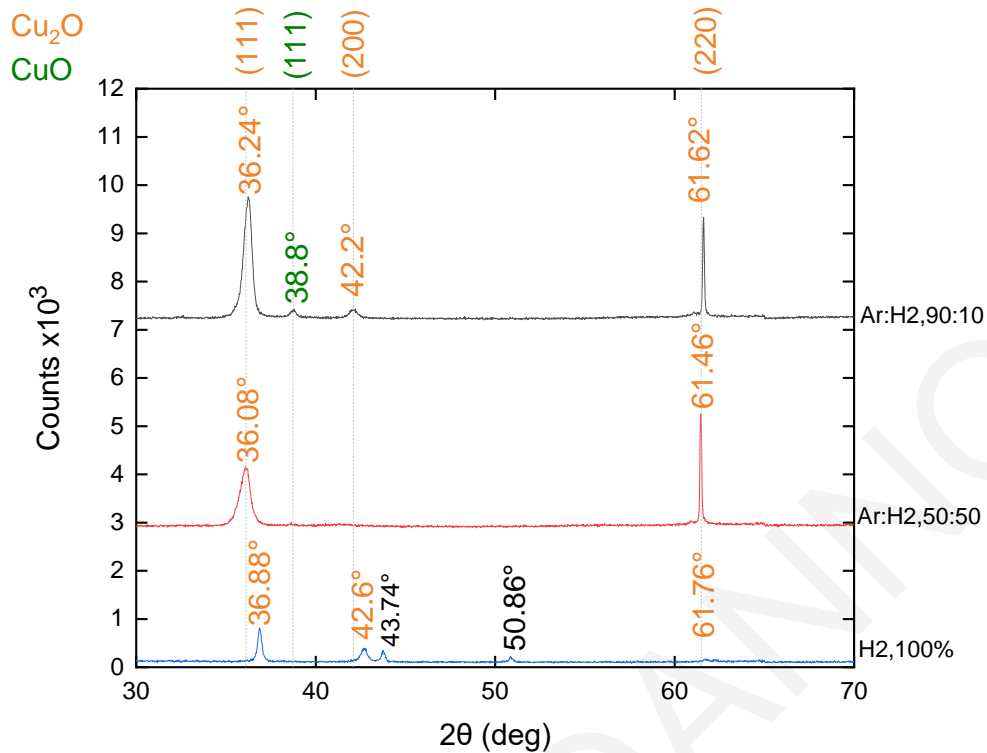


Figure 4.18: Si/Cu₂O TFs, Constant T at 500°C, Constant Ar:O₂ - 90:10, Decrease of H₂

With 50% of H₂ in the mixture gas, we succeed pure Cu₂O with only 2 peaks at 36°, and 61°, with lower peak at 36°. The important is that this sample has only our material. At 100% of H₂, we can observe low peaks, succeed of Cu₂O, but we have two more peaks from completely different material. So, the range of H₂ in the inlet gases, must me from 10% to 50%.

After the results with pure Cu₂O with 50% of H₂, 500°C, we keep constant these parameters and we vary the O₂, to compare the three different ratios at the figure 4.19. As we can see the best XRD graph is this with the less quantity of O₂, of 10%. At the other two percentages of 25% and 50%, we have materials near to Cu₂O, but are not good and pure the first one. For example, the peak on 62°, at 50% of O₂, shows as a shift on the right. In summary, we can say that we have execute very good parameters for growth of desirable material on Si substrate until now. The temperature at 500°C, the low O₂ at 10% and 50% of H₂.

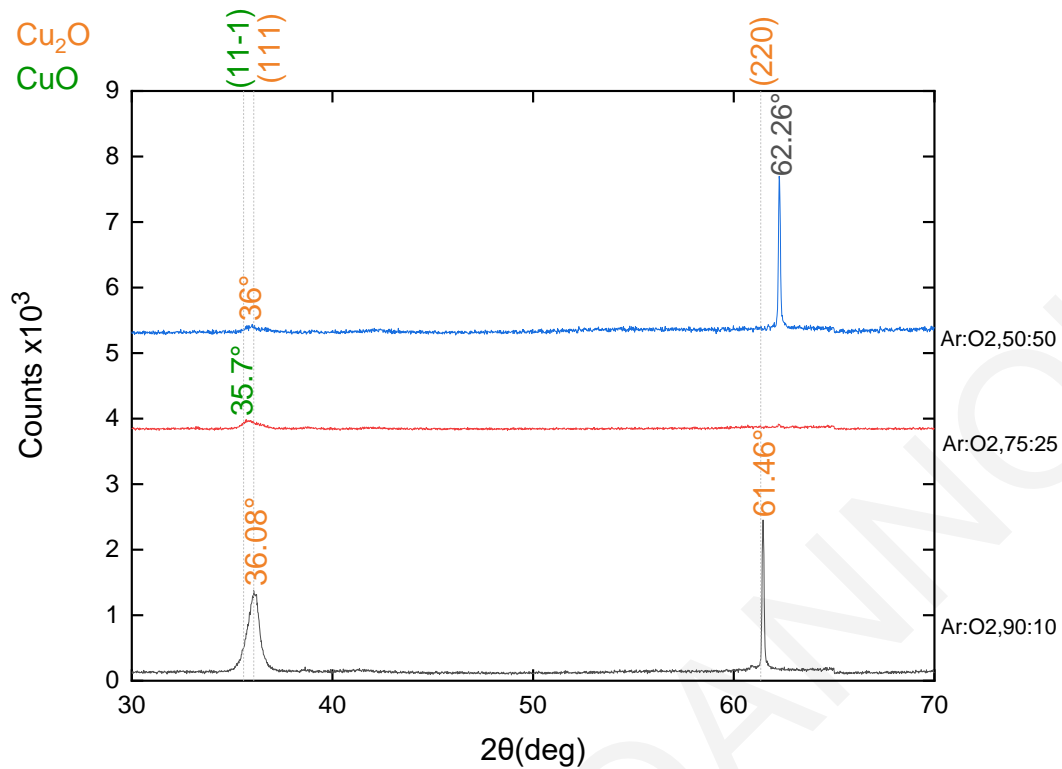


Figure 4.19: Si/Cu₂O TFs, Constant T at 500°C, Constant Ar:H₂ at 50:50, Increase of O₂

Below we have two more combination graphs with Si substrate, with changing of temperature and time in CVD process. On the figure 4.20 we change and keep constant the time from one to two hours of annealing, we reduce the temperature at 300°C, and we vary the O₂, from 50% to 25%. Also, we keep constant the H₂ at 50% because we succeed before pure Cu₂O at this ratio. For the ratio of O₂, we verified that in higher quantities we don't succeed our material. Also, we have one peak only from our material. In combination with these two changes, we observed that we don't have a better growth of Cu₂O. Unlike, we have less and lower peaks, and less uniformity on the film.

At figure 4.21, we keep constant the O₂ and H₂ at 10%, and we compared the two annealing temperatures, 300°C and 500°C. As we observed at 500°C, there is more much better growth of material than the 300°C, because we have higher, stronger and more peaks at 500°C.

So, we verified these very good parameters for growth of Cu₂O on Si substrates. The temperature at 500°C, the low O₂ at 10% and 50% of H₂.

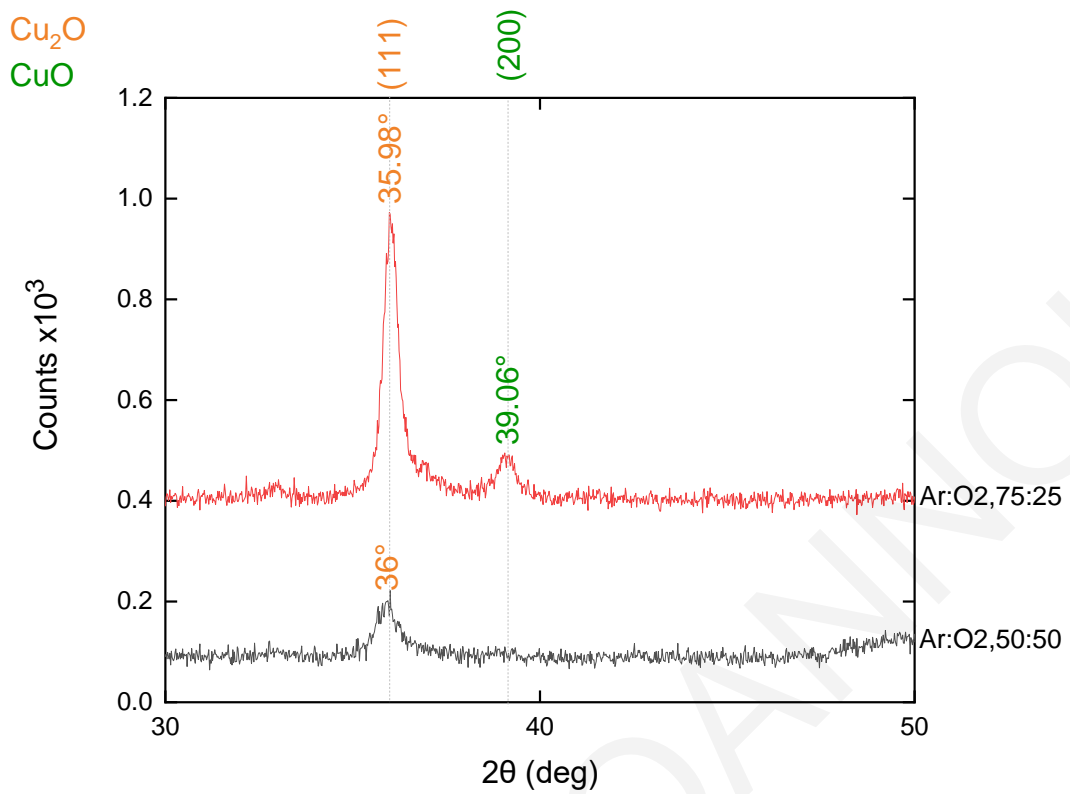


Figure 4.20: Si/Cu₂O TFs, Constant T at 300°C, Constant Ar:H₂ at 50:50, 300°C, 2hrs Increase of O₂

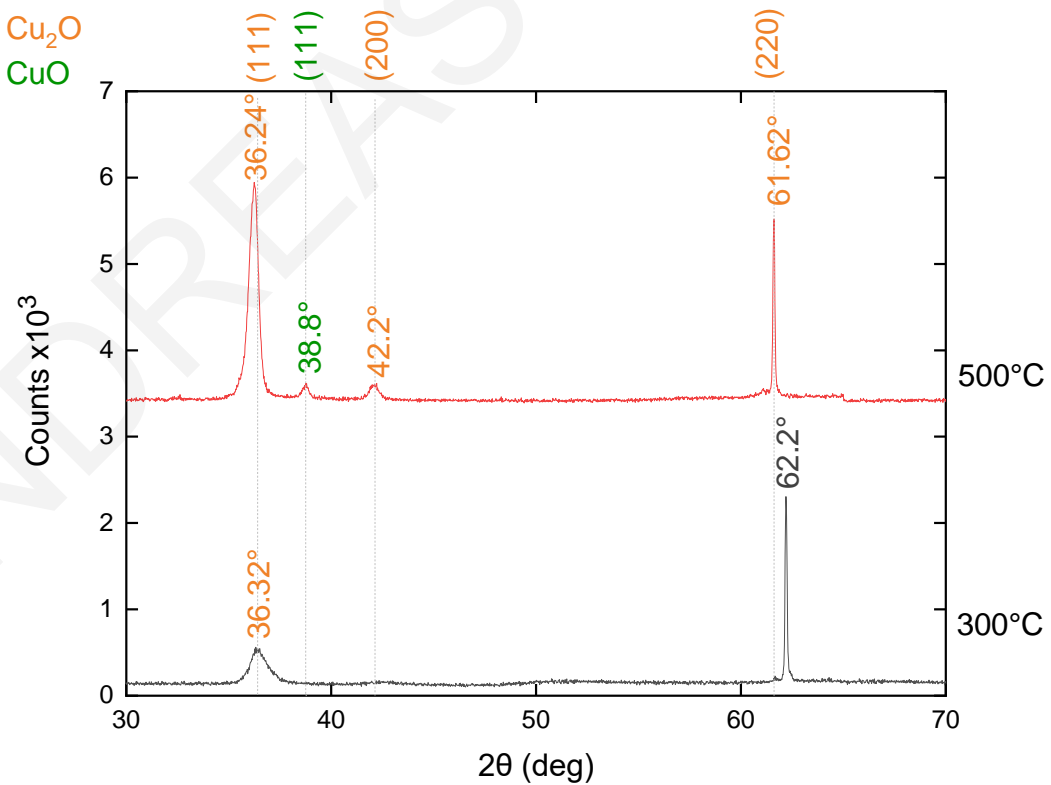


Figure 4.21: Si/Cu₂O TFs, Constant Ar:H₂ & Ar:O₂ at 90:10, Increase of T

Following the growth of Cu_2O on Si substrates, we have the results from the growth of Cu_2O on SLG substrates. Generally, the H_2 offers more uniformity on samples, but as we know the SLG is an amorphous material, so we don't have the same uniformity as the Si substrates.

In this analysis we started with constant O_2 and H_2 at 10%, to compare the growth on two annealing temperatures of 300°C and 500°C . As we observed at 300°C , we don't have pure Cu_2O , and we don't have the CuO which is near to Cu_2O . At 500°C we succeed a very good pure Cu_2O , with strong peaks at the main theoretical points, also we have the appearance of two more identical peaks of Cu_2O at 30° and at 73° , which is important. So, from this result we can say that for SLG substrates in addition to previous optimum conditions, the H_2 at 10% is also optimum.

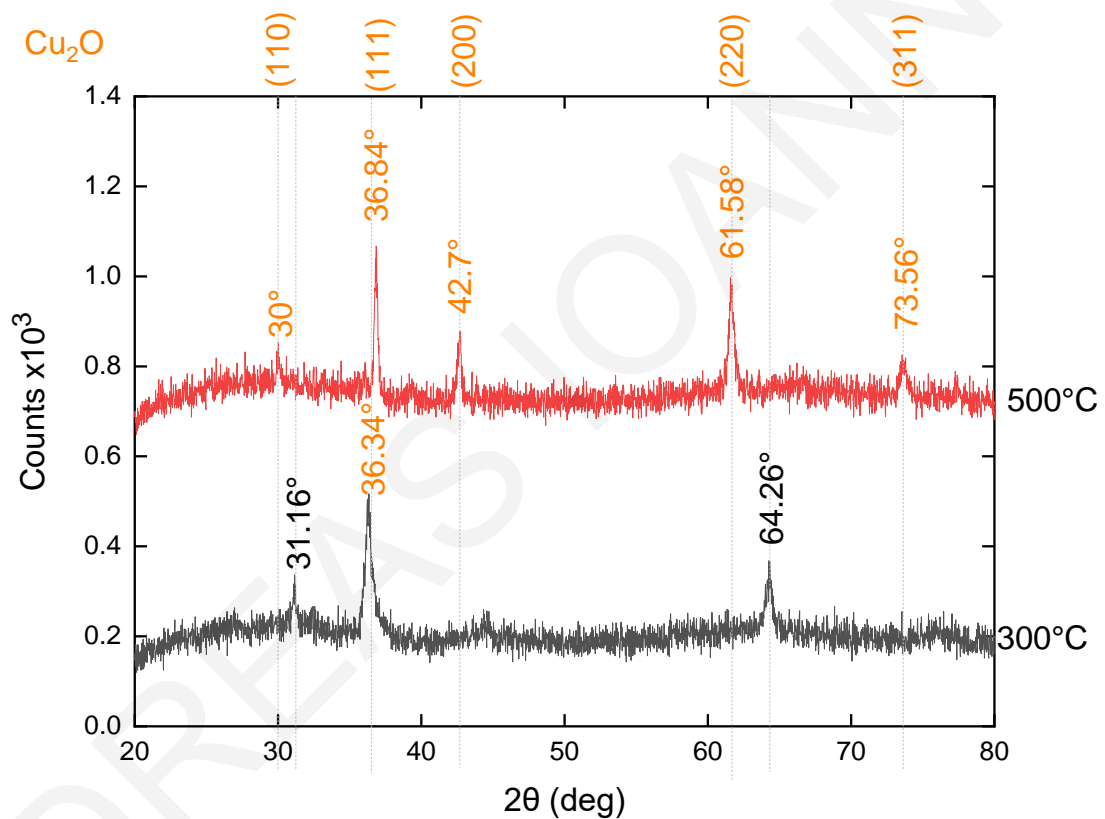


Figure 4.22: SLG/ Cu_2O TFs, Constant $\text{Ar}:\text{H}_2$ & $\text{Ar}:\text{O}_2$ at 90:10, Increase of T

At figure 4.23 we have a combination of previous optimum conditions for Si substrate, thus 500°C , 50% H_2 , and the three ratios of O_2 at Reactive Sputtering. With decrease of O_2 from 50% to 10% we observe clearly that the growth of Cu_2O is much better. The material is not pure Cu_2O but also has peaks from CuO . The important is that we verified the previous optimum conditions at 10% of O_2 . Furthermore, we have again the appearance of more than 3 peaks of Cu_2O at SLG substrate. These results are important, even though we have the low peak of CuO at 39° . Also, is important that the theoretical peak of Cu_2O with the highest intensity at 36° , is on this graph the highest.

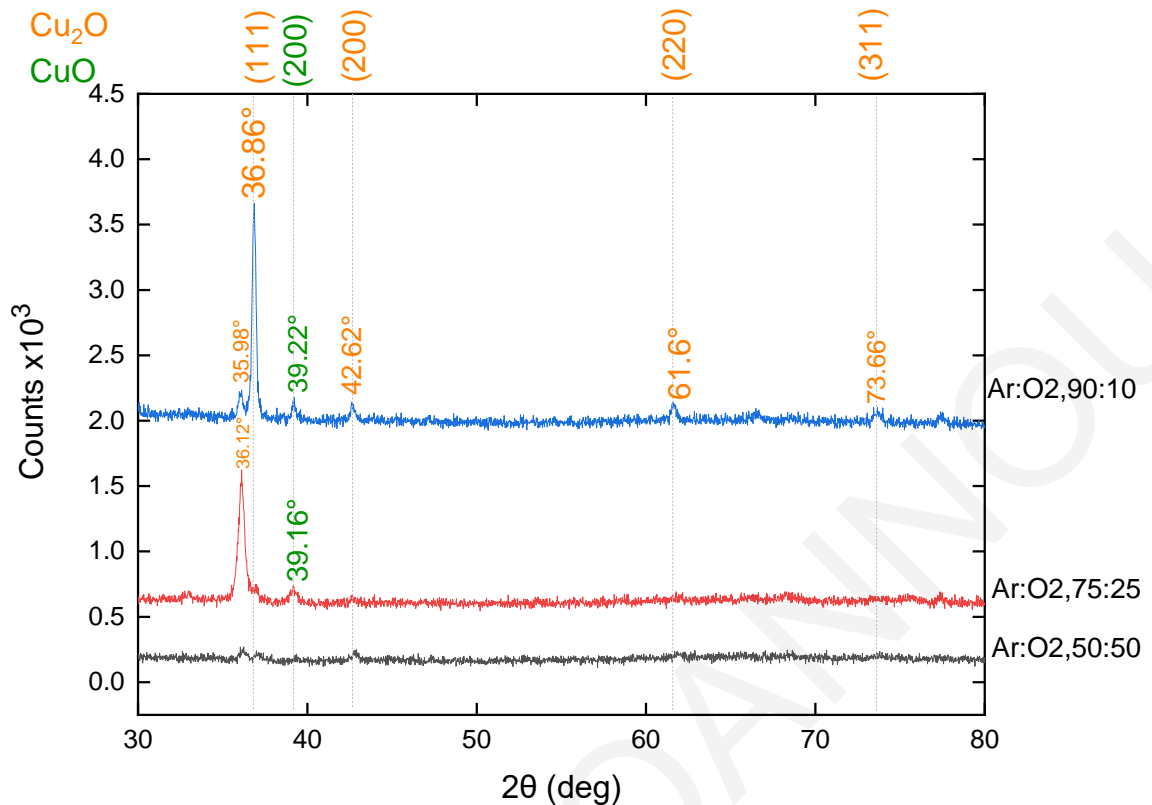


Figure 4.23: SLG/Cu₂O TFs, Constant T=500°C, Constant Ar:H₂ at 50:50, Decrease of O₂

Subsequently, at figure 4.24 we keep again constant the temperature at 500°C, the O₂ at 10%, and we increase the H₂, from 10% to 100%. We have pure material at 10% and 50%. Compared to previous results on Si substrate at 100% of H₂, now at SLG substrate we have very good growth of Cu₂O with strong peaks and only the low peak of CuO at 39°.

At the next three graphs we present other combinations of conditions. At figure 4.25 we keep constant the H₂ at 50% as an optimum condition to increase and keep constant the O₂ at 25%. The graph shows as the growth on two annealing temperatures 300°C and 500°C. At both of temperatures we have a simple growth of Cu₂O, with one peak at 36°, and not pure material because we have and one lower peak of CuO at 39°. What we can say is that, from one peak of material we don't have a good, deposited film.

The same is happened at figure 4.26. The change from previous graph, is that we increase the O₂ at 50%. The material is pure Cu₂O with not peaks from other materials on both of temperatures, but the peaks are few and lower than the previous graphs on SLG substrate. Again, we have a simple growth of material.

At last graph (figure 4.27) we reduce and keep constant the temperature at 300°C. The H₂ is on 50%, and we have two materials with 25% and 50% of O₂, in Reactive Sputtering. As expected, the growth with less O₂ is better, but again the growth of Cu₂O on both samples, is simple and not the best, we have few and lower peaks.

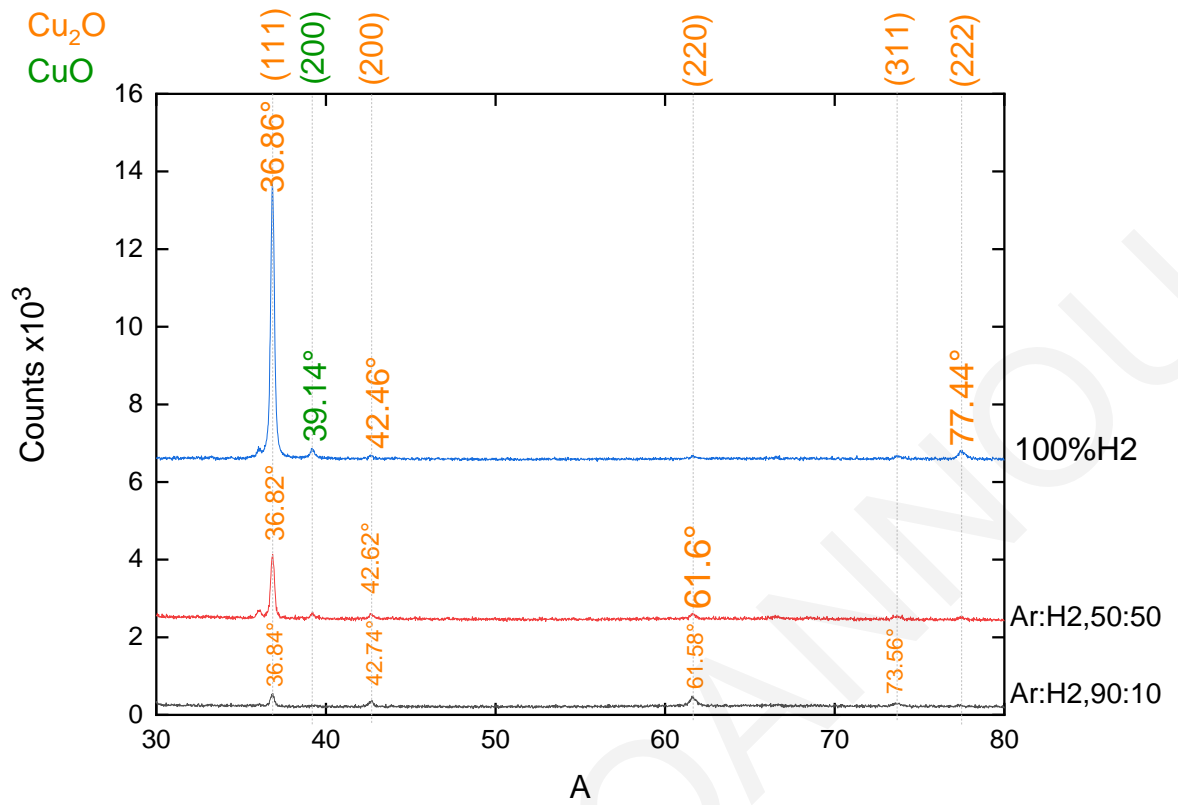


Figure 4.24: SLG/Cu₂O TFs, Constant T at 500°C, Constant Ar:O₂ at 90:10, Increase of H₂

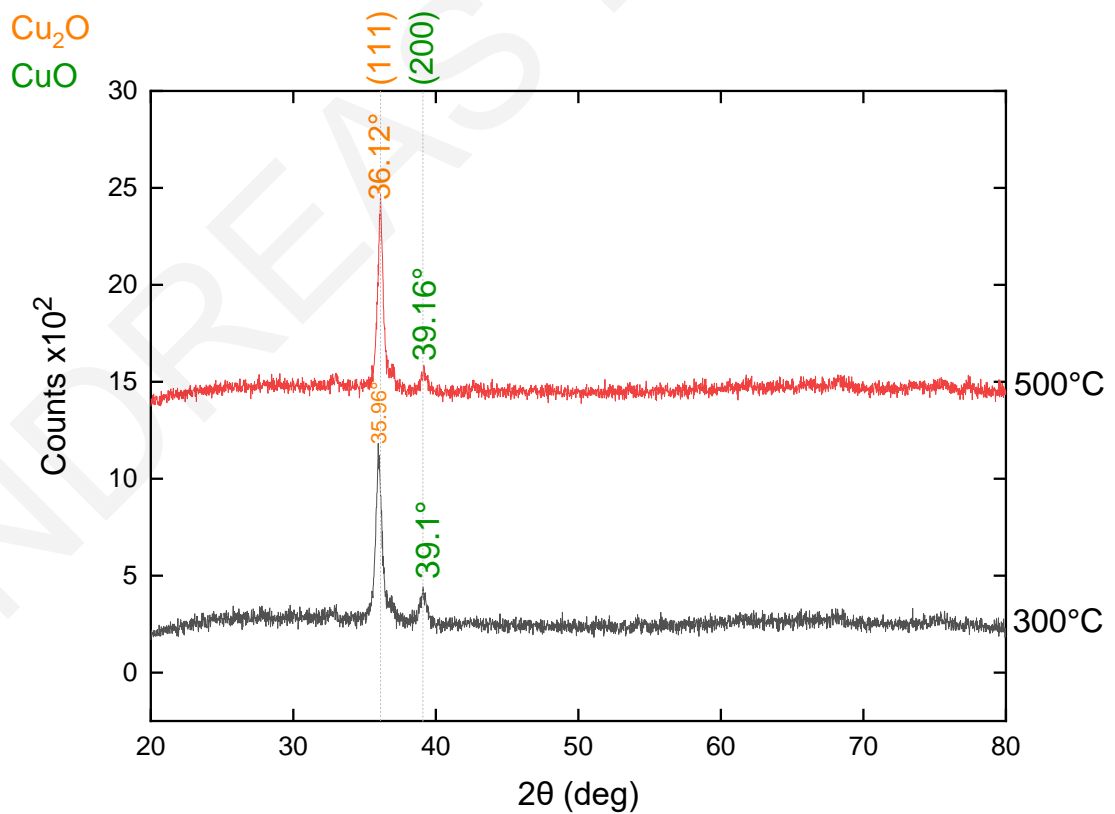


Figure 4.25: SLG/Cu₂O TFs, Constant Ar:H₂ at 50:50, Ar:O₂ at 75:25, Increase of T

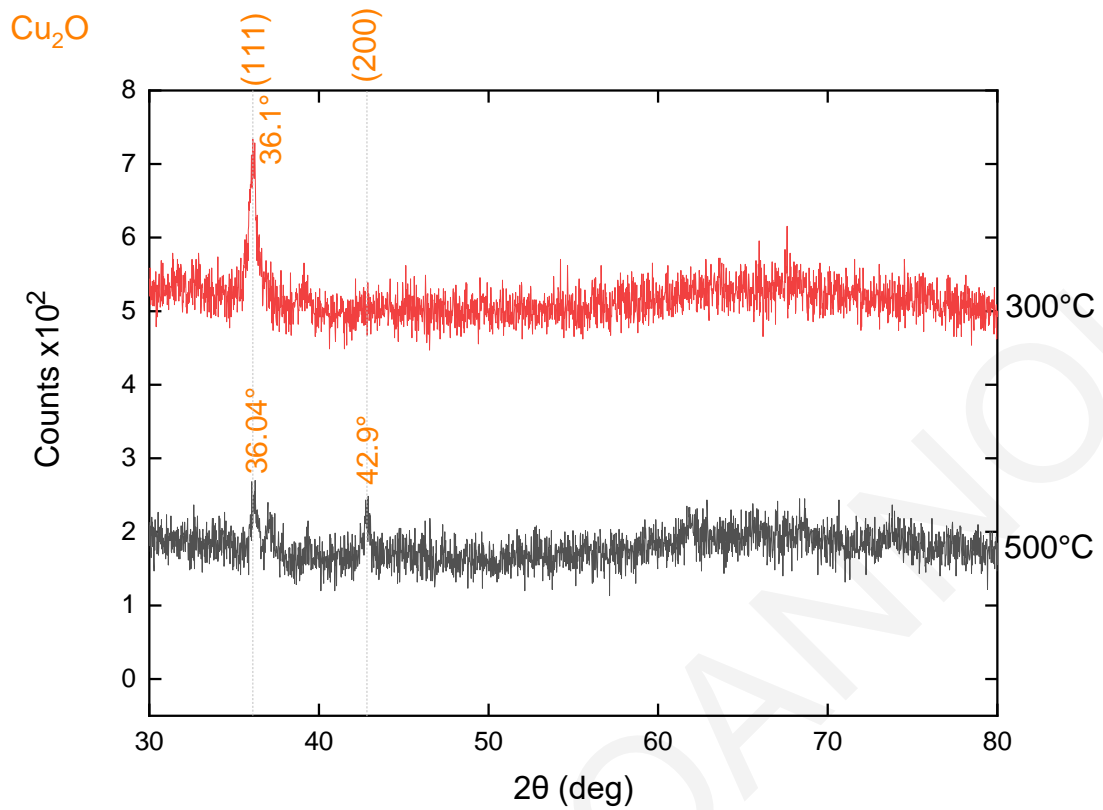


Figure 4.26: SLG/Cu₂O TFs, Constant Ar:H₂ & Ar:O₂ at 50:50, Decrease of T

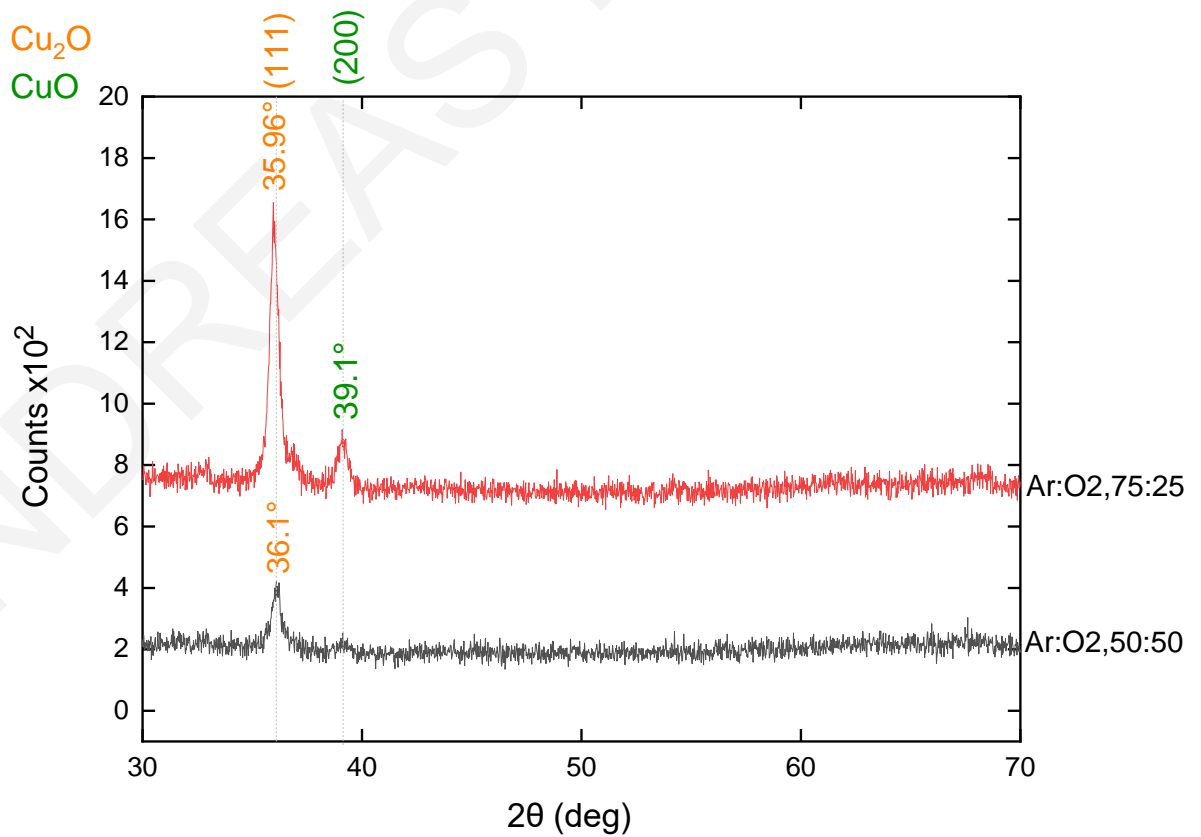


Figure 4.27: SLG/Cu₂O TFs, Constant T= 300°C, Constant Ar:H₂ at 50:50, Decrease of O₂

4.5.5. Optimum Conditions for pure Cu₂O

In conclusion, the optimum conditions with the introduction of H₂ in experiment is clearer now. However, differ on two substrates at some points. The optimum temperature is 500°C on both of substrates. The vacuum pressure of 10⁻¹mbar has very good effect at the annealing process, so we keep this pressure as the best. The O₂ in Reactive Sputtering is 10% at all of cases. Compared to other two quantities of 25% and 50%, the 10% is the best because is what we need, the less O₂ to form Cu₂O instead of CuO. However, if we change something else and we keep the 25% may be and this quantity very good for the growth of desirable material.

Generally, the growth layers of Cu₂O exhibited clear and well resolved peaks belonging to the cubic crystal structure of Cu₂O. The last condition is the H₂. Generally, the optimum quantity is on 50%. The addition of 10% of H₂ was not enough to suppress the oxidation of Cu₂O according to the chemical reaction: $2\text{Cu}_2\text{O} + \text{O}_2 \rightarrow 4\text{CuO}$, and we observed peaks belonging to the monoclinic crystal structure of CuO. Furthermore, the addition of 100% of H₂, give us the reduction of Cu₂O and CuO to metallic Cu, according to the following chemical reaction: $\text{Cu}_2\text{O} + \text{H}_2 \rightarrow 2\text{Cu} + \text{H}_2\text{O}$. As we said before, the optimum quantity is the 50% of H₂, because is capable to prevent the oxidation and reduction of Cu₂O. This is happened because the intersecting grain boundaries and the porosity of Cu₂O provide diffusion paths and traps for hydrogen. So, the higher grain boundary density of Cu₂O layers give us a faster reduction, which is starts when a certain density of accumulated oxygen vacancies is reached at the periphery of the Cu₂O grains. For those reasons, is important to find the optimum flow of H₂ at the annealing of Cu₂O.

4.6. Preparation of samples for SEM Characterization, Raman Spectroscopy and Ultrafast Pump Probe Spectroscopy (UPPS)

The previous results are very good for the growth of a pure Cu₂O. After that we must do a preparation of substrates in same way as the previous experiments, to have further analysis on characteristics with different substrates. The new substrates are the m, r, a - Al₂O₃. We chose these substrates because the process of annealing of Cu₂O at higher temperatures leads to thermal diffusion and reacts with previous substrates. The sapphire can be used as a barrier against the thermal diffusion of copper up to 750°C, so we can do our experiments on the optimum temperature that we found before, 500°C. The second reason is that we need these substrates due to their characteristics, to probe the electronic band structure and gap states of Cu₂O by UPPS, ultrafast pump probe spectroscopy. The Cu₂O layers on these three substrates, were semi-transparent, had a light-yellow color. The purpose is to understand the mechanism of generation and recombination, which is important from an applied and fundamental point of view.

4.6.1. Experimental process - Preparation of Cu₂O thin films

The process is same as the previous experiments, the preparation the cleaning the deposition in Reactive Sputtering. Now, the substrates are the Si, and r-Al₂O₃, m-Al₂O₃, a-Al₂O₃. The size of them is smaller than the Si and SLG substrates. The dimensions are 5x5mm.

For the Reactive Sputtering we use the same inlet mixture gases, the three ratios of 10%, 25%, 50% of O₂ with Argon. The target is again pure Cu. The sputter current is the same on 120mA, 4 minutes on each cycle and 3 cycles per sample. At some runs we reduce the number of cycles from 3 to 1, to reduce the thickness of deposited material. The thickness from 300nm is reduced to 100nm. This was happened to make the samples measurable for optical measurements (experiment 4). All information about the reactive sputtering conditions is on Supplement at Table 4.7.

For the thermal vacuum annealing we use the optimum conditions. The temperature is on 500°C, 60 minutes, the pressure is on 10⁻¹mbar, and the inlet mixture gas is on 50% of H₂, with 50% of Argon. Only one run on CVD was done by 100% of H₂. All information about the thermal vacuum annealing conditions is on Supplement at Table 4.8.

4.6.2. SEM and Raman Spectroscopy Results

According to the characterization of Cu₂O layers by SEM the grains have a size of 89.62 ± 7.87nm, as shown by the SEM image (figure 4.28). At this figure is introduced the corresponding histogram. The layers are nanostructured, and the protrusions on the surface with a diameter of d ~ 1μm, were found to be slightly richer in Cu by ~5 at %. By the EDS, which is on the same setup with SEM, we have the chemical composition of Cu₂O. We find that the Cu₂O layers consist of Cu and O, which are the basics components of the material. Also, EDS detect Al, due to the substrate Al₂O₃.

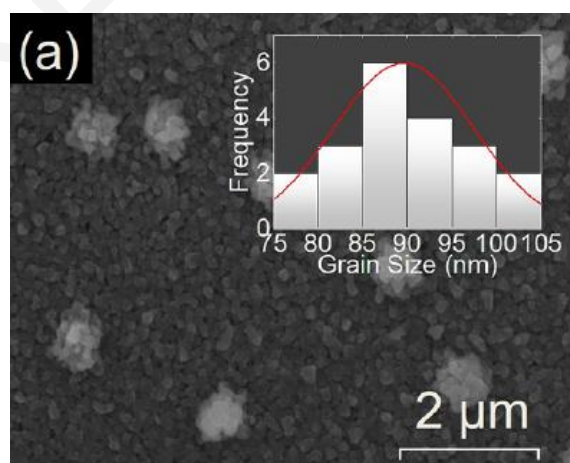


Figure 4.28: SEM image of a 300nm Cu₂O layer on m-Al₂O₃ with histogram of grain size [8] .

The Raman Spectroscopy is used for further investigation of structural and properties and composition of Cu_2O layers. The Raman spectra on r- Al_2O_3 , m- Al_2O_3 , a- Al_2O_3 is on figure 4.29.

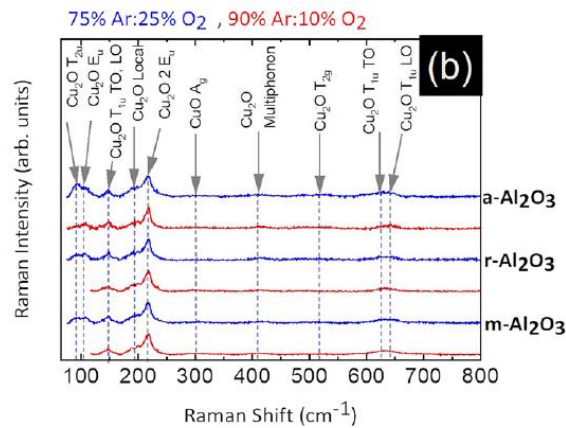


Figure 4.29: Raman spectra on m-, r-, a- Al_2O_3 [8].

4.6.3 UPPS Results and Discussion

By using the same Cu_2O layers on m-, r-, a- Al_2O_3 and the ultra-fast pump probe spectroscopy (UPPS), we measured the temporal evolution of the differential transmission through these layers. The purpose of UPPS is to generate and recombined the photogenerated electron-holes at this semiconductor material with direct energy bandgap. On figure 4.30 is the schematic illustration of the mechanisms that UPPS did, the generation and recombination of direct energy bandgap semiconductor.

For this operation, the pump gives a short pulse of energetic photons, which result in the excitation of electrons from the valence band into the conduction band. After the excitation, the electrons will gradually lose their energy, and from high above the conduction band minimum, now occupy lower energy states. They occupy the energy states closer to the conduction band minimum (E_c), and the empty states of Cu_2O which are crystallographic imperfections (E_i), that are located energetically in the energy gap of Cu_2O . The temporal evolution of the occupancy of these states is probed by a separate light beam by varying the wavelength from $\lambda_{\text{PR}} = 450$ to 750 nm and measuring the change in transmission or differential transmission (dT/T).

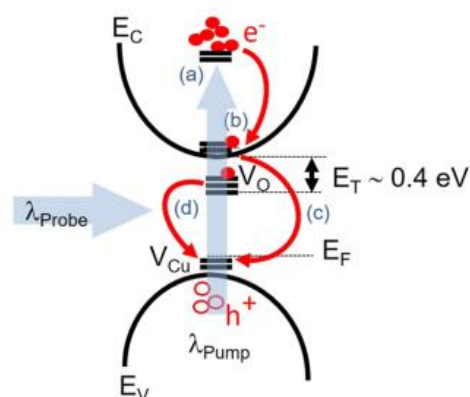


Figure 4.30: Mechanisms of generation and recombination of direct energy bandgap semiconductor, with crystal imperfections [8].

So, if a state is occupied by an electron, then the photon with a specific λ_{PR} will not be absorbed, resulting in a positive increase in differential transmission. In contrast, if a state is not occupied by a photoexcited electron, then a photon with a specific energy will be absorbed, with result the reducing transmission at a specific λ_{PR} . On this way we can find the fundamental direct energy bandgap of Cu_2O , and the states with crystal imperfections.

The results from UPPS measurements are at two below figures. At figure 4.31 the measurements obtained on Cu_2O layers on $m\text{-Al}_2\text{O}_3$ substrate using $\text{Ar}:\text{O}_2$ 90:10%. The case (a) is for 100 nm thickness of Cu_2O layer, and (b) for 300 nm thickness of Cu_2O layer. At both of cases, we observe two major peaks corresponding to a positive and negative maximum in dT/T at $\lambda_{PR} = 450$ and 487 nm which correspond to 2.75 and 2.54 eV, respectively.

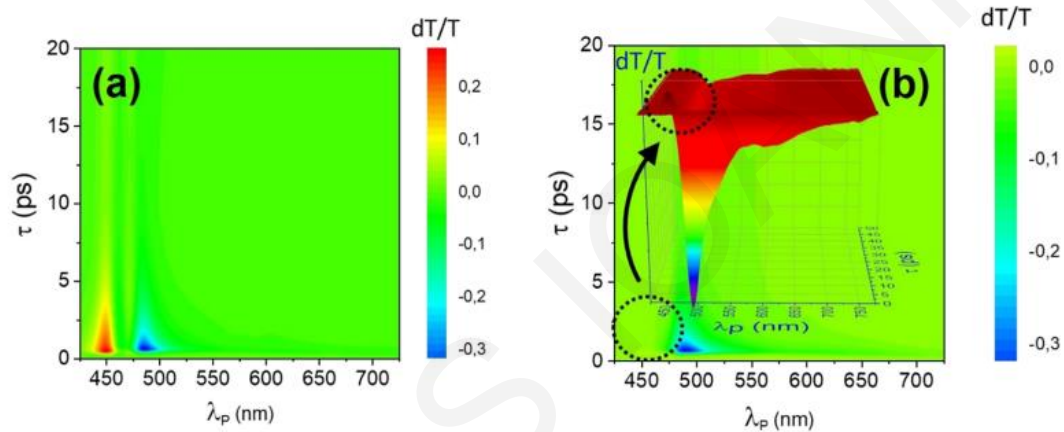


Figure 4.31: Differential transmission dT/T (no units) vs time delay τ (ps) and probe wavelength λ_p (nm) for the Cu_2O layers on $m\text{-Al}_2\text{O}_3$ obtained using $\text{Ar}:\text{O}_2$ 90:10% with a thickness of (a) 100 nm and (b) 300 nm [8].

At figure 4.32, the only difference with first one is the gases that are used for annealing of Cu_2O layer, which is now $\text{Ar}:\text{O}_2$ 75:25%. The peaks that were observed on previous measurements, obtained again, but we have the occurrence of two more peaks at $\lambda_{PR} = 570$ nm and at $\lambda_{PR} = 687$ nm which correspond to 2.17 and 1.8 eV, respectively.

The two maximum peaks 1.84 and 2.75 eV corresponds to positive dT/T , so are occupied by electrons. In contrast, the two maximum peaks 2.17 and 2.62 eV corresponds to negative dT/T , so here the photons absorbed, implying that these states are empty after the excitation and generation of excess electrons and holes. Consequently, the photogenerated electrons occupy the highest conduction band and after that move into lower states of crystal imperfections which are located energetically in the energy band gap of Cu_2O .

Also, we have not changes by increasing the excitation energy from 1 to 10 μJ , by increasing the thickness of layers from 100 to 300 nm and by using $\text{Ar}:\text{O}_2$ 50:50%.

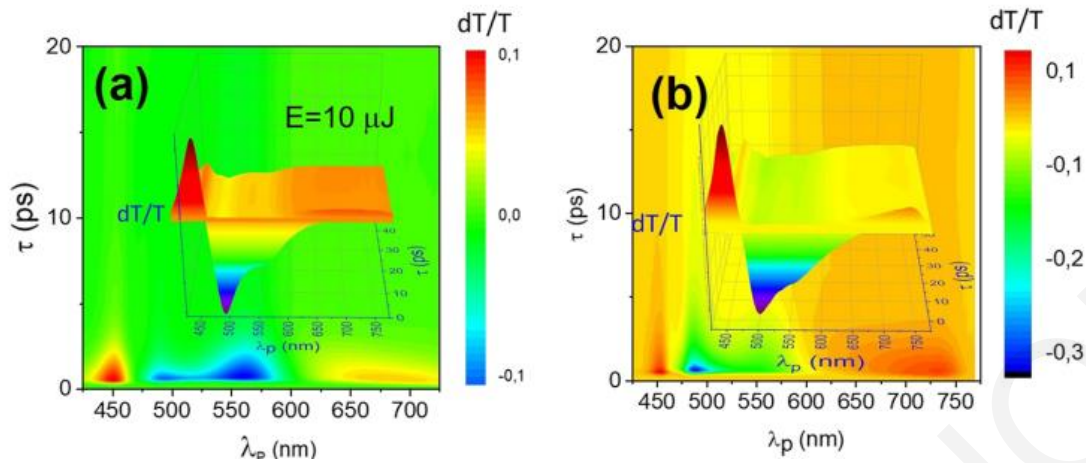


Figure 4.32: Differential transmission dT/T (no units) vs time delay τ (ps) and probe wavelength λ_p (nm) for the Cu_2O layers on $m\text{-Al}_2\text{O}_3$ obtained using $\text{Ar}:\text{O}_2$ 75:25% with a thickness of (a) 100nm and (b) 300nm [8].

Furthermore, the peaks observed at 2.17, 2.54, and 2.75 eV are related to the corresponding yellow, blue, and indigo direct gap transitions of Cu_2O . This observation was succeeded at room temperature due to the careful optimization that we did for the growth and annealing of Cu_2O layers under H_2 . Also, the direct gap transitions observed suggest that the Cu_2O layers are not coherently strained to the underlying m -, r -, and $a\text{-Al}_2\text{O}_3$, and there is not any dependence of layers on orientation (m -, r -, a -). The suggestion is that the Cu_2O layers are bulk-relaxed, and this is happened because of deposition by reactive sputtering at room temperature.

Also, there is observation of one more broad maximum peak at 1.84 eV, at the Cu_2O layers which annealed by higher amounts of oxygen, $\text{Ar}:\text{O}_2$ 75:25 and 50:50%. It seems like there is dependence of increase of oxygen and the occurrence of this broad peak. This is explained as a local density of states between 0.3 and 0.5 eV below the conduction band minimum inside the energy gap and comes to agreement with previous investigations that have proposed that oxygen vacancies, V_o , behave as donor-like states that reside 0.4 eV below the conduction band minimum at 2.2 eV. The occurrence of V_o donor-like states that are positively charged leads in surface band bending and depletion, so the Fermi level of Cu_2O is at V_o state, figure 4.33.

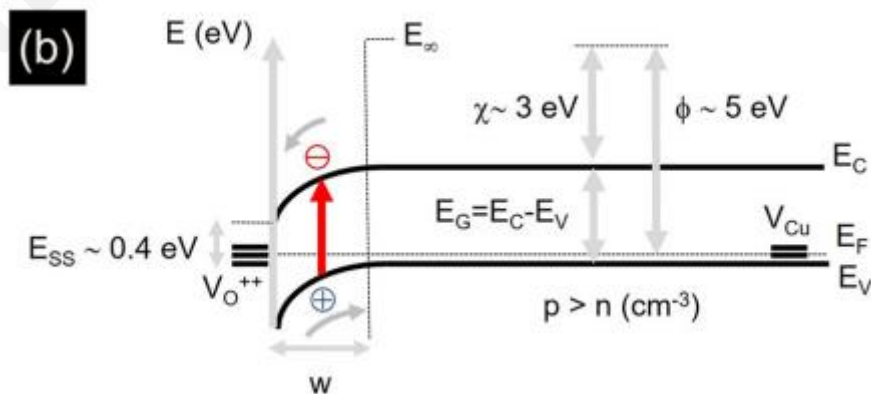


Figure 4.33: Potential conduction and valence band of Cu_2O with surface band bending and depletion [8].

The photoconductivity phenomenon in Cu_2O is due to the interaction between negatively charged copper vacancies V_{Cu}^- and positively charged oxygen vacancies V_{O}^+ or V_{O}^{++} that form pairs due to electrostatic interactions. A lot of researchers proposed that the positive charge of V_{O} influence the electrical and optical properties of Cu_2O , but Scanlon et al [38], proposed that V_{O} is not charged due to their theoretical calculations, and is energetically located close to the valence band.

Consequently, the origin of the maximum at 1.8 eV, is controversial, and it is necessary to explain. One other explanation is that the states corresponding to the maximum of 1.8 eV may be related to the formation of $\text{Cu}_2\text{O}/\text{CuO}$ nanostructures at the surface and/or grain boundaries. This formation was done by traces of CuO which are in Cu_2O layer, and act as traps considering that the $\text{Cu}_2\text{O}/\text{CuO}$ heterojunction has a straddled (type I) band line-up and conduction band discontinuity ΔE_c of 1.0 eV as shown at figure 4.34.

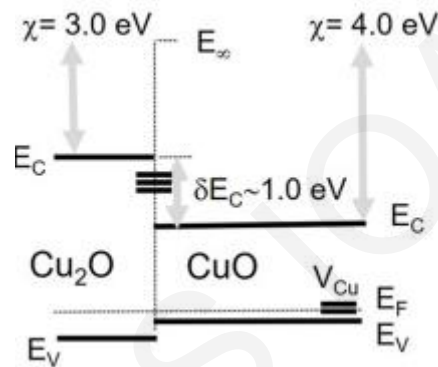


Figure 4.34: Band line-up of $\text{Cu}_2\text{O}/\text{CuO}$ nanostructures [8].

So, there is expectation of quantization inside $\text{Cu}_2\text{O}/\text{CuO}$ nanostructure, which in turn will give rise to a quantum confined level that will act as a trap. Also, if we consider that the size of $\text{Cu}_2\text{O}/\text{CuO}$ nanostructure vary and we have a broad transmission with a maximum at 1.8 eV, this will lead to an energetic distribution of traps. However, the crystal structures of these two materials, are different. The crystal structure of CuO is monoclinic with a lattice constant of 4.68 Å, and the Cu_2O has a cubic crystal structure with lattice constant of 4.2696 Å, which is smaller than the CuO lattice constant. This leads to a rising to a plethora of states related to crystallographic defects at the $\text{Cu}_2\text{O}/\text{CuO}$ interface.

Also, the high density of crystallographic defects at the $\text{Cu}_2\text{O}/\text{CuO}$ interface verified by the experiments for growing Cu_2O by thermal oxidation of a Cu foil under O_2 , as well and the poor properties and quality of this interface. The reaction starts between Cu and O_2 , leading to the formation of Cu_2O , but the latter keep the reaction to create a CuO layer above the Cu_2O . Subsequently, the two layers will separate from each other after reaching a certain thickness due to the different crystal structure that they have, and lattice mismatch. This high density may be responsible for the distribution of states at 0.4 eV below the conduction band minimum. This suggestion agrees with

other investigations, like Zivkovic and de Leeuw [39], who showed that both Cu and O₂ point imperfections give rise to states energetically located below the conduction band minimum inside the energy band gap of CuO. Also, with Shibasaki et al [17], who succeed the highest efficiency of all-oxide p-n junction solar cell, 8.4%, when Cu₂O contained minimal Cu and CuO.

So, the formation of Cu₂O/CuO nanostructure in Cu₂O layers is important because Cu₂O layers react over time with ambient O₂, which means that it is necessary to passivate their surface with a suitable oxide that will be transparent like the n-type Ga₂O₃ which is used by Shibasaki et al. Also, for the observation of Rydberg excitons in thin layers of Cu₂O as opposed to natural occurring crystals. Furthermore, for the application at solar cells the nanostructure of Cu₂O/CuO has better photocatalytic performance compared to Cu₂O or CuO single-component materials.

In conclusion, we said that suppressing the formation of crystallographic imperfections due to the oxidation of Cu₂O is critical in exploiting the properties of this novel metal-oxide semiconductor from a fundamental but also applied point of view in the context of energy conversion.

Chapter 5 – Conclusion

The pure Cu_2O was done successfully by the optimum conditions. These conditions are the deposition of Cu using $\text{Ar}:\text{O}_2$, by reactive sputtering and the next ratio: 90:10, 75:25, 50:50, and the post annealing by optimum conditions at 500°C under $\text{Ar}:\text{H}_2$, at ratio of 50:50 at 10^{-1}mbar . We find that the use of H_2 is important because suppress the oxidation and reduction of Cu_2O layers. Also, to prevent the further reaction of O_2 with Cu_2O (oxidation), and the form of CuO , we need to reduce the partial pressure of oxygen during cooling. This was happened using vacuum pressure on thermal annealing. Also, vacuum pressure prevents collisions between the vapor particles as a result the higher uniformity of material.

It has been done fundamental research on Cu_2O . According to the executed information by characterization methods, XRD, SEM, Raman Spectroscopy and UPPS, the Cu_2O layers have a cubic structure, consist of bulk-relaxed grains, and do not contain CuO , as observed by Raman Spectroscopy. By results on XRD we identify a pure Cu_2O without other impurities. Also, Cu_2O layers exhibited a detailed spectral structure and distinct peaks at 2.75, 2.5, and 2.17 eV corresponding to the indigo, blue and yellow direct gap transitions of Cu_2O as a result from ultrafast pump probe spectroscopy at room temperature.

However, we also observed a transition at 1.8 eV, which is related to a local density of states that is energetically located between ~ 0.3 and 0.5 eV below the conduction band minimum inside the energy gap. This is usually attributed to positively charged donor-like oxygen vacancies, but alternative explanations must also be considered, like the formation of $\text{CuO}/\text{Cu}_2\text{O}$ nanostructures at the surface and grain boundaries of the Cu_2O layers. It is then necessary to suppress completely the formation of $\text{CuO}/\text{Cu}_2\text{O}$ nanostructures, which we identify as one of the most important challenges in attaining high efficiency solar cells, as well as the observation of Rydberg excitons in Cu_2O layers, not just natural occurring crystals.

In conclusion, the cuprous oxide is a novel metal-oxide semiconductor according to the fundamental research that was done. Consequently, it is important to have a technological point of view in the context of energy conversion, for high efficiency solar cells, for photocatalysis e.g. water splitting, and for the reduction of CO_2 which is important in view of escalating climate crisis.

Supplementary Material

Experiment 1

Table 4.1

Constant parameters: Target: Pure Cu, inlet gases: 90%Ar – 10%O₂, Sputter Current/Time/ Cycles:120mA/4'/3cycles

Sputtering Conditions	
#_SP	Substrate
4_1	Si
4_2	Si
4_3	Si
4_4	Si
5_1	SLG
5_2	SLG
5_3	SLG
5_4	SLG

Table 4.2

Constant parameters: Inlet Gases : 100% Ar, Time / Pressure: 60'/1bar

CVD Conditions			
#_CVD	#_SP	Material	T (°C)
3374_1	4_1	Si/Cu ₂ O	300
3374_2	5_1	SLG/Cu ₂ O	300
3375_1	4_2	Si/Cu ₂ O	400
3375_2	5_2	SLG/Cu ₂ O	400
3376_1	4_3	Si/Cu ₂ O	500
3376_2	5_3	SLG/Cu ₂ O	500
3377_1	4_4	Si/Cu ₂ O	600
3377_2	5_4	SLG/Cu ₂ O	600

Experiment 2

Table 4.3

Constant parameters: Target: Pure Cu, Sputter Current/Time/Cycles: 120mA/4'/3cycles

Sputtering Conditions		
#_SP	Substrate	Inlet Gases
6_1	Si	90%Ar – 10%O ₂
6_2	Si	90%Ar – 10%O ₂
6_3	Si	90%Ar – 10%O ₂
6_4	Si	90%Ar – 10%O ₂
7_1	SLG	90%Ar – 10%O ₂
7_2	SLG	90%Ar – 10%O ₂
7_3	SLG	90%Ar – 10%O ₂
7_4	SLG	90%Ar – 10%O ₂
8_1	Si	75%Ar – 25%O ₂
8_2	Si	75%Ar – 25%O ₂
8_3	Si	75%Ar – 25%O ₂
8_4	Si	75%Ar – 25%O ₂
9_1	SLG	75%Ar – 25%O ₂
9_2	SLG	75%Ar – 25%O ₂
9_3	SLG	75%Ar – 25%O ₂
9_4	SLG	75%Ar – 25%O ₂
10_1	Si	50%Ar – 50%O ₂
10_2	Si	50%Ar – 50%O ₂
10_3	Si	50%Ar – 50%O ₂
10_4	Si	50%Ar – 50%O ₂
11_1	SLG	50%Ar – 50%O ₂
11_2	SLG	50%Ar – 50%O ₂
11_3	SLG	50%Ar – 50%O ₂
11_4	SLG	50%Ar – 50%O ₂
12_1	Si	100%O ₂
12_2	SLG	100%O ₂

Table 4.4

Constant parameters: Inlet Gases: 100%Ar, Time/ Pressure: 60'/10⁻¹mbar

CVD Conditions			
#_CVD	#_SP	T (°C)	Material
355_1	6_1	600	Si/Cu ₂ O
355_2	7_1	600	SLG/Cu ₂ O
356_1	6_2	300	Si/Cu ₂ O
356_2	7_2	300	SLG/Cu ₂ O

357_1	6_3	500	Si/Cu ₂ O
357_2	7_3	500	SLG/Cu ₂ O
358_1	6_4	400	Si/Cu ₂ O
358_2	7_4	400	SLG/Cu ₂ O
360_1	8_1	600	Si/Cu ₂ O
360_2	8_2	600	SLG/Cu ₂ O
361_1	8_3	400	Si/Cu ₂ O
361_2	8_4	400	SLG/Cu ₂ O
362_1	9_1	500	Si/Cu ₂ O
362_2	9_2	500	SLG/Cu ₂ O
362_3	10_1	500	Si/Cu ₂ O
362_4	11_1	500	SLG/Cu ₂ O
363_1	9_3	300	Si/Cu ₂ O
363_2	9_4	300	SLG/Cu ₂ O
363_3	10_2	300	Si/Cu ₂ O
363_4	11_2	300	SLG/Cu ₂ O
364_1	10_3	400	Si/Cu ₂ O
364_2	11_3	400	SLG/Cu ₂ O
365_1	10_4	600	Si/Cu ₂ O
365_2	11_4	600	SLG/Cu ₂ O
366_1	12_1	500	Si/Cu ₂ O
366_2	12_2	500	SLG/Cu ₂ O

Experiment 3

Table 4.5

Constant parameters: Target: Pure Cu, Sputter Current/Time/Cycles: 120mA/4'/3cycles

Sputtering Conditions		
#_SP	Substrate	Inlet Gases
13_1	Si	90%Ar – 10%O ₂
13_2	Si	90%Ar – 10%O ₂
13_3	Si	90%Ar – 10%O ₂
13_4	Si	90%Ar – 10%O ₂
14_1	SLG	90%Ar – 10%O ₂
14_2	SLG	90%Ar – 10%O ₂
14_3	SLG	90%Ar – 10%O ₂
14_4	SLG	90%Ar – 10%O ₂
15_1	Si	75%Ar – 25%O ₂
15_2	Si	75%Ar – 25%O ₂
15_3	Si	75%Ar – 25%O ₂
15_4	Si	75%Ar – 25%O ₂
16_1	SLG	75%Ar – 25%O ₂

16_2	SLG	75%Ar – 25%O ₂
16_3	SLG	75%Ar – 25%O ₂
16_4	SLG	75%Ar – 25%O ₂
17_1	Si	50%Ar – 50%O ₂
17_2	Si	50%Ar – 50%O ₂
17_3	Si	50%Ar – 50%O ₂
17_4	Si	50%Ar – 50%O ₂
18_1	SLG	50%Ar – 50%O ₂
18_2	SLG	50%Ar – 50%O ₂
18_3	SLG	50%Ar – 50%O ₂
18_4	SLG	50%Ar – 50%O ₂

Table 4.6

CVD Conditions					
#_CVD	#_SP	T (°C)	Material	Inlet Gases	Time/Pressure
3397_1	13_1	500	Si/Cu ₂ O	90%Ar – 10%H ₂	60'/10 ⁻¹ mbar
3397_2	14_1	500	SLG/Cu ₂ O	90%Ar – 10%H ₂	60'/10 ⁻¹ mbar
3398_1	13_2	300	Si/Cu ₂ O	90%Ar – 10%H ₂	60'/10 ⁻¹ mbar
3398_2	14_2	300	SLG/Cu ₂ O	90%Ar – 10%H ₂	60'/10 ⁻¹ mbar
3399_1	13_3	500	Si/Cu ₂ O	50%Ar – 50%H ₂	60'/10 ⁻¹ mbar
3399_2	14_3	500	SLG/Cu ₂ O	50%Ar – 50%H ₂	60'/10 ⁻¹ mbar
3400_1	13_4	500	Si/Cu ₂ O	100%H ₂	60'/10 ⁻¹ mbar
3400_2	14_4	500	SLG/Cu ₂ O	100%H ₂	60'/10 ⁻¹ mbar
3401_1	15_1	500	Si/Cu ₂ O	50%Ar – 50%H ₂	60'/10 ⁻¹ mbar
3401_2	16_1	500	SLG/Cu ₂ O	50%Ar – 50%H ₂	60'/10 ⁻¹ mbar
3401_3	17_1	500	Si/Cu ₂ O	50%Ar – 50%H ₂	60'/10 ⁻¹ mbar
3401_4	18_1	500	SLG/Cu ₂ O	50%Ar – 50%H ₂	60'/10 ⁻¹ mbar
3402_1	15_2	800	Si/Cu ₂ O	50%Ar – 50%H ₂	60'/10 ⁻¹ mbar
3402_2	17_2	800	Si/Cu ₂ O	50%Ar – 50%H ₂	60'/10 ⁻¹ mbar
3403_1	15_3	300	Si/Cu ₂ O	50%Ar – 50%H ₂	60'/10 ⁻¹ mbar
3403_2	16_2	300	SLG/Cu ₂ O	50%Ar – 50%H ₂	60'/10 ⁻¹ mbar
3403_3	17_3	300	Si/Cu ₂ O	50%Ar – 50%H ₂	60'/10 ⁻¹ mbar
3403_4	18_2	300	SLG/Cu ₂ O	50%Ar – 50%H ₂	60'/10 ⁻¹ mbar
3404_1	15_4	300	Si/Cu ₂ O	50%Ar – 50%H ₂	120'/10 ⁻¹ mbar
3404_2	16_3	300	SLG/Cu ₂ O	50%Ar – 50%H ₂	120'/10 ⁻¹ mbar
3404_3	17_4	300	Si/Cu ₂ O	50%Ar – 50%H ₂	120'/10 ⁻¹ mbar
3404_4	18_3	300	SLG/Cu ₂ O	50%Ar – 50%H ₂	120'/10 ⁻¹ mbar

Experiment 4

Table 4.7

Constant parameters: Target: Pure Cu

Sputtering Conditions			
#_SP	Substrate	Inlet Gases	Sputter Current/Time/Cycles
19_1	r-Al ₂ O ₃	50%Ar – 50%O ₂	120mA/4'/3cycles
19_2	m-Al ₂ O ₃	50%Ar – 50%O ₂	120mA/4'/3cycles
19_3	Si	50%Ar – 50%O ₂	120mA/4'/3cycles
19_4	Si	50%Ar – 50%O ₂	120mA/4'/3cycles
19_5	Si	50%Ar – 50%O ₂	120mA/4'/3cycles
20_1	r-Al ₂ O ₃	90%Ar – 10%O ₂	120mA/4'/3cycles
20_2	m-Al ₂ O ₃	90%Ar – 10%O ₂	120mA/4'/3cycles
20_3	a-Al ₂ O ₃	90%Ar – 10%O ₂	120mA/4'/3cycles
20_4	Si	90%Ar – 10%O ₂	120mA/4'/3cycles
20_5	Si	90%Ar – 10%O ₂	120mA/4'/3cycles
20_6	Si	90%Ar – 10%O ₂	120mA/4'/3cycles
21_1	r-Al ₂ O ₃	75%Ar – 25%O ₂	120mA/4'/3cycles
21_2	m-Al ₂ O ₃	75%Ar – 25%O ₂	120mA/4'/3cycles
21_3	a-Al ₂ O ₃	75%Ar – 25%O ₂	120mA/4'/3cycles
21_4	Si	75%Ar – 25%O ₂	120mA/4'/3cycles
21_5	Si	75%Ar – 25%O ₂	120mA/4'/3cycles
21_6	Si	75%Ar – 25%O ₂	120mA/4'/3cycles
22_1	r-Al ₂ O ₃	75%Ar – 25%O ₂	120mA/4'/1cycle
22_2	m-Al ₂ O ₃	75%Ar – 25%O ₂	120mA/4'/1cycle
22_3	a-Al ₂ O ₃	75%Ar – 25%O ₂	120mA/4'/1cycle
22_4	Si	75%Ar – 25%O ₂	120mA/4'/1cycle
22_5	Si	75%Ar – 25%O ₂	120mA/4'/1cycle
23_1	r-Al ₂ O ₃	90%Ar – 10%O ₂	120mA/4'/1cycle
23_2	m-Al ₂ O ₃	90%Ar – 10%O ₂	120mA/4'/1cycle
23_3	a-Al ₂ O ₃	90%Ar – 10%O ₂	120mA/4'/1cycle
23_4	Si	90%Ar – 10%O ₂	120mA/4'/1cycle
23_5	Si	90%Ar – 10%O ₂	120mA/4'/1cycle
24_1	r-Al ₂ O ₃	50%Ar – 50%O ₂	120mA/4'/1cycle
24_2	m-Al ₂ O ₃	50%Ar – 50%O ₂	120mA/4'/1cycle
24_3	a-Al ₂ O ₃	50%Ar – 50%O ₂	120mA/4'/1cycle
24_4	Si	50%Ar – 50%O ₂	120mA/4'/1cycle
24_5	Si	50%Ar – 50%O ₂	120mA/4'/1cycle

Table 4.8Constant parameters: T= 500°C, Time/Pressure: 60'/10⁻¹mbar

CVD Conditions			
#_CVD	#_SP	Material	Inlet Gases
3426_1	20_1	r-Al ₂ O ₃	50%Ar – 50%H ₂
3426_2	20_2	m-Al ₂ O ₃	50%Ar – 50%H ₂
3426_3	20_3	a-Al ₂ O ₃	50%Ar – 50%H ₂
3426_4	20_4	Si	50%Ar – 50%H ₂
3426_5	21_4	Si	50%Ar – 50%H ₂
3426_6	19_3	Si	50%Ar – 50%H ₂
3427_1	23_1	r-Al ₂ O ₃	50%Ar – 50%H ₂
3427_2	23_2	m-Al ₂ O ₃	50%Ar – 50%H ₂
3427_3	23_3	a-Al ₂ O ₃	50%Ar – 50%H ₂
3427_4	23_4	Si	50%Ar – 50%H ₂
3427_5	22_4	Si	50%Ar – 50%H ₂
3427_6	24_4	Si	50%Ar – 50%H ₂
3428_1	21_1	r-Al ₂ O ₃	50%Ar – 50%H ₂
3428_2	21_2	m-Al ₂ O ₃	50%Ar – 50%H ₂
3428_3	21_3	a-Al ₂ O ₃	50%Ar – 50%H ₂
3428_4	22_1	Si	50%Ar – 50%H ₂
3428_5	22_2	Si	50%Ar – 50%H ₂
3428_6	22_3	Si	50%Ar – 50%H ₂
3429_1	24_1	r-Al ₂ O ₃	50%Ar – 50%H ₂
3429_2	24_2	m-Al ₂ O ₃	50%Ar – 50%H ₂
3429_3	24_3	a-Al ₂ O ₃	50%Ar – 50%H ₂
3429_4	20_5	Si	50%Ar – 50%H ₂
3429_5	22_5	Si	50%Ar – 50%H ₂
3429_6	24_5	Si	50%Ar – 50%H ₂
3430_1	19_1	r-Al ₂ O ₃	100%H ₂
3430_2	19_2	m-Al ₂ O ₃	100%H ₂
3430_3	20_6	Si	100%H ₂
3430_4	21_5	Si	100%H ₂
3430_5	19_4	Si	100%H ₂

References

- [1] S. Communication, "Nanotechnology : The Future Medicine," vol. 3, no. 1, pp. 32–33, 2010, doi: 10.4103/0974-2077.63301.
- [2] J. Pastuszak, "Photovoltaic Cell Generations and Current Research Directions for Their Development," 2022.
- [3] A. Mittiga, E. Salza, F. Sarto, M. Tucci, and R. Vasanthi, "Heterojunction solar cell with 2% efficiency based on a Cu₂O substrate," *Appl. Phys. Lett.*, vol. 88, no. 16, pp. 2–4, 2006, doi: 10.1063/1.2194315.
- [4] "Climate Change: Atmospheric Carbon Dioxide | NOAA Climate.gov." <https://www.climate.gov/news-features/understanding-climate/climate-change-atmospheric-carbon-dioxide> (accessed Mar. 29, 2024).
- [5] S. Mohan *et al.*, "A Critical Study of Cu₂O: Synthesis and Its Application in CO₂ Reduction by Photochemical and Electrochemical Approaches," *Catalysts*, vol. 12, no. 4, 2022, doi: 10.3390/catal12040445.
- [6] I. V. Bagal *et al.*, "Cu₂O as an emerging photocathode for solar water splitting - A status review," *Int. J. Hydrogen Energy*, vol. 44, no. 39, pp. 21351–21378, Aug. 2019, doi: 10.1016/j.ijhydene.2019.06.184.
- [7] V. Loosdrecht, "Para-excitons in Cu₂O — a new approach," 2005, doi: 10.1016/j.jlumin.2004.09.038.
- [8] E. Proutzou *et al.*, "Critical and controversial issues pertaining to the growth and properties of Cu₂O in the context of energy conversion," 2023, doi: 10.1063/5.0165856.
- [9] S. Noda, H. Shima, and H. Akinaga, "Cu₂O/ZnO Heterojunction Solar Cells Fabricated by Magnetron-Sputter Deposition Method Films Using Sintered Ceramics Targets," *J. Phys. Conf. Ser.*, vol. 433, no. 1, p. 012027, Apr. 2013, doi: 10.1088/1742-6596/433/1/012027.
- [10] S. Nandy, A. Banerjee, E. Fortunato, and R. Martins, "A Review on Cu₂O and Cu⁺-Based *p*-Type Semiconducting Transparent Oxide Materials: Promising Candidates for New Generation Oxide Based Electronics," *Rev. Adv. Sci. Eng.*, vol. 2, no. 4, pp. 273–304, 2013, doi: 10.1166/rase.2013.1045.
- [11] D. S. C. Halin, I. A. Talib, A. R. Daud, and M. A. A. Hamid, "Characterizations of cuprous oxide thin films prepared by sol-gel spin coating technique with different additives for the photoelectrochemical solar cell," *Int. J. Photoenergy*, vol. 2014, 2014, doi: 10.1155/2014/352156.
- [12] C. Qin, Y. Wang, Z. Lou, S. Yue, W. Niu, and L. Zhu, "Surface modification and stoichiometry control of Cu₂O/SnO₂ heterojunction solar cell by an ultrathin MgO tunneling layer," *J. Alloys Compd.*, vol. 779, pp. 387–393, 2019, doi: 10.1016/j.jallcom.2018.11.155.

- [13] R. Kumar, K. Bergum, H. N. Riise, E. Monakhov, A. Galeckas, and B. G. Svensson, "Impact of post annealing and hydrogen implantation on functional properties of Cu₂O thin films for photovoltaic applications," *J. Alloys Compd.*, vol. 825, p. 153982, Jun. 2020, doi: 10.1016/J.JALLCOM.2020.153982.
- [14] G. Liu *et al.*, "Investigation and mitigation of degradation mechanisms in Cu₂O photoelectrodes for CO₂ reduction to ethylene," *Nat. Energy*, vol. 6, no. 12, pp. 1124–1132, Dec. 2021, doi: 10.1038/S41560-021-00927-1.
- [15] S. Ghosh *et al.*, "Deposition of thin films of different oxides of copper by RF reactive sputtering and their characterization," *Vacuum*, vol. 57, no. 4, pp. 377–385, 2000, doi: 10.1016/S0042-207X(00)00151-2.
- [16] Ø. Nordseth, R. Kumar, K. Bergum, I. Chilibon, S. E. Foss, and E. Monakhov, "Nitrogen-Doped Cu₂O Thin Films for Photovoltaic Applications," pp. 1–9, 2019.
- [17] S. Shibasaki *et al.*, "Highly transparent Cu₂O absorbing layer for thin film solar cells," *Appl. Phys. Lett.*, vol. 119, no. 24, p. 242102, Dec. 2021, doi: 10.1063/5.0072310.
- [18] C. L. Chu, H. C. Lu, C. Y. Lo, C. Y. Lai, and Y. H. Wang, "Physical properties of copper oxide thin films prepared by dc reactive magnetron sputtering under different oxygen partial pressures," *Phys. B Condens. Matter*, vol. 404, no. 23–24, pp. 4831–4834, 2009, doi: 10.1016/j.physb.2009.08.185.
- [19] M. F.K, "International Journal of Thin Film Science and Technology Optical characterization of Copper Oxide thin films prepared by reactive dc magnetron sputtering for solar cell applications © 2012 NSP characterization of Copper Oxide thin films prepared by Optic," vol. 2, no. 1, 2013.
- [20] A. Ogwu, T. H. Darma, and E. Bouquerel, "Electrical resistivity of copper oxide thin films prepared by reactive magnetron sputtering," no. June 2018, 2007.
- [21] Y. Okamoto *et al.*, "Passivation of defects in nitrogen-doped polycrystalline Cu₂O thin films by crown-ether cyanide treatment," *Appl. Phys. Lett.*, vol. 82, no. 7, p. 1060, Feb. 2003, doi: 10.1063/1.1555267.
- [22] S. Ishizuka, S. Kato, Y. Okamoto, and K. Akimoto, "Hydrogen treatment for polycrystalline nitrogen-doped Cu₂O thin film," *J. Cryst. Growth*, vol. 237–239, no. 1-4 I, pp. 616–620, Apr. 2002, doi: 10.1016/S0022-0248(01)01975-3.
- [23] K. P. Hering, C. Kandzia, J. Benz, B. G. Kramm, M. Eickhoff, and P. J. Klar, "Hydrogen induced mobility enhancement in RF sputtered Cu₂O thin films," *J. Appl. Phys.*, vol. 120, no. 18, p. 185705, Nov. 2016, doi: 10.1063/1.4966605.
- [24] T. Miyata, H. Tokunaga, K. Watanabe, N. Ikenaga, and T. Minami, "Photovoltaic properties of low-damage magnetron-sputtered n-type ZnO thin film/p-type Cu₂O sheet heterojunction solar cells," *Thin Solid Films*, vol. 697, Mar. 2020, doi: 10.1016/J.TSF.2020.137825.
- [25] H. A. Al-Jawhari, "A review of recent advances in transparent p-type Cu₂O-based thin film transistors," *Mater. Sci. Semicond. Process.*, vol. 40, pp. 241–








- 252, Dec. 2015, doi: 10.1016/J.MSSP.2015.06.063.
- [26] S. C. Chen *et al.*, "Optoelectronic properties of Cu₃N thin films deposited by reactive magnetron sputtering and its diode rectification characteristics," *Journal of Alloys and Compounds*, vol. 789, pp. 428–434, 2019, doi: 10.1016/j.jallcom.2019.02.268.
- [27] L. C. Chen, "Review of preparation and optoelectronic characteristics BN of Cu₂O-based solar cells with nanostructure," *Mater. Sci. Semicond. Process.*, vol. 16, no. 5, pp. 1172–1185, 2013, doi: 10.1016/j.mssp.2012.12.028.
- [28] D. S. Murali, S. Kumar, R. J. Choudhary, A. D. Wadikar, M. K. Jain, and A. Subrahmanyam, "Synthesis of Cu₂O from CuO thin films: Optical and electrical properties," *AIP Adv.*, vol. 5, no. 4, p. 047143, Apr. 2015, doi: 10.1063/1.4919323.
- [29] Y. S. Lee, M. T. Winkler, S. C. Siah, R. Brandt, and T. Buonassisi, "Hall mobility of cuprous oxide thin films deposited by reactive direct-current magnetron sputtering," *Appl. Phys. Lett.*, vol. 98, no. 19, May 2011, doi: 10.1063/1.3589810.
- [30] D. Płoch, M. Bester, G. Wisz, P. Sawicka-chudy, and M. Sibi, "TiO₂ / CuO / Cu₂O Photovoltaic Nanostructures Prepared by DC Reactive Magnetron Sputtering," pp. 1–11, 2022.
- [31] T. Minami, T. Miyata, and Y. Nishi, "Efficiency improvement of Cu₂O-based heterojunction solar cells fabricated using thermally oxidized copper sheets," *Thin Solid Films*, vol. 559, pp. 105–111, 2014, doi: 10.1016/j.tsf.2013.11.026.
- [32] T. M. Besmann, D. P. Stinton, and R. A. Lowden, "Chemical Vapor Deposition Techniques," *MRS Bull.*, vol. 13, no. 11, pp. 45–51, 1988, doi: 10.1557/S0883769400063910.
- [33] J. R. Creighton and P. Ho, "Introduction to Chemical Vapour Deposition," pp. 1–28, 2010, doi: 10.1007/978-1-84882-894-0_1.
- [34] J. Epp, *X-Ray Diffraction (XRD) Techniques for Materials Characterization*. Elsevier Ltd, 2016.
- [35] R. Cremer *et al.*, "Deposition and characterization of metastable Cu₃N layers for applications in optical data storage," *Mikrochim. Acta*, vol. 133, no. 1–4, pp. 299–302, 2000, doi: 10.1007/s006040070109.
- [36] A. Chauhan, "Powder XRD Technique and its Applications in Science and Technology," *J. Anal. Bioanal. Tech.*, vol. 5, no. 6, 2014, doi: 10.4172/2155-9872.1000212.
- [37] M. D. A. Pereira-da-silva and F. A. Ferri, *1 - Scanning Electron Microscopy*. Elsevier Inc., 2017.
- [38] D. O. Scanlon, B. J. Morgan, G. W. Watson, and A. Walsh, "Acceptor levels in p-type Cu₂O: Rationalizing theory and Experiment," *Phys. Rev. Lett.*, vol. 103, no. 9, pp. 1–4, 2009, doi: 10.1103/PhysRevLett.103.096405.

- [39] A. Živković and N. H. De Leeuw, “Exploring the formation of intrinsic p -type and n -type defects in CuO,” *Phys. Rev. Mater.*, vol. 4, no. 7, 2020, doi: 10.1103/PhysRevMaterials.4.074606.

ANDREAS IOANNOU

RESEARCH ARTICLE | OCTOBER 20 2023

Critical and controversial issues pertaining to the growth and properties of Cu_2O in the context of energy conversion

Eleni Prountzou ; Andreas Ioannou ; Dimitrios Sapalidis ; Eleni Pavlidou; Maria Katsikini ; Andreas Othonos ; Matthew Zervos  



APL Energy 1, 036102 (2023)
<https://doi.org/10.1063/5.0165856>



View
Online



Export
Citation



APL Quantum
First Articles Online
No Article Processing Charges for Submissions
Through December 31, 2024
[Read Now](#)



Critical and controversial issues pertaining to the growth and properties of Cu_2O in the context of energy conversion

Cite as: APL Energy 1, 036102 (2023); doi: 10.1063/5.0165856

Submitted: 30 June 2023 • Accepted: 9 October 2023 •

Published Online: 20 October 2023



Eleni Prountzou,¹ Andreas Ioannou,² Dimitrios Sapalidis,¹ Eleni Pavlidou,¹ Maria Katsikini,¹ Andreas Othonos,³ and Matthew Zervos^{2,a)}

AFFILIATIONS

¹School of Physics, Aristotle University of Thessaloniki, GR-54124 Thessaloniki, Greece

²Nanostructured Materials and Devices Laboratory, School of Engineering, University of Cyprus, P.O. Box 20537, Nicosia 1678, Cyprus

³Laboratory of Ultrafast Science, School of Physical Sciences, University of Cyprus, P.O. Box 20537, Nicosia 1678, Cyprus

^{a)}Author to whom correspondence should be addressed: zervos@ucy.ac.cy

ABSTRACT

Cu_2O has been deposited on m-, r-, and a- Al_2O_3 by reactive sputtering of Cu using Ar with different contents of O_2 followed by annealing under carefully optimized conditions at 500°C under Ar: H_2 in order to prevent the oxidation and reduction of the Cu_2O layers, which have a cubic crystal structure and are bulk-relaxed. We find that the content of O_2 influences the structural and optical properties of the Cu_2O layers that exhibited a detailed spectral structure and distinct peaks at 2.75, 2.54, and 2.17 eV corresponding to the indigo, blue, and yellow direct gap transitions of Cu_2O as observed by ultrafast pump-probe spectroscopy at room temperature. However, we also observed a transition at 1.8 eV that is related to the occurrence of states ~ 0.4 eV below the conduction band minimum of Cu_2O . We discuss the controversial origin of these states, which are usually attributed to donor-like oxygen vacancy states, and suggest that the origin of these states may be related to traps at the interfaces of $\text{CuO}/\text{Cu}_2\text{O}$ nanostructures, which is important in the context of energy conversion pertaining to solar cells and photocatalysis.

© 2023 Author(s). All article content, except where otherwise noted, is licensed under a Creative Commons Attribution (CC BY) license (<http://creativecommons.org/licenses/by/4.0/>). <https://doi.org/10.1063/5.0165856>

I. INTRODUCTION

Cuprous oxide (Cu_2O) is a p-type metal-oxide semiconductor that has a fundamental, direct energy bandgap of 2.1 eV and a cubic crystal structure belonging to the $\text{Pn}3\text{m}$ crystallographic space group with a lattice constant of $a = 4.2696 \text{ \AA}$. The native p-type conductivity of Cu_2O is related to the occurrence of copper vacancies, V_{Cu} , that give rise to acceptor-like states located at $E_{\text{A}} \sim 0.2$ eV above the valence band maximum.¹

Cu_2O has been suggested to be suitable as a solar cell absorber for a long time due to the fact that it has a direct energy gap but also an absorption coefficient that can reach $\alpha = 10^5$ in the visible.² However, so far, device efficiencies have been limited to less than 10%, despite the fact that the theoretical efficiency of Cu_2O solar cells is $\sim 20\%$.³

A Cu_2O p-n junction solar cell with an efficiency of $\sim 2\%$ was fabricated by Elfadill *et al.*⁴ using Cl-doped n-type Cu_2O and Na-doped p-type Cu_2O , while a Cu_2O heterojunction solar cell (HJSC), with an efficiency of 3.4% and a very small cell area of $8 \times 10^{-3} \text{ cm}^2$, was fabricated by Ravindra *et al.*⁵ Others, like Markose *et al.*,⁶ fabricated an $\text{ITO}/\text{B}:\text{Cu}_2\text{O}/\text{SiO}_x/\text{n-Si}/\text{Ag}$ HJSC that exhibited an open-circuit voltage of 370 mV, a short-circuit current density of 36.5 mA/cm^2 , and an efficiency of 5.4%, but this was obtained on Si. Similarly, Liu *et al.*⁷ employed a variety of interfacial engineering and light management strategies to push the efficiency limit of $\text{Cu}_2\text{O}/\text{Si}$ solar cells and obtained a power conversion efficiency of 9.54%. More importantly, an all-oxide HJSC based on p-type Cu_2O and n-type Ga_2O_3 was fabricated by Shibasaki *et al.*⁸ on glass and displayed an efficiency of 8.4% when the Cu_2O contained minimal Cu and CuO.

In contrast to solar cells, Cu₂O/CuO layers have been shown to have better photocatalytic performance compared to Cu₂O or CuO single-component materials.⁹ Cu₂O is, therefore, an active topic of investigation for the fabrication of solar cells and photocatalysis, i.e., water splitting,¹⁰ but also for CO₂ reduction,¹¹ which is important in view of the escalating climate crisis.^{10,12} Furthermore, Cu₂O is interesting from a fundamental point of view, as excitons were observed for the first time in Cu₂O by Gross¹³ in 1956, after which it has been used as an archetype for understanding the novel properties of excitons.^{14–16} Rydberg excitons with principal quantum numbers as large as $n = 25$ and giant wavefunction extensions in excess of $2 \mu\text{m}$ were observed by Kazimierczuk *et al.* in natural gem crystals of Cu₂O.^{17,18} Excitons with principal quantum numbers up to $n = 3$ have been observed in other semiconductors such as GaAs,¹⁹ but excitons with principal quantum numbers as large as $n = 25$ have only been observed in Cu₂O. Very recently, Rydberg exciton-polaritons were also detected in a SiO₂/Ta₂O₅/Cu₂O/Ta₂O₅/SiO₂ Fabry–Pérot cavity in which the Cu₂O layer was cut from a naturally occurring crystal and attached with epoxy to Ta₂O₅/SiO₂.²⁰ It is desirable then to obtain high purity and good crystal quality Cu₂O layers, which are important not just from a fundamental but also a technological point of view.

Cu₂O has been deposited using many different methods such as molecular beam epitaxy (MBE), atomic layer deposition (ALD),²¹ pulsed laser deposition (PLD), electrodeposition (ELD),²² aerosol assisted chemical vapor deposition (AACVD),²³ successive ionic layer adsorption and reaction (SILAR),²⁴ sputtering,^{8,25} or the thermal oxidation of copper.²⁶ The hole density of un-doped (u/d) Cu₂O is of the order of $p \sim 10^{15} \text{ cm}^{-3}$,²⁷ and room temperature hole mobilities of $\mu_p = 100 \text{ cm}^2/\text{Vs}$ have been achieved,²⁸ while the mobility of holes in Cu₂O at 4.2 K has been shown to reach quite large values of $\mu_p = 1.8 \times 10^5 \text{ cm}^2/\text{Vs}$.²⁹ In general, p-type doping of Cu₂O has been carried out using Si,³⁰ Mg,³¹ and N,³² while n-type doping is possible with F, Cl, and Br³³ but also with Al.³⁴

However, despite ongoing efforts, single crystal epitaxial Cu₂O is not easy to obtain even by MBE on MgO (100), which has a lattice mismatch of $\sim 1\%$ with Cu₂O. In other words, the epitaxy of Cu₂O on MgO (100) is not trivial and differs from simple cube-on-cube epitaxy, thereby giving Cu₂O epi-layers with multiple orientations.³⁵ Consequently, it is necessary to anneal the Cu₂O layers in order to improve their crystallinity. It is useful to mention at this point that single crystal Cu₂O has been obtained in the past by Toth *et al.*²⁶ back in the 1960s via the thermal oxidation of metallic Cu foils between 1020 and 1050 °C, which resulted in polycrystalline Cu₂O that was annealed at even higher temperatures. This promoted recrystallization and the formation of single-crystals, but Cu₂O reacts with O₂ according to $2\text{Cu}_2\text{O} + \text{O}_2 \rightarrow 4\text{CuO}$ at the surface or grain boundaries. The suppression of this reaction is critical in obtaining high efficiency solar cells, like the p-type Cu₂O/n-type Ga₂O₃ solar cell fabricated by reactive sputtering on glass by Shibasaki *et al.*⁸ This can be achieved by reducing the partial pressure of oxygen during cooling in order to prevent a transition across the phase boundary between Cu₂O and CuO, in accordance with Schmidt-Whitley *et al.*³⁶ However, the process of annealing Cu₂O layers at elevated temperatures is complicated due to thermal inter-diffusion and reactions that will occur between the Cu₂O and the underlying substrate of choice. It has been shown that sapphire,

i.e., Al₂O₃, can be used as a barrier against the thermal diffusion of copper up to 750 °C.^{37,38} Wagner *et al.*³⁹ obtained Cu₂O on a-Al₂O₃ by Vapor Phase Epitaxy (VPE) via melting Cu at 1080 °C. Others, like Ottosson and Carlsson,⁴⁰ have grown Cu₂O on r-Al₂O₃, but the Cu₂O will react with Al₂O₃ according to the reaction $\text{Cu}_2\text{O} + \text{Al}_2\text{O}_3 \rightarrow \text{CuAlO}_2$ under N₂ at temperatures higher than 700 °C.⁴¹ Lower temperatures between 450 and 550 °C have been shown to yield lower crystallinity CuAlO₂,⁴² which is a p-type transparent conducting oxide (TCO) with an energy bandgap of 3.4 eV.⁴³ It is then necessary to anneal the Cu₂O layers on Al₂O₃ at intermediate temperatures to prevent thermal inter-diffusion and reactions.

Here we have deposited Cu₂O on m-, r-, and a-Al₂O₃ by reactive sputtering of Cu using Ar:O₂ with different ratios of 90:10, 75:25, or 50:50% v/v, followed by annealing under optimum conditions at 500 °C under Ar:H₂ at 10^{-1} mbar. In the past, only a few, like Unutulmazsoy *et al.*,⁴⁴ annealed Cu₂O using Ar containing 5% v/v H₂ at 10^{-4} mbar and 300 °C. Here we have carried out a systematic investigation into the optimization of the annealing conditions over a wider temperature range and flows of H₂ in order to suppress the oxidation and reduction of the Cu₂O layers and subsequently *probe* the electronic band structure and gap states of this novel p-type metal-oxide semiconductor by ultrafast *pump-probe* spectroscopy (UPPS) in order to gain an understanding of the generation and recombination mechanisms that are important from an applied and fundamental point of view. The Cu₂O layers obtained in this fashion exhibited a detailed spectral structure and distinct peaks corresponding to the indigo, blue, and yellow direct gap transitions of Cu₂O as observed by UPPS at room temperature, but we also observed a transition related to the occurrence of states ~ 0.4 eV below the conduction band minimum of Cu₂O. We discuss the controversial origin of these states, which are usually attributed to oxygen vacancy donor-like states, and suggest that their origin may instead be related to the formation of CuO/Cu₂O nanostructures.

II. EXPERIMENTAL

Square samples ($10 \times 10 \text{ mm}^2$) were cut from m-, r-, and a-Al₂O₃ and n-type Si (001), after which they were cleaned sequentially in trichloroethylene, methanol, and acetone and rinsed in isopropanol and de-ionized water at 20 °C. Subsequently, they were dried with nitrogen, followed by a dehydration bake at 120 °C. A Cu₂O layer was deposited by reactive sputtering of a Cu (99.999%) target with Ar:O₂ at 10^{-2} mbar. The thickness of the Cu₂O layers was either 100 nm or 300 nm, and the Ar:O₂ ratio used during deposition was 90:10, 75:25, or 50:50% v/v. The Cu₂O layers were deposited on m-, r-, and a-Al₂O₃ at room temperature and were subsequently annealed under optimum conditions in a 1 in. hot wall, low pressure chemical vapor deposition reactor capable of reaching 1100 °C, which was fed by a manifold consisting of four mass flow controllers connected to Ar, NH₃, O₂, and H₂. The reactor was initially purged for 10 min, and then the temperature was ramped up to 500 °C at 30 °C/min. Upon reaching 500 °C, the Cu₂O layers were annealed for 1 h, after which cooling took place. The samples were removed only when the temperature fell below 100 °C. A constant flow of 50 ml/min of Ar and 50 ml/min of H₂ was maintained throughout the entire process.

The surface morphology of the Cu_2O thin films was investigated using JSM-7610F+ Field-Emission Scanning Electron Microscopy (FESEM). The samples were coated with carbon film using a JEOL-4X vacuum evaporator, and the thickness of the carbon coating did not exceed 200 Å. The composition of the Cu_2O was measured using an Oxford (AZtec Energy Advanced) Energy Dispersive X-ray Spectroscopy (EDS) system attached to the FESEM.

The Raman spectra were recorded in the backscattering geometry using a DILOR spectrometer equipped with an optical microscope and 100× objective along with an Ar+ laser operating at 514.532 and 487.986 nm that was used for excitation with a power of about 4.5 and 7.5 mW on sample for the green (514.532 nm) and blue (487.986 nm) laser lines, respectively. Energy calibration of the spectra was performed utilizing a neon lamp.

The structural properties of the Cu_2O films were also investigated by X-Ray Diffraction (XRD) in the Bragg–Brentano geometry using a two-cycle Rigaku Ultima+ powder x-ray diffractometer with $\text{CuK}\alpha$ radiation ($\lambda = 1.54056 \text{ \AA}$) operating at 40 kV and 30 mA.

Finally, the properties of the Cu_2O layers were investigated by measuring the time evolution of the differential transmission (dT/T) on a ps time scale by ultrafast pump–probe spectroscopy (UPPS) using a pump of $\lambda_{\text{PU}} = 400$ or 260 nm and a probe that was varied between $\lambda_{\text{PR}} = 450$ and 750 nm. The measurements were carried out in a typical pump–probe optical setup, as described in detail elsewhere.⁴⁵

III. RESULTS AND DISCUSSION

It is instructive to begin by describing the optimization of the growth and annealing conditions of Cu_2O . Initially, Cu_2O layers were deposited on n-type Si (001) and soda lime glass (SLG) by reactive sputtering of Cu under Ar: O_2 with a ratio of 90:10, 75:25, or 50:50% v/v and annealed at temperatures ranging from 300 to 600 °C under a flow of 100 ml/min Ar for 60 min at 10^{-1} mbar. All of the Cu_2O layers obtained in this way exhibited small but clear and well resolved peaks in the XRD corresponding to both CuO and Cu_2O . Consequently, an identical set of Cu_2O layers was prepared and annealed between 300 and 600 °C under Ar: H_2 . The content of H_2 was 10, 50, or 100% v/v at 10^{-1} mbar, keeping all

else equal. We find that the optimum annealing temperature for the Cu_2O layers is 500 °C. The Cu_2O layers exhibited clear and well resolved peaks belonging to the cubic crystal structure of Cu_2O , as shown in Fig. 1(a), but the addition of 10% H_2 was not adequate to suppress the oxidation of Cu_2O , i.e., $2\text{Cu}_2\text{O} + \text{O}_2 \rightarrow 4\text{CuO}$, as we also observed peaks belonging to the monoclinic crystal structure of CuO in Fig. 1(a). On the other hand, 100% H_2 leads to the reduction of Cu_2O and CuO to metallic Cu according to $\text{Cu}_2\text{O} + \text{H}_2 \rightarrow 2\text{Cu} + \text{H}_2\text{O}$. In contrast, 50% H_2 was sufficient to prevent the oxidation as well as the reduction of Cu_2O , which has a cubic crystal structure and corresponding unit cell shown in Fig. 1(b). These findings are consistent with Kim *et al.*,⁴⁶ who showed that a large flow of H_2 will reduce CuO into metallic Cu without the formation of intermediate Cu_4O_3 or Cu_2O . However, only a few have investigated the effect of H_2 on the reduction of Cu_2O layers, such as Unutulmazsoy *et al.*,⁴⁴ who annealed Cu_2O using Ar containing 5% v/v H_2 at 10^{-4} mbar and 300 °C and argued that intersecting grain boundaries and the porosity of Cu_2O provide diffusion paths and traps for hydrogen. Consequently, the higher grain boundary density of the thinner Cu_2O layers results in a faster reduction that starts once a certain density of accumulated oxygen vacancies is reached at the periphery of the Cu_2O grains. Hence, a careful adjustment of the reducing conditions and flow of H_2 needs to be carried out when annealing Cu_2O .

After optimization, Cu_2O layers with a thickness of 100 and 300 nm were deposited on m-, r-, and a- Al_2O_3 by reactive sputtering under Ar: O_2 (90:10, 75:25, 50:50% v/v), which were annealed under 50 ml/min Ar: 50 ml/min H_2 at 500 °C. The Cu_2O layers on m-, r-, and a- Al_2O_3 were semi-transparent, had a light-yellow color, and consist of grains with a size of $89.62 \pm 7.87 \text{ nm}$, as shown by the Scanning Electron Microscopy (SEM) image of the Cu_2O and corresponding histogram shown as an inset in Fig. 2(a). Evidently, the Cu_2O layers are nanostructured, and the protrusions on the surface with a diameter of $d \sim 1 \mu\text{m}$ were found to be slightly richer in Cu by $\sim 5 \text{ at. \%}$. We find that the Cu_2O layers consist of Cu and O by EDS; Al was also detected due to the underlying Al_2O_3 , as the information depth of EDS is about $1.5\text{--}2 \mu\text{m}$.^{47,48} The structural properties and composition of the Cu_2O layers were investigated further by Raman spectroscopy. The Raman spectra of the Cu_2O layers grown on m-, r-, and a- Al_2O_3 , which were obtained with different Ar: O_2 contents, are shown in Fig. 2(b). The unit cell of Cu_2O contains six atoms, resulting in 18 phonon modes, 15 of which are optical lattice vibrations and 3 are acoustic vibrational modes. The vibrational mode symmetries at the center of the Brillouin zone ($k = 0$) are^{49–51} $A_{2u} \oplus E_u \oplus T_{2g} \oplus 3T_{1u} \oplus T_{2u}$. A, E, and T symmetries correspond to one-, two-, and threefold-degenerate phonons, respectively. All symmetries represent optical phonons except for T_{1u} , which corresponds to the three acoustic vibrational modes. Phonons having T_{2g} symmetry are the only Raman active vibrational modes of Cu_2O , while the two remaining T_{1u} symmetry modes are infrared active optical modes, and the rest, i.e., phonons having A_{2u} , E_u , and T_{2u} symmetry, are non-active Raman and infrared modes, i.e., silent modes.⁵¹ According to group theory, only the peak due to the threefold-degenerate T_{2g} lattice vibrational mode should appear in the Raman spectra of a natural Cu_2O crystal. However, more peaks are usually observed in the Raman spectra of Cu_2O , despite the fact that they are either silent or infrared active phonon modes. This is due to^{49–51} (a) the excitation conditions and resonance with excitonic states of

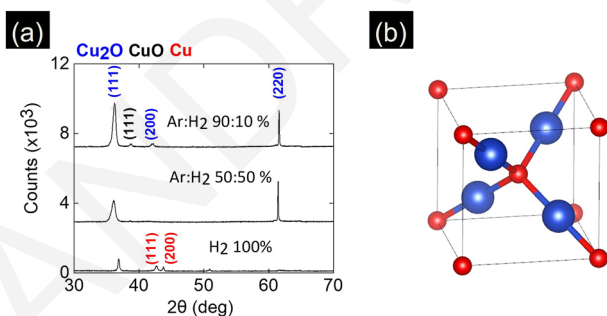


FIG. 1. (a) XRD of a 300 nm-thick Cu_2O layer obtained on glass with Ar: O_2 (75:25% v/v) that was annealed for 60 min at 500 °C under Ar: H_2 . The Cu_2O layer annealed under Ar: H_2 (50:50% v/v) has no peaks corresponding to CuO, Cu (b) unit cell of cubic Cu_2O .

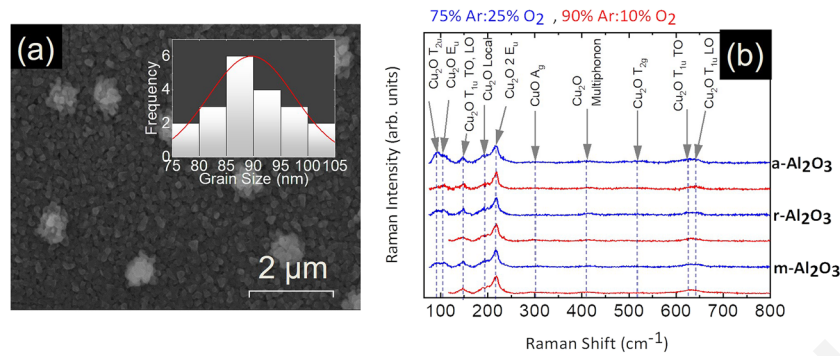


FIG. 2. (a) FE-SEM image of a 300 nm Cu_2O layer on $m\text{-Al}_2\text{O}_3$; inset shows the histogram of grain size along with normal distribution fit (red line); similar surface morphology was observed on r - and $\alpha\text{-Al}_2\text{O}_3$ substrates. (b) Raman spectra of the Cu_2O layers on m -, r -, and $\alpha\text{-Al}_2\text{O}_3$ obtained with different $\text{Ar}:\text{O}_2$ contents and annealed under $\text{Ar}:\text{H}_2$ (50%:50% v/v) at 500 °C for 60 min. The vertical line at 300 cm^{-1} corresponds to CuO (A_g), but we do not observe any clear peak, suggesting that the Cu_2O layers do not contain the CuO phase.

Cu_2O , (b) the polarization and scattering geometry used, and (c) the surface treatment. The non-stoichiometry of Cu_2O also plays a key role in the emergence of the non-active Raman lattice modes in the spectra, inducing several intrinsic defects, i.e., anti-sites, interstitials, and vacancies in the lattice.^{49,50} Point imperfections reduce the local symmetry of a perfect Cu_2O crystal, thereby relaxing the selection rules and activating Raman-forbidden vibrational modes.

The Cu_2O layers on m -, r -, and $\alpha\text{-Al}_2\text{O}_3$ peaks due to the following vibrational modes are detected: 93.2 cm^{-1} (T_{2u}),^{50,51} 108 cm^{-1} (E_u),^{50,51} 148.6 cm^{-1} [T_{1u} , Transverse Optical (TO) and Longitudinal Optical (LO) phonons],^{50,51} 217.5 cm^{-1} ($2 E_u$),^{50,52} 516.7 cm^{-1} (T_{2g}),⁵⁰⁻⁵² and 626.9 and 643.5 cm^{-1} (T_{1u} , TO and LO phonons, respectively).^{50,51} A multi-phonon Raman scattering mode appears at 413.7 cm^{-1} , consistent with the literature,^{52,53} while at 196 cm^{-1} , a peak is observed due to local vibrations of Cu on O-sites with T_d point symmetry.^{50,53} Moreover, the A_g Raman active mode of CuO appears at 302.1 cm^{-1} .⁵⁴⁻⁵⁸ As evident, the Cu_2O phase is dominant, and the Raman active mode of CuO that occurs via the oxidation of Cu_2O is not observable. In addition, we find no evidence for the formation of CuAlO_2 , suggesting that there is no reaction between Cu_2O and Al_2O_3 . Moreover, we do not find any significant dependence of the properties of the Cu_2O layers on the different orientations, m -, r -, and α -, of the Al_2O_3 substrate. Nevertheless, the T_{1u} peak of Cu_2O at $\sim 150 \text{ cm}^{-1}$, which is detected in the Raman spectra of the Cu_2O layers deposited on Si , gains intensity as the O_2 content in the $\text{Ar}:\text{O}_2$ mixture increases and is attributed to the formation of intrinsic point imperfections in the crystal lattice of Cu_2O (see the supplementary material for more details).

The temporal evolution of the differential transmission through the Cu_2O layers was measured by UPPS. Before considering in detail the spectra obtained from the Cu_2O layers it is useful to describe the generation and recombination of photogenerated electron-hole pairs during UPPS in direct energy bandgap semiconductors.

Initially, the pump, i.e., a short pulse of energetic photons with energy of $E_{PU} = 3.1$ or 4.77 eV corresponding to $\lambda_{PU} = 400$ or 260 nm, will result in the excitation of electrons from the valence band into the conduction band, as shown in Fig. 3. The photogenerated electrons will initially occupy empty states residing high above

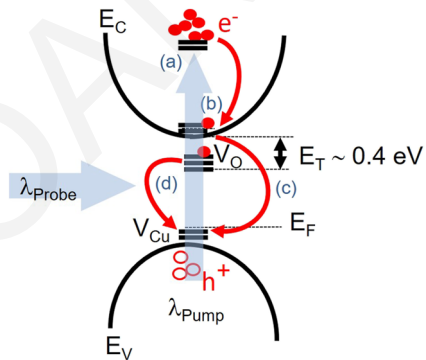


FIG. 3. Generation and recombination, mechanisms, and pathways of photogenerated electron-hole pairs in a direct semiconductor with states related to crystal point-imperfections residing in the energy bandgap.

the conduction band minimum. These hot electrons will gradually lose energy via electron-phonon or electron-electron interactions and will occupy lower energy states closer to the conduction band minimum (E_C) as well as empty states related to crystallographic imperfections (E_i) that are located energetically in the energy gap of Cu_2O . A separate light beam is used to probe the temporal evolution of the occupancy of the above-mentioned states located at different energies by varying the wavelength between $\lambda_{PR} = 450$ and 750 nm and measuring the change in transmission or differential transmission (dT/T). If a state is occupied by an electron, then the photon with a specific λ_{PR} will not be absorbed, resulting in a positive increase in differential transmission at the specific wavelength corresponding to a particular energy state. In contrast, if a state is not occupied by a photoexcited electron, then a photon with a specific energy will be absorbed, thereby reducing transmission at a specific λ_{PR} . In essence, one may find the fundamental direct energy bandgap(s) of a semiconductor as well as the energetic location of states lying in the energy gap that are related to crystal imperfections, similar to deep level transient spectroscopy.

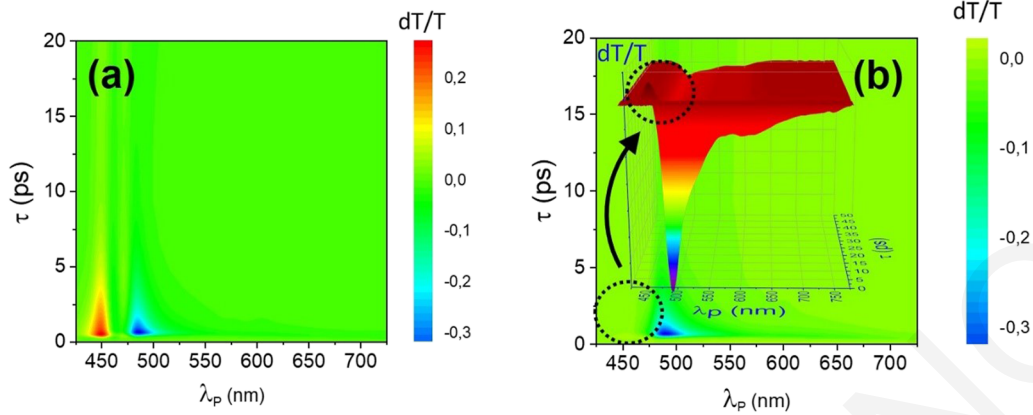


FIG. 4. Differential transmission dT/T (no units) vs time delay τ (ps) and probe wavelength λ_p (nm) for the Cu_2O layers on $m\text{-Al}_2\text{O}_3$ obtained using $\text{Ar}:\text{O}_2$ 90:10% v/v with a thickness of (a) 100 nm and (b) 300 nm; inset shows the peak at 450 nm in 3D.

The variation of dT/T vs τ and λ_{PR} for the 100 nm Cu_2O layers on $m\text{-Al}_2\text{O}_3$ that were obtained using $\text{Ar}:\text{O}_2$ (90:10% v/v) is shown in Fig. 4(a). One may observe the occurrence of two major peaks corresponding to a positive and negative maximum in dT/T at $\lambda_{PR} = 450$ and 487 nm, i.e., 2.75 and 2.54 eV, respectively. We also observe these by increasing the thickness of the Cu_2O layer from 100 to 300 nm, as shown in Fig. 4(b) but the maximum at $\lambda_{PR} = 450$ nm is not so pronounced compared to that in Fig. 4(a).

Similarly, the variation of dT/T vs τ and λ_{PR} for the 100 nm Cu_2O layers on $m\text{-Al}_2\text{O}_3$ that were obtained using $\text{Ar}:\text{O}_2$ 75:25% v/v is shown in Fig. 5(a). One may observe the occurrence of the peaks that appear in Figs. 4(a) and 4(b), but also the emergence of a maximum at $\lambda_{PR} = 570$ nm and a broad one at $\lambda_{PR} = 687$ nm, i.e., 2.17 and 1.8 eV, respectively.

It should be pointed out that the maxima at 1.84 and 2.75 eV correspond to positive dT/T , indicating that these states are in fact

occupied by electrons. In contrast, the maxima at 2.17 and 2.62 eV correspond to negative dT/T , implying absorption, and these conduction band minima states are in fact empty after excitation and the generation of excess electrons and holes. It appears then that photogenerated electrons occupy the highest conduction band and subsequently move into states related to point-imperfections that are energetically located in the energy gap of Cu_2O . No changes occurred by increasing the excitation energy from 1 to 10 μJ , as shown by the inset in Fig. 5(a). In addition, no significant changes occurred by increasing the thickness of the Cu_2O layer from 100 to 300 nm, as shown in Fig. 5(b).

The spectral structure obtained from Cu_2O on $m\text{-Al}_2\text{O}_3$ using $\text{Ar}:\text{O}_2$ 50:50% v/v is also similar and shown as an inset in Fig. 5(b). We find that the spectral structure obtained by UPPS is not dependent on the thickness of the Cu_2O and is also the same for m -, r -, and $a\text{-Al}_2\text{O}_3$.

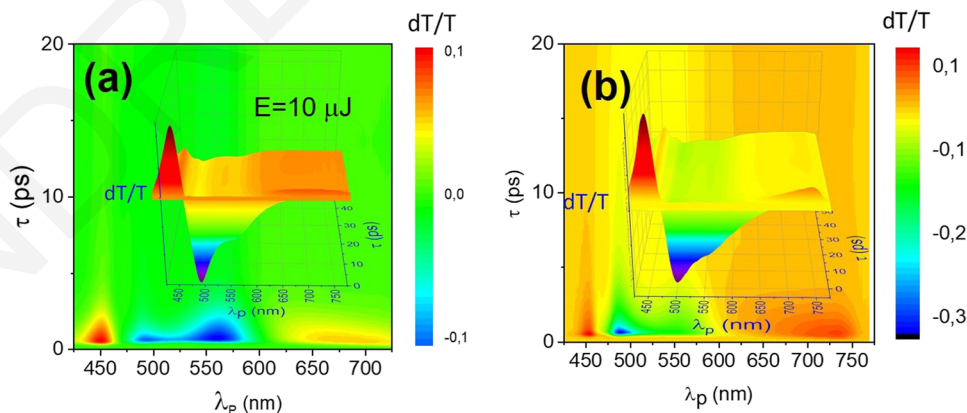


FIG. 5. Differential transmission dT/T (no units) vs time delay τ (ps) and probe wavelength λ_p (nm) for the Cu_2O layers on $m\text{-Al}_2\text{O}_3$ obtained using $\text{Ar}:\text{O}_2$ 75:25% v/v with a thickness of (a) 100 nm; inset shows the spectrum obtained with an excitation of 10 μJ in 3D and (b) 300 nm; inset shows the spectrum for Cu_2O obtained on $m\text{-Al}_2\text{O}_3$ using $\text{Ar}:\text{O}_2$ 50:50% v/v in 3D.

The four peaks observed at $\lambda_{PR} = 450, 487, 570,$ and 687 nm correspond to $2.75, 2.54, 2.17,$ and 1.84 eV, respectively. In order to understand the origin of these optical transitions, it is necessary to consider the electronic structure of Cu_2O , as shown in Fig. 6(a). The top of the valence band and bottom of the conduction band are derived from states belonging to the same ion, so they have the same parity, and dipole transitions are forbidden. The two upmost valence bands, with Γ_7^+ and Γ_8^+ symmetry, are related to Cu_{3d} electrons. The lowest conduction band with Γ_6^+ symmetry is related to Cu_{4s} electrons, and the next higher conduction band with Γ_8^- symmetry is related to O_{2p} electrons.

Excitation from the two valence bands to the two conduction bands results in a four-exciton series with energies of $2.17, 2.30, 2.62,$ and 2.75 eV,⁵⁹ which are usually observed at low temperatures and described as the yellow, green, blue, and indigo transitions, respectively, as shown in Fig. 6(a). Evidently, the peaks observed at $2.17, 2.54,$ and 2.75 eV are very close indeed to the corresponding yellow, blue, and indigo transitions of Cu_2O . These transitions are not related to transitions of photogenerated electrons from the conduction band minima into the continuum at higher energies inside the conduction band following excitation, as suggested by Shenje *et al.*,⁶⁰ otherwise, we would have observed a host of other energetic transitions. Similarly, they are not related to the excitation of electrons occupying states below the top of the valence E_V into empty holes near the top of the E_V . The peaks observed at $2.17, 2.54,$ and 2.75 eV are related to the corresponding yellow, blue, and indigo direct gap transitions of Cu_2O . Their observation at room temperature is due to the careful optimization of the annealing conditions under H_2 , and the direct gap transitions observed suggest that the Cu_2O is not coherently strained to the underlying $m-, r-,$ and $a\text{-Al}_2\text{O}_3$. This may be understood by considering that $m\text{-Al}_2\text{O}_3$ is ideally suited for the growth of cubic crystals such as Cu_2O as it has an oxygen

terminated surface with a tetragonal, two-dimensional unit cell of $4.34 \times 4.76 \text{ \AA}^2$, which is expected to result in Cu_2O under a biaxial tensile strain of 1.6% and 11.5% if epitaxial growth occurs, considering that the lattice constant of Cu_2O is $a = 4.2696 \text{ \AA}$. The tensile strain is expected to be even larger in the case of epitaxial Cu_2O on $r\text{-Al}_2\text{O}_3$, which also has a surface consisting of oxygen atoms arranged in a tetragonal two-dimensional unit cell of $5.12 \times 4.76 \text{ \AA}^2$, and this in turn is expected to change the energy gap of Cu_2O , which is strongly dependent on strain.⁶¹ However, we do not observe any dependence of the direct gap transitions of the Cu_2O layers on orientation, i.e., $m-, r-,$ and $a\text{-Al}_2\text{O}_3$, suggesting that the Cu_2O layers are bulk-relaxed, not coherently strained, due to the fact that they were deposited by reactive sputtering at room temperature.

In addition to the above direct gap transitions, we also observed a broad peak with a maximum at 1.84 eV in the Cu_2O layers deposited under $\text{Ar}:\text{O}_2$ $75:25$ and $50:50\%$ v/v. In other words, the broad peak appears to be dependent on the content of oxygen in the Cu_2O layers during deposition. It is reasonable then to suggest that it is related to a local density of states that is energetically located between ~ 0.3 and 0.5 eV below the conduction band minimum inside the energy gap. This is consistent and in very good agreement with those who have proposed that oxygen vacancies, i.e., V_{O} , behave as donor-like states that reside ~ 0.4 eV below the conduction band minimum at 2.2 eV.^{18,62–66} The occurrence of V_{O} donor-like states that are positively charged results in surface band bending and depletion, as shown in Fig. 6(b). In fact, it has been suggested that the Fermi level (E_F) of Cu_2O is actually pinned at surface states related to V_{O} that reside energetically at ~ 0.4 eV below the conduction band minimum. The energetic position of the Fermi level with respect to the conduction band edge at the surface and in the bulk governs the overall band bending. In the bulk, a flat band condition exists, provided that the surface depletion is smaller than the

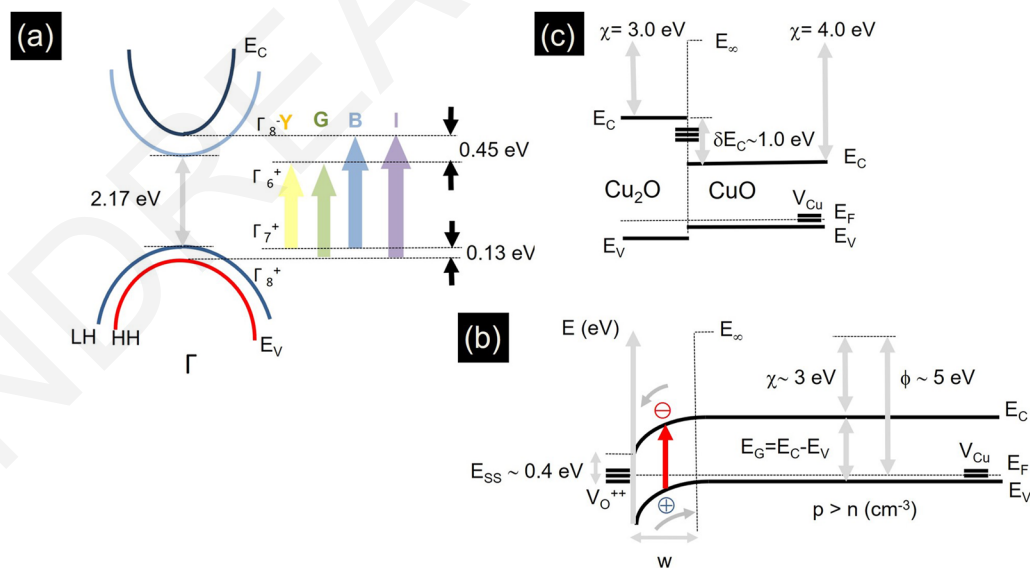


FIG. 6. (a) The yellow, green, blue, and indigo exciton transitions of Cu_2O ; (b) conduction and valence band potential profiles of u/d Cu_2O showing the surface depletion, downward band-bending, work function ϕ , and electron affinity χ ; (c) band line-up of $\text{CuO}/\text{Cu}_2\text{O}$ showing also trap states at the interface.

thickness of the Cu_2O layer. The surface depletion width is of the order of a few tens of nm's in $\text{u/d Cu}_2\text{O}$ as the static dielectric constant of Cu_2O is rather low, i.e., $\epsilon_R = 4$. For completeness, it is instructive to mention that the persistent photoconductivity effect in Cu_2O is due to the interplay between negatively charged copper vacancies V_{Cu}^- and positively charged oxygen vacancies V_{O}^+ or V_{O}^{++} that forms pairs, e.g., V_{Cu}^- and V_{O}^+ or V_{Cu}^- and V_{O}^{++} , due to electrostatic interaction. According to Mittiga *et al.*,⁶⁷ V_{O}^{++} reside energetically in the upper half of the energy bandgap of Cu_2O .

Evidently, many have proposed that V_{O} donor-like states that are positively charged influence the electrical and optical properties of Cu_2O ,^{18,62–66} but according to the theoretical calculations of Scanlon *et al.*,⁶⁸ V_{O} is not charged and is energetically located close to the valence band, so this is still a matter of controversy. It is then necessary to find alternative explanations for the origin of the maximum at 1.8 eV, which may be attributed to a transition between acceptor-like states related to V_{Cu} that reside energetically ~ 0.2 eV above the valence band maximum and states in the conduction band. However, the V_{Cu} acts as acceptor-like states, not donor-like states, and does not lead to surface depletion or downward band bending as observed experimentally.^{18,62–66} Hence, one cannot rule out the existence of states residing energetically ~ 0.4 eV below the conduction band minima. We suggest that these states corresponding to the maximum at 1.8 eV may be related to the formation of $\text{Cu}_2\text{O}/\text{CuO}$ nanostructures at the surface and/or grain boundaries. Despite the fact that we have not observed a significant content of CuO in the Raman spectra of Fig. 2, the Cu_2O layers may well contain traces of CuO leading to the formation of $\text{Cu}_2\text{O}/\text{CuO}$ nanostructures that will act in essence as traps considering that the $\text{Cu}_2\text{O}/\text{CuO}$ heterojunction has a straddled (type I) band line-up and conduction band discontinuity $\Delta E_{\text{C}}(\text{Cu}_2\text{O}/\text{CuO}) \sim 1.0$ eV as shown in Fig. 6(c). The size of these $\text{Cu}_2\text{O}/\text{CuO}$ nanostructures is going to be of the order of a few tens of nm's considering that the Cu_2O is nanostructured, i.e., consists of grains with average sizes of less than 100 nm. Consequently, one may expect quantization to occur inside the $\text{Cu}_2\text{O}/\text{CuO}$ nanostructures, which in turn will give rise to a quantum confined level that will act as a trap. Considering that the size of the $\text{Cu}_2\text{O}/\text{CuO}$ nanostructures will also vary, this in turn will lead to an energetic distribution of traps commensurate with the fact that we observed a broad transition with a maximum at 1.8 eV. However, one must also keep in mind that CuO has a monoclinic crystal structure with a lattice constant of 4.68 Å that is larger than the lattice constant of cubic Cu_2O , which is 4.2696 Å, and as such will give rise to a plethora of states related to crystallographic defects at the $\text{Cu}_2\text{O}/\text{CuO}$ interface. The poor properties and quality of the $\text{CuO}/\text{Cu}_2\text{O}$ interface are well known and clearly manifested when trying to grow Cu_2O via thermal oxidation of a Cu foil under O_2 . Initially, the Cu reacts with O_2 , leading to the formation of Cu_2O , but the latter reacts again with O_2 , leading to the formation of a CuO layer on top of Cu_2O that will separate after reaching a certain thickness due to the lattice mismatch between the CuO and Cu_2O , which inevitably leads to a very high density of crystallographic defects at the $\text{CuO}/\text{Cu}_2\text{O}$ heterojunction interface that may be responsible for the distribution of states ~ 0.4 eV below the conduction band minima as shown in Fig. 6(c). This hypothesis is consistent with Živković and de Leeuw,⁶⁹ who showed that both oxygen and copper point imperfections give rise to states energetically located below the

conduction band minimum inside the energy gap of CuO . It is also consistent with the fact that the all-oxide p-n junction solar cell of Shibasaki *et al.*⁸ displayed the highest efficiency of 8.4% when the Cu_2O contained minimal Cu and CuO .

The formation of CuO on top of Cu_2O at the surface is also consistent with the observations of surface depletion and downward band bending, which occur due to the band line-up and difference in the energy gaps as opposed to the electrostatic band-bending induced by positively charged donors.

Considering the above-mentioned arguments, we suggest that the formation of $\text{CuO}/\text{Cu}_2\text{O}$ nanostructures in Cu_2O layers is especially important as Cu_2O layers react over time with ambient O_2 , which means that it is necessary to passivate their surface with a suitable oxide that will be transparent like, for instance, the n-type Ga_2O_3 used by Shibasaki *et al.*⁸ This is of paramount importance not just for devices but also for the observation of Rydberg excitons in thin layers of Cu_2O as opposed to natural occurring crystals. In contrast to solar cells, $\text{Cu}_2\text{O}/\text{CuO}$ layers have better photocatalytic performance compared to Cu_2O or CuO single-component materials.^{9,70–73} This might seem perplexing at first, but it can be explained by an increase in the surface area and porosity of the $\text{Cu}_2\text{O}/\text{CuO}$ structure due to the formation of voids at the $\text{Cu}_2\text{O}/\text{CuO}$ interface, which allows the infiltration of liquids. This is very similar to the case of quantum dot sensitized solar cells, in which CdS/CdSe quantum dots are deposited on top of a scaffold of TiO_2 particles with high porosity and surface area that is critical for the infiltration of the liquid electrolytes.

We suggest in closing that suppressing the formation of crystallographic imperfections due to the oxidation of Cu_2O is critical in exploiting the properties of this novel metal-oxide semiconductor from a fundamental but also applied point of view in the context of energy conversion.

IV. CONCLUSIONS

Cu_2O has been deposited on m-, r-, and a- Al_2O_3 by reactive sputtering of Cu using $\text{Ar}:\text{O}_2$ (90:10, 75:25, or 50:50% v/v), after which it was annealed under optimum conditions at 500 °C under $\text{Ar}:\text{H}_2$ (50:50% v/v) at 10^{-1} mbar. The Cu_2O layers have a cubic crystal structure, consist of bulk-relaxed grains, and do not contain CuO , as observed by Raman spectroscopy. The Cu_2O layers exhibited a detailed spectral structure and distinct peaks at 2.75, 2.54, and 2.17 eV corresponding to the indigo, blue, and yellow direct gap transitions of Cu_2O as observed by ultrafast pump–probe spectroscopy at room temperature. However, we also observed a transition at 1.8 eV, which is related to a local density of states that is energetically located between ~ 0.3 and 0.5 eV below the conduction band minimum inside the energy gap. This is usually attributed to positively charged donor-like oxygen vacancies, but alternative explanations must also be considered, like the formation of $\text{CuO}/\text{Cu}_2\text{O}$ nanostructures at the surface and grain boundaries of the Cu_2O layers. It is then necessary to suppress completely the formation of $\text{CuO}/\text{Cu}_2\text{O}$ nanostructures, which we identify as one of the most important challenges in attaining high efficiency solar cells, as well as the observation of Rydberg excitons in Cu_2O layers, not just natural occurring crystals.

SUPPLEMENTARY MATERIAL

The Raman spectra of the Cu₂O layers deposited on n-type Si (001) with different oxygen contents are described for completeness in the supplementary material so that one may compare with the Cu₂O layers deposited on m-, r-, and a-Al₂O₃.

AUTHOR DECLARATIONS

Conflict of Interest

The authors have no conflicts to disclose.

Author Contributions

E. Prountzou: Raman, EDS, SEM, XRD, Writing. **A. Ioannou:** Growth/Annealing, XRD Investigation. **D. Sapalidis:** Raman, EDS, SEM, XRD. **E. Pavlidou:** SEM, EDS. **M. Katsikini:** Supervision of E. Prountzou and D. Sapalidis. **A. Othonos:** UPPS. **M. Zervos:** Conceptualization, Growth/Annealing, Supervision, Writing (Lead).

Eleni Prountzou: Formal analysis (equal); Investigation (equal); Methodology (equal); Validation (equal); Visualization (equal); Writing – original draft (supporting). **Andreas Ioannou:** Formal analysis (equal); Investigation (equal); Methodology (equal); Validation (equal); Visualization (equal). **Dimitrios Sapalidis:** Formal analysis (equal); Investigation (equal); Methodology (equal); Validation (equal); Visualization (equal). **Eleni Pavlidou:** Formal analysis (equal); Investigation (equal); Methodology (equal). **Maria Katsikini:** Supervision (equal). **Andreas Othonos:** Investigation (equal); Methodology (equal); Validation (equal); Visualization (equal). **Matthew Zervos:** Conceptualization (lead); Data curation (equal); Formal analysis (lead); Investigation (lead); Methodology (lead); Project administration (lead); Resources (equal); Supervision (equal); Validation (lead); Visualization (lead); Writing – original draft (lead).

DATA AVAILABILITY

The data that support the findings of this study are available within the article and its supplementary material.

REFERENCES

- D. O. Scanlon and G. W. Watson, “Undoped n-type Cu₂O: Fact or fiction?,” *J. Phys. Chem. Lett.* **1**, 2582–2585 (2010).
- C. Malerba, F. Biccari, C. Leonor Azanza Ricardo, M. D’incapu, P. Scardi, and A. Mittiga, “Absorption coefficient of bulk and thin film Cu₂O,” *Sol. Energy Mater. Sol. Cells* **95**, 2848–2854 (2011).
- A. Lakshmanan, Z. C. Alex, and S. R. Meher, “Recent advances in cuprous oxide thin film based photovoltaics,” *Mater. Today Sustainability* **20**, 100244 (2022).
- N. G. Elfadill, M. R. Hashim, K. M. Chahrour, and S. A. Mohammed, “Preparation of p-type Na-doped Cu₂O by electrodeposition for a p-n homojunction thin film solar cell,” *Semicond. Sci. Technol.* **31**, 065001 (2016).
- P. Ravindra, R. Mukherjee, and S. Avasthi, “Hole-selective electron-blocking copper oxide contact for silicon solar cells,” *IEEE J. Photovoltaics* **7**, 1278–1283 (2017).
- K. K. Markose, M. Shaji, S. Bhatia, P. R. Nair, K. J. Saji, A. Antony, and M. K. Jayaraj, “Novel boron-doped p-type Cu₂O thin films as a hole-selective contact in c-Si solar cells,” *ACS Appl. Mater. Interfaces* **12**, 12972–12981 (2020).

- Y. Liu, J. Zhu, L. Cai, Z. Yao, C. Duan, Z. Zhao, C. Zhao, and W. Mai, “Solution-processed high-quality Cu₂O thin films as hole transport layers for pushing the conversion efficiency limit of Cu₂O/Si heterojunction solar cells,” *Sol. RRL* **4**, 1900339 (2020).
- S. Shibasaki, Y. Honishi, N. Nakagawa, M. Yamazaki, Y. Mizuno, Y. Nishida, K. Sugimoto, and K. Yamamoto, “Highly transparent Cu₂O absorbing layer for thin film solar cells,” *Appl. Phys. Lett.* **119**, 242102 (2021).
- X. Liu, J. Chen, P. Liu, H. Zhang, G. Li, T. An, and H. Zhao, “Controlled growth of CuO/Cu₂O hollow microsphere composites as efficient visible-light-active photocatalysts,” *Appl. Catal., A* **521**, 34 (2016).
- B. Koiki and O. Arotiba, “Cu₂O as an emerging semiconductor in photocatalytic and photoelectrocatalytic treatment of water contaminated with organic substances: A review,” *RSC Adv.* **10**, 36514–36525 (2020).
- G. Liu, F. Zheng, J. Li, G. Zeng, Y. Ye, D. M. Larson, J. Yano, E. J. Crumlin, J. W. Ager, L. Wang, and F. M. Toma, “Investigation and mitigation of degradation mechanisms in Cu₂O photoelectrodes for CO₂ reduction to ethylene,” *Nat. Energy* **6**, 1124–1132 (2021).
- Y. Zhang, M.-M. Liu, J. Chen, S. Fang, and P. Zhou, “Recent advances in Cu₂O-based composites for photocatalysis: A review,” *Dalton Trans.* **50**, 4091 (2021).
- E. F. Gross, “Optical spectrum of excitons in the crystal lattice,” *Nuovo Cimento* **3**, 672–701 (1956).
- M. Kuwata-Gonokami, M. Kubouchi, R. Shimano, and A. Mysyrowicz, “Time-resolved excitonic Lyman spectroscopy of Cu₂O,” *J. Phys. Soc. Jpn.* **73**, 1065–1069 (2004).
- K. Karpinska, P. H. M. van Loosdrecht, I. P. Handayani, and A. Revcolevschi, “Para-excitons in Cu₂O—A new approach,” *J. Lumin.* **112**, 17–20 (2005).
- R. A. Kaindl, R. Huber, B. A. Schmid, Y. R. Shen, and D. S. Chemla, in *15th International Conference on Ultrafast Phenomena* (Optica Publishing Group, 2006), p. MG7.
- T. Kazimierzczuk, D. Fröhlich, S. Scheel, H. Stolz, and M. Bayer, “Giant Rydberg excitons in the copper oxide Cu₂O,” *Nature* **514**, 343–347 (2014).
- M. Borgwardt, S. T. Omelchenko, M. Favaro, P. Plate, C. Höhn, D. Abou-Ras, K. Schwarzburg, R. van de Krol, H. A. Atwater, N. S. Lewis, R. Eichberger, and D. Friedrich, “Femtosecond time-resolved two-photon photoemission studies of ultrafast carrier relaxation in Cu₂O photoelectrodes,” *Nat. Commun.* **10**, 2106 (2019).
- G. W. Fehrenbach, W. Schäfer, J. Treusch, and R. G. Ulbrich, “Transient optical spectra of a dense exciton gas in a direct-gap semiconductor,” *Phys. Rev. Lett.* **49**, 1281–1284 (1982).
- K. Orfanakis, S. K. Rajendran, V. Walther, T. Volz, T. Pohl, and H. Ohadi, “Rydberg exciton-polaritons in a Cu₂O microcavity,” *Nat. Mater.* **21**, 767–772 (2022).
- T. Iivonen, M. J. Heikkilä, G. Popov, H. E. Nieminen, M. Kaipio, M. Kemell, M. Mattinen, K. Meinander, K. Mizohata, J. Räisänen, M. Ritala, and M. Leskelä, “Atomic layer deposition of photoconductive Cu₂O thin films,” *ACS Omega* **4**, 11205–11214 (2019).
- A. S. M. S. Rahman, M. A. Islam, and K. M. Shorowordi, “Electrodeposition and characterization of copper oxide thin films for solar cell applications,” *Procedia Eng.* **105**, 679–685 (2015).
- H. Liu, V. H. Nguyen, H. Roussel, I. Gélard, L. Rapenne, J. Deschanvres, C. Jiménez, and D. Muñoz-Rojas, “The role of humidity in tuning the texture and electrical properties of Cu₂O thin films deposited via aerosol-assisted CVD,” *Adv. Mater. Interfaces* **6**, 1801364 (2018).
- S. Chatterjee and A. J. Pal, “Introducing Cu₂O thin films as a hole-transport layer in efficient planar perovskite solar cell structures,” *J. Phys. Chem. C* **120**, 1428–1437 (2016).
- J. Jo, Z. Deng, N. Sanders, E. Kioupakis, and R. L. Peterson, “Experimental and theoretical study of hole scattering in RF sputtered p-type Cu₂O thin films,” *Appl. Phys. Lett.* **120**, 112105 (2022).
- R. S. Toth, R. Kilkson, and D. Trivich, “Preparation of large area single-crystal cuprous oxide,” *J. Appl. Phys.* **31**, 1117–1121 (1960).
- G. Aggarwal, S. K. Maurya, A. J. Singh, A. K. Singh, and B. Kavaipatti, “Intrinsic acceptor-like defects and their effect on carrier transport in polycrystalline Cu₂O photocathodes,” *J. Phys. Chem. C* **123**, 26057 (2019).
- Y. Tolstova, S. Wilson, S. Omelchenko, N. Lewis, and H. Atwater, in *IEEE Conference on Photovoltaic Specialists* (IEEE, 2015).

- ²⁹T. Ito, H. Yamaguchi, K. Okabe, and T. Masumi, "Single crystal growth and characterization of Cu_2O and CuO ," *J. Mater. Sci.* **33**, 3555–3566 (1998).
- ³⁰S. Ishizuka, S. Kato, Y. Okamoto, and K. Akimoto, "Control of hole carrier density of polycrystalline Cu_2O thin films by Si doping," *Appl. Phys. Lett.* **80**, 950–952 (2002).
- ³¹J. Resende, V.-S. Nguyen, C. Fleischmann, L. Bottiglieri, S. Brochen, W. Vandervorst, W. Favre, C. Jiménez, J.-L. Deschamps, and N. D. Nguyen, "Grain-boundary segregation of magnesium in doped cuprous oxide and impact on electrical transport properties," *Sci. Rep.* **11**, 7788 (2021).
- ³²Ø. Nordseth, R. Kumar, K. Bergum, I. Chilibon, S. E. Foss, and E. Monakhov, "Nitrogen-doped Cu_2O thin films for photovoltaic applications," *Materials* **12**, 3038 (2019).
- ³³Q. Bai, W. Wang, Q. Zhang, and M. Tao, "n-type doping in Cu_2O with F, Cl, and Br: A first-principles study," *J. Appl. Phys.* **111**, 023709 (2012).
- ³⁴S. R. Meher, A. Lakshmanan, D. Gupta, and Z. C. Alex, "N-type doping feasibility of Cu_2O with In and Al for cost-effective photovoltaics: An ab initio investigation," *Mater. Today Commun.* **26**, 102015 (2021).
- ³⁵K. Matsuzaki, K. Nomura, H. Yanagi, T. Kamiya, M. Hirano, and H. Hosono, "Epitaxial growth of high mobility Cu_2O thin films and application to p-channel thin film transistor," *Appl. Phys. Lett.* **93**, 202107 (2008).
- ³⁶R. D. Schmidt-Whitley, M. Martinez-Clemente, and A. Revcolevschi, "Growth and microstructural control of single crystal cuprous oxide Cu_2O ," *J. Cryst. Growth* **23**, 113–120 (1974).
- ³⁷P. Majumder, R. Katamreddy, and C. Takoudis, "Atomic layer deposited ultrathin HfO_2 and Al_2O_3 films as diffusion barriers in copper interconnects," *Electrochem. Solid-State Lett.* **10**, H291 (2007).
- ³⁸M. Rühle, A. Liedtke, U. Alber, R. Schweinfest, and G. Elßner, in *Interfacial Science in Ceramic Joining*, edited by A. Bellosi, T. Kosmač, and A. P. Tomsia (Springer Netherlands, Dordrecht, 1998), pp. 3–14.
- ³⁹A. Wagner, H. Scherg-Kurmes, A. Waag, and A. Bakin, "Vapour phase epitaxy of Cu_2O on a-plane Al_2O_3 ," *Phys. Status Solidi C* **10**, 1284–1287 (2010).
- ⁴⁰M. Ottosson and J. O. Carlsson, "Chemical vapour deposition of Cu_2O and CuO from CuI and O_2 or N_2O ," *Surf. Coat. Technol.* **78**, 263–273 (1996).
- ⁴¹R. S. Yu and H. H. Yin, "Structural and optoelectronic properties of p-type semiconductor CuAlO_2 thin films," *Thin Solid Films* **526**, 103–108 (2012).
- ⁴²J. C. Lee, S. Y. Um, Y. W. Heo, J. H. Lee, and J. J. Kim, "Phase development and crystallization of CuAlO_2 thin films prepared by pulsed laser deposition," *J. Eur. Ceram. Soc.* **30**, 509–512 (2010).
- ⁴³S. K. Lee and W. H. Tuan, "Formation of CuAlO_2 at the $\text{Cu}/\text{Al}_2\text{O}_3$ interface and its influence on interface strength and thermal conductivity," *Int. J. Appl. Ceram. Technol.* **10**, 780–789 (2013).
- ⁴⁴Y. Unutulmazsoy, C. Cancellieri, L. Lin, and L. P. H. Jeurgens, "Reduction of thermally grown single-phase CuO and Cu_2O thin films by in-situ time-resolved XRD," *Appl. Surf. Sci.* **588**, 152896 (2022).
- ⁴⁵M. Zervos, A. Othonos, M. Sergides, T. Pavloudis, and J. Kioseoglou, "Observation of the direct energy band gaps of defect tolerant Cu_3N by ultrafast pump-probe spectroscopy," *J. Phys. Chem. C* **124**(6), 3459–3469 (2020).
- ⁴⁶J. A. Kim, J. H. Park, S. G. Park, C. S. Son, Y. G. Son, and D. H. Hwang, "Effect of substrate temperature on variations in the structural and optical properties of Cu_2O thin films deposited via RF magnetron sputtering," *Crystals* **13**, 643 (2023).
- ⁴⁷D. Titus, E. James Jebaseelan Samuel, and S. M. Roopan, in *Green Synthesis, Characterization and Applications of Nanoparticles*, edited by A. K. Shukla and S. Irvani (Elsevier, 2019), pp. 303–319.
- ⁴⁸T. Roodbar Shojaei, S. Soltani, and M. Derakhshani, in *Fundamentals of Bio-nanomaterials*, edited by A. Barhoum, J. Jeevanandam, and M. K. Danquah (Elsevier, 2022), pp. 139–174.
- ⁴⁹B. K. Meyer, A. Polity, D. Reppin, M. Becker, P. Hering, P. J. Klar, T. Sander, C. Reindl, J. Benz, M. Eickhoff, C. Heiliger, M. Heinemann, J. Bläsing, A. Krost, S. Shokovets, C. Müller, and C. Ronning, "Binary copper oxide semiconductors: From materials towards devices," *Phys. Status Solidi B* **249**, 1487–1509 (2012).
- ⁵⁰B. K. Meyer, A. Polity, D. Reppin, M. Becker, P. Hering, B. Kramm, P. J. Klar, T. Sander, C. Reindl, C. Heiliger, M. Heinemann, C. Müller, and C. Ronning, *Semicond. Semimetals* **88**, 201–226 (2013).
- ⁵¹T. Sander, C. T. Reindl, M. Giar, B. Eifert, M. Heinemann, C. Heiliger, and P. J. Klar, "Correlation of intrinsic point defects and the Raman modes of cuprous oxide," *Phys. Rev. B* **90**, 045203 (2014).
- ⁵²P. Dawson, M. M. Hargreave, and G. R. Wilkinson, "The dielectric and lattice vibrational spectrum of cuprous oxide," *J. Phys. Chem. Solids* **34**, 2201–2208 (1973).
- ⁵³J. Reydellet, M. Balkanski, and D. Trivich, "Light scattering and infrared absorption in cuprous oxide," *Phys. Status Solidi B* **52**, 175–185 (1972).
- ⁵⁴W. Wang, Q. Zhou, X. Fei, Y. He, P. Zhang, G. Zhang, L. Peng, and W. Xie, "Synthesis of CuO nano- and micro-structures and their Raman spectroscopic studies," *CrystEngComm* **12**, 2232–2237 (2010).
- ⁵⁵L. Debbichi, M. C. Marco de Lucas, J. F. Pierson, and P. Krüger, "Vibrational properties of CuO and Cu_4O_3 from first-principles calculations, and Raman and infrared spectroscopy," *J. Phys. Chem. C* **116**, 10232–10237 (2012).
- ⁵⁶G. Kliche and Z. V. Popovic, "Far-infrared spectroscopic investigations on CuO ," *Phys. Rev. B* **42**, 10060–10066 (1990).
- ⁵⁷X. K. Chen, J. C. Irwin, and J. P. Franck, "Evidence for a strong spin-phonon interaction in cupric oxide," *Phys. Rev. B* **52**, R13130 (1995).
- ⁵⁸T. H. Tran and V. T. Nguyen, "Copper oxide nanomaterials prepared by solution methods, some properties, and potential applications: A brief review," *Int. Scholarly Res. Not.* **2014**, 856592.
- ⁵⁹A. Živković, N. H. de Leeuw, B. G. Searle, and L. Bernasconi, "Electronic excitations in copper oxides: Time-dependent density functional theory calculations with a self-consistent hybrid kernel," *J. Phys. Chem. C* **124**, 24995–25003 (2020).
- ⁶⁰L. Shenje, S. Larson, Y. Zhao, and S. Ullrich, "Composition effects on ultrafast optical properties of Cu_xO_y thin films: A transient absorption study," *J. Phys. Chem. C* **124**, 24908–24918 (2020).
- ⁶¹A. Visibile, R. B. Wang, A. Vertova, S. Rondinini, A. Minguzzi, E. Ahlberg, and M. Busch, "Influence of strain on the band gap of Cu_2O ," *Chem. Mater.* **31**, 4787–4792 (2019).
- ⁶²S. Han, K. M. Niang, G. Rughoobur, and A. J. Flewitt, "Effects of post-deposition vacuum annealing on film characteristics of p-type Cu_2O and its impact on thin film transistor characteristics," *Appl. Phys. Lett.* **109**, 173502 (2016).
- ⁶³S. Han and A. J. Flewitt, "Analysis of the conduction mechanism and copper vacancy density in p-type Cu_2O thin films," *Sci. Rep.* **7**, 5766 (2017).
- ⁶⁴S. Han and A. J. Flewitt, "The origin of the high off-state current in p-type Cu_2O thin film transistors," *IEEE Electron Device Lett.* **38**, 1394–1397 (2017).
- ⁶⁵R. Zhang, L. Li, L. Frazer, K. B. Chang, K. R. Poeppelmeier, M. K. Y. Chan, and J. R. Guest, "Atomistic determination of the surface structure of $\text{Cu}_2\text{O}(111)$: Experiment and theory," *Phys. Chem. Chem. Phys.* **20**, 27456–27463 (2018).
- ⁶⁶L. Grad, Z. Novotny, M. Hengsberger, and J. Osterwalder, "Influence of surface defect density on the ultrafast hot carrier relaxation and transport in Cu_2O photoelectrodes," *Sci. Rep.* **10**, 10686 (2020).
- ⁶⁷A. Mittiga, F. Biccari, and C. Malerba, "Intrinsic defects and metastability effects in Cu_2O ," *Thin Solid Films* **517**, 2469–2472 (2009).
- ⁶⁸D. O. Scanlon, B. J. Morgan, G. W. Watson, and A. Walsh, "Acceptor levels in p-type Cu_2O : Rationalizing theory and experiment," *Phys. Rev. Lett.* **103**, 096405 (2009).
- ⁶⁹A. Živković and N. H. de Leeuw, "Exploring the formation of intrinsic p-type and n-type defects in CuO ," *Phys. Rev. Mater.* **4**, 074606 (2020).
- ⁷⁰Y. Zhu, Z. Xu, K. Yan, H. Zhao, and J. Zhang, "One-step synthesis of $\text{CuO-Cu}_2\text{O}$ heterojunction by flame spray pyrolysis for cathodic photoelectrochemical sensing of L-cysteine," *ACS Appl. Mater. Interfaces* **9**, 40452–40460 (2017).
- ⁷¹A. Dubale, A. Gedamu, H. M. Chen, T. Berhe, W.-N. Su, and B. J. Hwang, "Highly stable CuS and CuS-Pt catalyzed $\text{Cu}_2\text{O}/\text{CuO}$ heterostructure as efficient photocathode for hydrogen evolution reaction," *J. Mater. Chem. A* **4**, 2205 (2015).
- ⁷²D. Jiang, J. Xue, L. Wu, W. Zhou, Y. Zhang, and X. Li, "Photocatalytic performance enhancement of $\text{CuO}/\text{Cu}_2\text{O}$ heterostructures for photodegradation of organic dyes: Effects of CuO morphology," *Appl. Catal., B* **211**, 199 (2017).
- ⁷³Y. Yang, D. Xu, Q. Wu, and P. Diao, " $\text{Cu}_2\text{O}/\text{CuO}$ bilayered composite as a high-efficiency photocathode for photoelectrochemical hydrogen evolution reaction," *Sci. Rep.* **6**, 35158 (2016).